JYU DISSERTATIONS 441

Esa Kukkonen

Nonlinear Optical Materials through Weak Interactions and their Application in 3D Printing

UNIVERSITY OF JYVÄSKYLÄ
FACULTY OF MATHEMATICS
AND SCIENCE

JYU DISSERTATIONS 441

Esa Kukkonen

Nonlinear Optical Materials through Weak Interactions and their Application in 3D Printing

Esitetään Jyväskylän yliopiston matemaattis-luonnontieteellisen tiedekunnan suostumuksella
julkisesti tarkastettavaksi Ambiotican auditoriossa YAA303
lokakuun 29. päivänä 2021 kello 12.

Academic dissertation to be publicly discussed, by permission of
the Faculty of Mathematics and Science of the University of Jyväskylä,
in building Ambiotica, auditorium YAA303, on October 29, 2021, at 12 o'clock.

JYVÄSKYLÄN YLIOPISTO
UNIVERSITY OF JYVÄSKYLÄ

JYVÄSKYLÄ 2021

Editors
Jari Konu
Department of Chemistry, University of Jyväskylä
Päivi Vuorio
Open Science Centre, University of Jyväskylä

ISBN 978-951-39-8884-5 (PDF)
URN:ISBN:978-951-39-8884-5
ISSN 2489-9003

Permanent link to this publication: http://urn.fi/URN:ISBN:978-951-39-8884-5

ABSTRACT

Kukkonen, Esa
Nonlinear optical materials through weak interactions and their application in 3D printing
Jyväskylä: University of Jyväskylä, 2021, 58 p.
(JYU Dissertations
ISSN 2489-9003; 441)
ISBN 978-951-39-8884-5 (PDF)

Nonlinear optical (NLO) materials are highly coveted for their ability to change the properties of incident radiation as this feature has a variety of applications in laser technology and optoelectronics. The primary focus of this study was second harmonic generation (SHG), also known as frequency doubling, which is one of the most sought-after and widely studied NLO phenomena.

In this work, several different approaches were used to study nonlinear optical materials and their potential applications. First, noncovalent interactions were investigated as a way to influence the packing of the molecules within crystals to achieve favourable, non-centrosymmetric structures necessary for second harmonic generation. Halogen bonding was studied via reactions between simple di- and interhalogens and 4-aminopyridine. Instead of forming co-crystal adducts, the halogens were observed to favour the formation of iodonium-bridged bis(pyridines) or protonation of the pyridine ring, leading to solely centrosymmetric structures.

Next, a variety of dipolar stilbenes and their diaromatic derivatives were synthesized to investigate the effects of structural changes like doubling the length of the ethylene bridge and replacement of one aromatic ring with thiophene. While most of the modifications led to centrosymmetric structures, the simple substituent changes afforded a compound with a significantly higher second harmonic generation intensity than the reference material urea.

Lastly, a novel method of utilizing optically active materials within transparent 3D printed objects was investigated. Powdered NLO active materials were mixed with a photopolymerizable resin, which was then used to print simple lenses via stereolithography. The lenses were able to generate the second harmonic, and its intensity was found to strengthen almost linearly with the increasing thickness of the 3D printed lens. This method offers a fast and simple way of manufacturing highly customizable functional objects for optical applications.

Keywords: Nonlinear Optics, Second Harmonic Generation, Noncovalent Interactions, 3D Printing, Stereolithography.

TIIVISTELMÄ

Kukkonen, Esa
Epälineaarisia optisia materiaaleja heikoilla vuorovaikutuksilla sekä niiden soveltaminen 3D-tulostuksessa
Jyväskylä: Jyväskylän yliopisto, 2021, 58 s.
(JYU Dissertations
ISSN 2489-9003; 441)
ISBN 978-951-39-8884-5 (PDF)

Epälineaariset optiset (NLO) materiaalit ovat hyvin tavoiteltuja johtuen niiden kyvystä muuttaa säteilyn ominaisuuksia, millä on useita sovelluskohteita laserteknologiassa ja optoelektroniikassa. Tämä tutkimus keskittyi toiseen harmonisen säteilyyn, joka tunnetaan myös taajuuden kaksinkertaistumisena ja joka on yksi halutuimmista ja eniten tutkituista NLO-ilmiöistä.

Tässä työssä epälineaarisia optisia materiaaleja sekä niiden mahdollisia sovellutuksia tutkittiin monella tavalla. Ensiksi testattiin ei-kovalenttisten vuorovaikutuksien vaikutusta molekyylien pakkautumiseen kiteissä, jotta saavutettaisiin toisen harmonisen säteilyn syntymiseen vaadittavia ei-sentrosymmetrisiä rakenteita. Halogeenisitoutumista tutkittiin yksinkertaisten di- ja interhalogeenien sekä 4-aminopyridiinin välisillä reaktioilla. Halogeenien havaittiin suosivan jodonium-siltaisten bis(pyridiini)en tai protonoitujen pyridiinien muodostumista adduktien sijaan, mikä johti yksinomaan sentrosymmetrisiin rakenteisiin.

Tutkimuksen seuraavassa vaiheessa syntetisoitiin useita dipolaarisia stilbeenejä sekä niiden diaromaattisia johdannaisia. Näiden molekyylien avulla tutkittiin rakenteellisten muutosten, kuten etyleenisillan pituuden kaksinkertaistumisen sekä yhden aromaattisen renkaan korvaamisen tiofeenillä, vaikutuksia yhdisteiden optisiin ominaisuuksiin. Vaikka suurin osa muutoksista johtikin sentrosymmetrisiin rakenteisiin, yksinkertaiset substituentinvaihdokset saivat aikaan yhdisteen, jonka tuottaman toisen harmonisen säteilyn intensiteetti oli merkittävästi korkeampi kuin vertailukohtana käytetyn urean.

Lopuksi tutkittiin mahdollisuutta hyödyntää optisesti aktiivisia materiaaleja läpinäkyvissä 3D-tulostetuissa kappaleissa. Jauhemaisia NLO-aktiivisia materiaaleja sekoitettiin fotopolymeroituvaan hartsiin, josta tulostettiin yksinkertaisia linssejä stereolitografia-menetelmällä. Linssit kykenivät tuottamaan toista harmonista säteilyä, jonka intensiteetin havaittiin voimistuvan lähes lineaarisesti 3D-tulostetun linssin paksuuden kasvaessa. Kehitetty metodi tarjoaa nopean ja helpon tavan valmistaa erittäin kustomoitavia funktionaalisia kappaleita optisiin sovellutuksiin.

Avainsanat: Epälineaarinen optiikka, Toinen harmoninen säteily, Ei-kovalenttiset vuorovaikutukset, 3D-tulostus, Stereolitografia.

Author's address

Esa Kukkonen
Department of Chemistry
P.O. Box 35
FI-40014 University of Jyväskylä
Finland
esa.p.kukkonen@jyu.fi

Supervisors

Adjunct Professor Jari Konu
Department of Chemistry
University of Jyväskylä
Finland

Professor Matti Haukka
Department of Chemistry
University of Jyväskylä
Finland

Reviewers

Adjunct Professor Ari Lehtonen
Department of Chemistry
University of Turku
Finland

Adjunct Professor Raija Oilunkaniemi
Laboratory of Inorganic Chemistry
Environmental and Chemical Engineering
University of Oulu
Finland

Opponent

Professor Evamarie Hey-Hawkins
Institute of Inorganic Chemistry
Faculty of Chemistry and Mineralogy
Leipzig University
Germany

PREFACE

The work presented in this thesis was carried out in the Department of Chemistry at the University of Jyväskylä during 2017-2021. Finnish Cultural Foundation is warmly acknowledged for funding the research.

I started my PhD adventure by the usual method of continuing on the project I worked on during my Master's studies. The years have flown past (too) fast, and along the way I've gotten familiar with the unexpectedness of both chemistry and the world beyond it. The pandemic set its own challenges for the latter half of my studies as the time I spent in the lab was cut to a minimum. As a silver lining, working from home allowed me to truly focus on writing and helped me get this thesis done in time. Although I feel that the scientific story presented in this work could've used one final piece of the puzzle, I still see it as a fitting summary of the past four years.

First and foremost, I would like to thank my supervisors Adjunct Professor Jari Konu and Professor Matti Haukka for all the help and advice during my studies, especially throughout writing my thesis. Equally big thanks go to all previous and current members of our research group I have had the pleasure to know over the years for creating the friendly atmosphere which made me feel welcome from the very first meeting. I could not have wished for better people to share my PhD journey with. I would also like to thank all my colleagues at the Department of Chemistry who have contributed to my studies in one way or another, as well as the reviewers of my thesis for their valuable comments.

Lastly, I would like to express my sincerest gratitude to my family and friends for their continuous and invaluable support over the years. Thank you for everything.

Jyväskylä 11.8.2021
Esa Kukkonen

LIST OF ORIGINAL PUBLICATIONS

I Kukkonen, E.; Lahtinen, E.; Myllyperkiö, P.; Konu, J.; and Haukka, M. Three-Dimensional Printing of Nonlinear Optical Lenses. *ACS Omega*, **2018**, 3 (*9*), 11558-11561.

II Kukkonen, E.; Malinen, H.; Haukka, M.; and Konu, J. Reactivity of 4-Aminopyridine with Halogens and Interhalogens: Weak Interactions Supported Networks of 4-Aminopyridine and 4-Aminopyridinium. *Cryst. Growth Des.*, **2019**, 19 (*4*), 2434-2445.

III Kukkonen, E., Lahtinen, E., Myllyperkiö, P., Haukka, M., and Konu, J. Nonlinear Optical Properties of Diaromatic Stilbene, Butadiene and Thiophene Derivatives. *New J. Chem.,* **2021**, 45 (*15*), 6640-6650.

Author's contributions

The author performed most of the 3D printing in paper **I** and a large part of the synthetic work in papers **II** and **III**. The author also carried out most of the structural characterizations and optical measurements in paper **III** and participated in SHG measurements in papers **I** and **III**. The author also wrote the initial drafts for all three papers.

Other related publications by the author:

IV Lahtinen, E.; Kukkonen, E.; Jokivartio, J.; Parkkonen, J.; Virkajärvi, J.; Kivijärvi, L.; Ahlskog, M.; and Haukka M., Preparation of Highly Porous Carbonous Electrodes by Selective Laser Sintering, *ACS Appl. Energy Mater.*, **2019**, 2 (*2*), 1314-1318.

V Lahtinen, E.; Kukkonen, E.; Kinnunen, V.; Lahtinen, M.; Kinnunen, K.; Suvanto, S.; Väisänen, A.; and Haukka M. Gold Nanoparticles on 3D-Printed Filters: From Waste to Catalysis, *ACS Omega*, **2019**, 4 (*16*), 16891-16898.

VI Kukkonen, E., Ayeah, V., Haukka, M., and Konu, J. Proton Transfer and Crystal Packing Motifs in the crystallization of Isonicotinamide and 4-Pyridinethioamide with Organic and Inorganic Acids. *Manuscript in preparation.*

VII Kukkonen, E., Ayeah, V., Myllyperkiö, P., Haukka, M., and Konu, J. Structural and Nonlinear Optical Properties of 4-Hydroxypyridine with Ammonia-borane, Inorganic, and Organic Acids. *Manuscript in preparation.*

CONTENTS

ABBREVIATIONS AND TERMINOLOGY

BBO	Barium Borate
CAD	Computer-Aided Design
CAHB	Charge-Assisted Hydrogen Bonding
CCD	Charge-Coupled Device
CLIP	Continuous Liquid Interface Production
DAST	4-N,N-dimethylamino-4′-N-methyl-stilbazolium tosylate
DIW	Direct Ink Writing
DLP	Digital Light Processing
DLW	Direct Laser Writing
DoD	Drop-on-Demand
EFISHG	Electric Field Induced Second Harmonic Generation
KDP	Potassium Dihydrogen Phosphate
KTP	Potassium Titanyl Phosphate
LBO	Lithium Triborate
MJM	MultiJet Modeling
MMONS	3-methyl-4-methoxy-4′-nitrostilbene
MOF	Metallo-Organic Framework
NLO	Nonlinear Optics
NMR	Nuclear Magnetic Resonance spectroscopy
PMT	Photomultiplier tube
SHG	Second Harmonic Generation
SLA	Stereolithography
SLS	Selective Laser Sintering
UV	Ultraviolet
YAG	Yttrium Aluminium Garnet

Birefringence	The dependence of the material's refractive index on the polarization or propagation direction of the radiation
Curing	Hardening of a polymeric material by cross-linking
Periodic poling	A method to create layers with alternating orientation within a material to prevent the cancellation of the material's nonlinear properties

1 INTRODUCTION

Nonlinear optics (NLO) is a branch of optics that studies materials that have the ability to modify incident radiation's properties, such as its phase or frequency. Consequently, NLO materials have a variety of current and potential technological applications in e.g. optical data storage, optoelectronics, and telecommunications, just to mention a few. One of the most sought-after nonlinear optical properties is second harmonic generation (SHG). This phenomenon is often referred to as frequency doubling since SHG active materials are able to combine two incident photons into one, creating radiation with twice the frequency and half the wavelength of the initial photons. This important phenomenon is widely utilized in e.g. laser technology[1] and SHG microscopy[2].

The majority of SHG active materials which are currently in commercial use are purely inorganic compounds that were discovered several decades ago, such as potassium titanyl phosphate (KTP)[3], β-barium borate (BBO)[4], and lithium triborate (LBO)[5]. The main assets of these compounds are their wide transparency ranges and good mechanical properties. As modern technology continues to strive towards more efficient materials, organic compounds have attracted a lot of scientific interest due to their large nonlinearities on both molecular and macroscopic scales. These superior properties fundamentally arise from the extensive conjugation of these systems, a feature that also gives rise to ultrafast response times which are highly coveted in technological applications.

Another advantage of using organic compounds for second harmonic generation is the ease of structural modifications in the molecules. This is an important factor as SHG, like all other second-order nonlinear phenomena, requires the material to have no inversion centre, which means that any form of control over the arrangement of molecules in crystals is highly beneficial. One way of trying to ensure a favourable alignment of molecules is to utilize noncovalent interactions for steering the molecular assembly towards non-centrosymmetry. Two types of noncovalent interactions with a particular significance to organic materials are the closely related hydrogen and halogen bonding. Both interactions are rather specific in nature and, importantly for

crystal engineering, have a relatively high directionality of the bonds which allows a rational approach to the structural design of the compounds.

However, some issues around the organic materials' practical use remain as is suggested by the inorganic materials' continued commercial domination. One of the biggest limitations in the use of organic materials has been the issue of growing large crystals with sufficient optical quality. The organic crystals also tend to lack the mechanical strength of their inorganic counterparts and are consequently not as easily shaped into optical parts. Therefore, in addition to investigating novel materials, searching for ways to circumvent the drawbacks of the efficient, already-known materials could help the organics to realize their potential in nonlinear optics.

The aim of this thesis was to develop novel nonlinear optical materials, with a particular focus on their second harmonic generation properties. The materials were designed to be based on dipolar conjugated organic molecules, which could then be further modified to promote the non-centrosymmetric arrangement of the molecules or adjust the orientation of molecular polarities within the structures. Non-covalent interactions, primarily halogen and hydrogen bonding, were studied as a way to influence the self-assembly of molecules into functional materials. Furthermore, the effects of structural modifications of stilbenes, one of the best-performing groups of organic NLO materials, were investigated. These studies included changing the length of the ethylene bridge between aromatic moieties as well as the nature of one of the aromatic rings.

Lastly, the possibility of using NLO active materials as a crystalline powder within 3D printed lenses was investigated. While the emergence of the scientific use of 3D printing has already led to reports of several optical applications, studies on the inclusion of functional additives are still scarce at best. The utilization of small crystals would eliminate the need for long and often tedious crystallizations of the organic materials, and the plastic matrix could provide additional protection to the active material against potentially unfavourable environmental factors such as moisture.

2 NONLINEAR OPTICS

Nonlinear optics (NLO) as a concept covers a wide variety of phenomena that all arise from the nonlinear response of the materials' polarization to the electric field of the incident light. This nonlinearity will cause changes in the phase, polarization, or frequency of the radiation travelling through the material. The polarization p of a single molecule can be formulated as

$$p = p_0 + \alpha E + \beta EE + \gamma EEE + \ldots, \quad (1)$$

where p_0 is the ground state polarization of the molecule, E is the external electric field (of the incident radiation), α the linear polarizability of the molecule, and β and γ its second and third-order hyperpolarizabilities, respectively. These parameters reflect the strength of the molecules' nonlinearity, and they can be measured experimentally. The molecular polarizability terms are replaced by susceptibilities $\chi^{(n)}$ on the macroscopic level, where the index n denotes the order of the susceptibility (e.g. the hyperpolarizability β gives rise to second-order susceptibility $\chi^{(2)}$ of the material). It is noteworthy that high values of the molecular parameters do not automatically lead to large susceptibilities, as the latter are also dependent on the three-dimensional arrangement of molecules within the material.[6]

Due to the inherently low intensities of the nonlinear optical phenomena, it took the invention of laser[7] in 1960 before they could be quantitatively determined. The first NLO discovery didn't have to wait for long as second harmonic generation was observed in quartz within a year from the first laser.[8] This started a whole new branch of research, and the amount of known nonlinear optical phenomena quickly grew during the following years. Especially frequency-mixing processes such as harmonic generation, optical parametric amplification, and optical parametric oscillation have seen a lot of scientific interest and technological applications thus far. One of the most important and widely utilized of these phenomena, second harmonic generation, is discussed in further detail in the following chapters.

2.1 Second harmonic generation

Second harmonic generation (SHG) is one of the most important NLO phenomena and has subsequently been the focus of a plethora of scientific studies. In SHG, two photons interact with matter to create a single photon with twice the frequency and thus half the wavelength of the original radiation. While usually incomplete, the conversion can get close to 100% under the right experimental conditions.[9] The phenomenon can be seen as a special case of sum-frequency generation, where two photons of different wavelengths combine into one. It also bears resemblance to two-photon fluorescence, but it does not require real electronic states, nor is there any energy loss involved.

The main prerequisite for the material to exhibit second harmonic generation, or any other second-order nonlinear property, is the non-centrosymmetry of its crystal structure. The lack of an inversion centre prevents the molecular second-order hyperpolarizabilities β from effectively cancelling each other, therefore leading to a non-zero susceptibility $\chi^{(2)}$. Several structural factors like the conjugation of the molecule and intramolecular charge transfer have also been found beneficial for compounds to exhibit high second-order nonlinearity.[10]

An important aspect when considering the usability of new SHG materials in practical applications is their phase-matching ability. This means the existence of an orientation of the crystal where the harmonics generated by individual dipoles interact constructively, significantly strengthening the overall SHG signal of the material. Conversely, the generated harmonics in crystals where phase-matching is not possible to achieve will stay weak, which severely hinders the use of the materials in most applications that are based on nonlinear wave mixing processes (Figure 1). Phase-matching is commonly achieved by utilizing the material's birefringence to overcome the dispersion of the radiation. In the so-called angle tuning method, the crystal is carefully oriented in a way that the incidence angle of the radiation fulfils the phase-matching condition. Another method called temperature tuning is possible in crystals where the birefringence is strongly dependent on temperature, like lithium niobate.[11] As the name suggests, phase-matching is achieved by keeping the incidence angle constant and varying the crystal's temperature instead. If neither method can be used, it is possible to achieve efficient NLO properties through quasi-phase-matching, where the materials' crystal domains are affected by e.g. periodic poling[12] to compensate for the mismatch of the generated nonlinear radiation.[9]

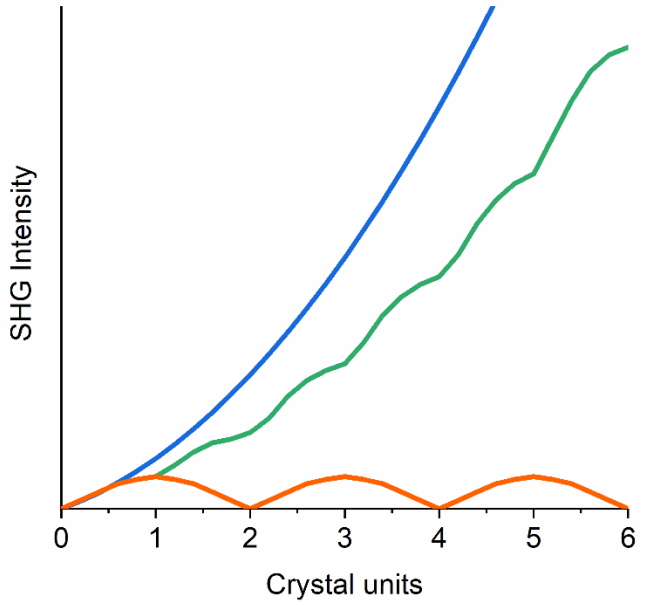

FIGURE 1 SHG intensity as a function of crystal size of perfectly phase-matched (blue), quasi-phase-matched (green), and non-phase-matching (orange) nonlinear optical materials.

2.1.1 Measurement techniques

A variety of measurement techniques that can be used to investigate materials' second harmonic generation properties have been developed. Each of these methods comes with different prerequisites and sample preparation methods, as well as advantages and limitations. They also differ by the nature of the parameters which can be obtained from the results. Commonly SHG measurements have been performed with Nd:YAG lasers operating at 1064 nm, meaning that the wavelength of the generated second harmonic is 532 nm, but the use of other wavelengths such as 1907 nm has also been reported.[13–15]

Kurtz-Perry (sometimes only referred to as Kurtz) method is one of the most common SHG measurement techniques due to its simplicity and suitability for quick scanning of materials (Figure 2). The technique was first reported[16] in 1968, not long after the invention of lasers and the subsequent discovery of nonlinear optics, and has been since named after its inventors. The measurement is performed on a powdered sample, eliminating the need for growing large crystal samples, and the produced SHG intensity is compared with a known reference material. Commonly either potassium dihydrogen phosphate (KDP) or urea is used since the relevant properties of both compounds are well-known in addition to them being widely available. In order for the obtained results to be comparable the samples should be of uniform crystal size, typically ranging from 5 µm to 150 µm, as the intensities produced by crystals of unequal size can vary drastically. It should be noted that the Kurtz-Perry technique does not provide accurate numerical data about the material's NLO properties; the resulting value is merely an estimate of the material's nonlinear optical coefficient. Nevertheless, it

provides valuable information about the relative efficiencies of NLO compounds without extensive sample preparation.

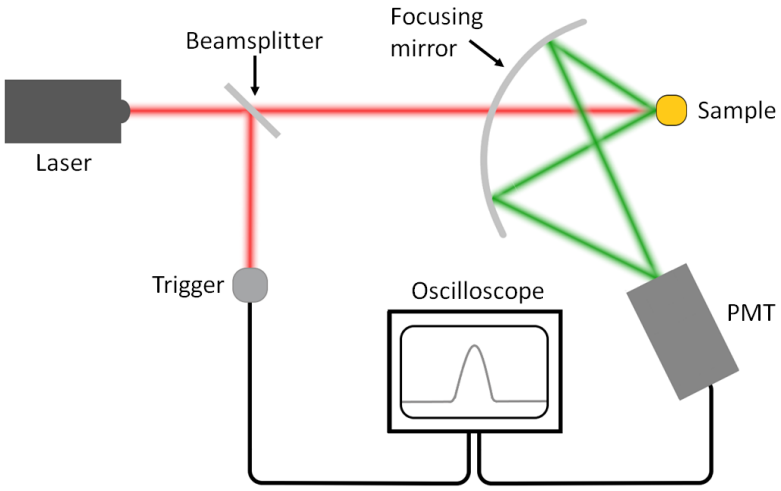

FIGURE 2 A schematic of a typical Kurtz-Perry measurement setup. The powder sample is irradiated with laser, the generated second harmonic is collected to a photomultiplier tube (PMT) and measured with an oscilloscope or a charge-coupled device (CCD).

Kurtz-Perry technique also enables the determination of whether the material under investigation is phase-matchable or not. The material is powdered into several distinct crystal sizes, and the second harmonic intensities obtained from the different portions are plotted against the crystal sizes (Figure 3). If the plot reaches an intensity maximum after which the intensities start to fall as the crystal size grows, the material is not phase-matchable. If the intensities do not fall but instead increase to a certain level after which they stay nearly constant despite the growing crystal size, the material is phase-matchable.

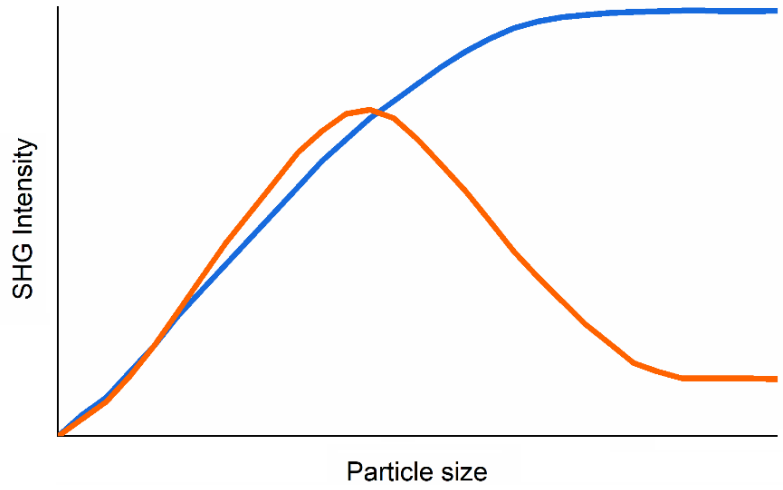

FIGURE 3 Schematic representation of the behaviour of phase-matchable (blue) and non-phase-matchable (orange) NLO materials in Kurtz-Perry SHG measurements as a function of increasing crystal size.

EFISHG (or EFISH, short for Electric Field Induced Second Harmonic Generation) is a common method for defining the molecular second-order hyperpolarizability β in the solution state, while also allowing measurements from the gas phase.[17,18] In the measurements a strong direct current electric field is applied to the solution, which breaks the isotropy of the solute, thus allowing the SHG to occur. However, in order to calculate the value of β from the obtained results, knowledge of other molecular parameters like dipole moment μ and third-order hyperpolarizability γ is required. Additionally, for this technique to be applicable, the compound of interest should be polar and non-ionic; restrictions which are not trivial for all SHG active materials. The technique also does not provide insight on the properties of the solid material as the hyperpolarizability β alone does not give any indication about the crystal's packing which also has a critical role in the material's macroscopic properties.

Another similar solution state technique is Hyper-Rayleigh scattering, but unlike EFISHG, it also allows non-polar and ionic samples due to the absence of the external electric field. In the method incoherently scattered second harmonic radiation is measured from an isotropic solution, and the second-order hyperpolarizability β can be obtained from the results without the prerequisites of EFISHG.[19,20] However, due to the scattered nature of the second harmonic, the obtained signals are typically much weaker. Additionally, effects like multiphoton fluorescence can interfere with the second harmonic signal, making the interpretation of the results less straightforward.[21]

Maker fringe technique is commonly used for accurate solid-state determination of the nonlinear coefficient d_{ij}. The method was discovered by Maker *et al.*[22] and its theory was further developed by Jerphagnon and Kurtz[23]. The measurement is performed on a single crystal which is rotated around an axis perpendicular to the laser beam direction, and the generated SHG intensity is plotted against the rotation angle. As the optical path length which the laser travels within the crystal changes, so does the interference and thus the intensity of the generated harmonic, which leads to a periodically oscillating SHG plot. The obtained peak amplitudes can then be used to determine the NLO coefficient.

2.2 Noncovalent interactions as tools for SHG material synthesis

Due to the importance of SHG, numerous studies to find novel materials with high second-order nonlinear activity have been carried out. Inorganic materials have been on the frontline of nonlinear optics ever since SHG was first observed in quartz[8]. They have continued to dominate the commercial use of nonlinear optics despite the organic materials displaying significantly higher nonlinearities, as the former are mechanically more durable as well as easier to crystallize in larger sizes that the applications often require. The inorganics also possess wider transparency regions extending to deep UV, whereas organic materials tend to be more limited due to the energy-absorbing vibrational states of the common covalent bonds in these systems.

Nevertheless, using organic materials as SHG generators offers profound advantages over their inorganic counterparts, and they have consequently been in the focus of intensive research for decades. The main appeal of these materials is their potential for extensively conjugated structures which have given rise to exceptionally strong nonlinearities. Especially π-bridged donor-acceptor molecular structures with intramolecular charge transfer (Figure 4) have been found to lead to high molecular hyperpolarizabilities.[10,24] The conjugation allows easier and faster electron movement which, in combination with the polarizability, causes large dipole moment changes upon photoexcitation. This, consequently, leads to strong nonlinear responses and ultrafast response times which are highly valued in technological applications.

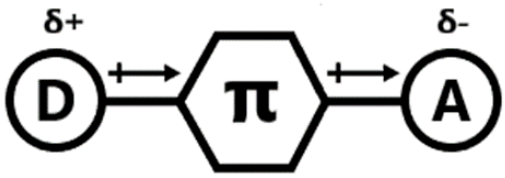

FIGURE 4 General schematic of a molecule with the so-called "push-pull" effect, intra-molecular charge transfer between the donor (D) and acceptor (A) groups combined with a conjugated (π) structure.

However, moving from good properties on the molecular level into the material level is not straightforward. For example, the utilization of strong electron donors like the dimethylamino group in an attempt to maximize molecular hyperpolarizability can lead to lower transparency on the material level. Therefore, weak donors like bromine have been studied as a tool towards wider transparency ranges without sacrificing the strength of the molecule's nonlinear response.[25,26] An even more critical challenge in synthesizing novel materials with second-order nonlinearity is trying to ensure their non-centrosymmetric crystal structure which prevents the molecular hyperpolarizabilities from effectively cancelling each other. Perhaps the most promising crystal engineering approach is to use weak noncovalent interactions in guiding the assembly of the molecules into NLO active materials. This method aims to take full advantage of the tailorability of the organic compounds and, at least in theory, should also allow structural control beyond mere symmetry considerations. For instance, even if the material's crystallization was non-centrosymmetric, an antiparallel alignment of the molecular chains or sheets would weaken the nonlinearity compared to a perfectly parallel alignment of all molecular dipoles (Figure 5), which is why the tools to fine-tune the crystallization behaviour are so essential.

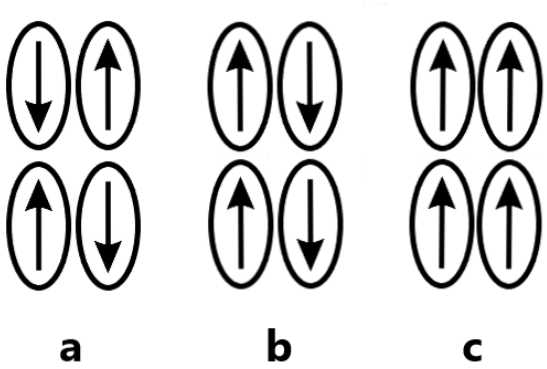

FIGURE 5 Simplified schematic representation of different molecular dipole arrangements: (a) individual dipoles cancelling each other out, (b) antiparallel alignment of polar chains/sheets, and (c) ideal, parallel alignment of all dipoles.

Noncovalent interactions refer to chemical interactions of atoms that do not share an electron pair between them. The strength of these forces varies greatly, from the weak van der Waals to the ionic and metal-ligand interactions reaching the strength of covalent bonds. The interactions have been intensively studied for decades for their crucial role in crystal engineering and materials science as the ordering of molecules in the crystal lattice often determines the properties of the entire material, like in the case of nonlinear optics. Two especially important interactions are hydrogen and halogen bonding, both of which arise primarily from electrostatic interactions while also having contributions from charge transfer and dispersion.[27,28] The predictable directionality of these forces, the like of which most other noncovalent interactions are lacking, enables better rationalization of the molecules' alignment during the crystallization of the compounds. The following chapters will go through some key compounds as well as examples of the use of different noncovalent interactions in the synthesis of NLO materials.

2.2.1 Ionic interactions

The vast majority of the inorganic NLO active compounds are ionic by nature. Metal oxides have traditionally been the key group of SHG studies, and materials like potassium dihydrogen phosphate KH_2PO_4 (KDP) and barium borate BaB_2O_4 (BBO)[4] (both strongly birefringent) continue to be widely utilized in NLO applications. Especially various borate compounds have gained a lot of interest due to the inherently large electronegativity differences between the anion's constituents as well as the anion's anisotropic electron distribution, both of which benefit the SHG properties. Due to their low cut-off wavelengths, these materials are especially useful in applications requiring second or higher harmonic generation in the deep UV region.[29,30] However, these compounds are less useful in middle and far-infrared applications due to their increasing absorption. As a result, research on novel chalcogenide and halide-based compounds for this wavelength region continues as the current commercial materials like $AgGaS_2$

(silver thiogallate) and $ZnGeP_2$ (zinc germanium phosphide) suffer from drawbacks that hinder their widespread use.[31,32]

In the case of organic compounds, the usefulness of the ionic interactions stems from the coulombic forces' ability to overtake the weaker dipole-dipole interactions which often lead to crystalline centrosymmetry.[33] One of the most extensively studied groups of such compounds are the stilbazolium salts. The first glimpse into the compounds' potential was obtained when Meredith reported[13] a series of 4'-dimethylamino-N-methyl-4-stilbazolium salts, the strongest of which reached SHG efficiency of around 220 times urea. The Kurtz-Perry measurements of the study used a longer wavelength of 1.91 μm due to the compounds' strongly coloured nature, preventing the absorption of the generated second harmonic. Some years later Marder *et al.*[14] systematically studied these compounds with a series of reactions that changed both the counteranion and the substituents of the stilbazolium cation. These reactions afforded among others 4-N,N-dimethylamino-4'-N-methyl-stilbazolium tosylate (DAST, Figure 6), which was measured to generate 1000 times stronger SHG than urea at 1907 nm. The study also confirmed the impact of the selected wavelength, as the measurements were performed at 1064 nm as well, giving an SHG efficiency of mere 15 times urea for DAST, and a similarly large variation was observed with several other compounds. Additionally, the selection of counteranion was found to have large implications on the materials' nonlinear properties through changes in the cations' packing. Further systematic studies have since been made[34] and materials exceeding DAST's SHG efficiency at 1907 nm have been reported.[35–37] In addition to strong SHG capabilities, stilbazolium salts have also been studied as potential optical THz radiation generators[38].

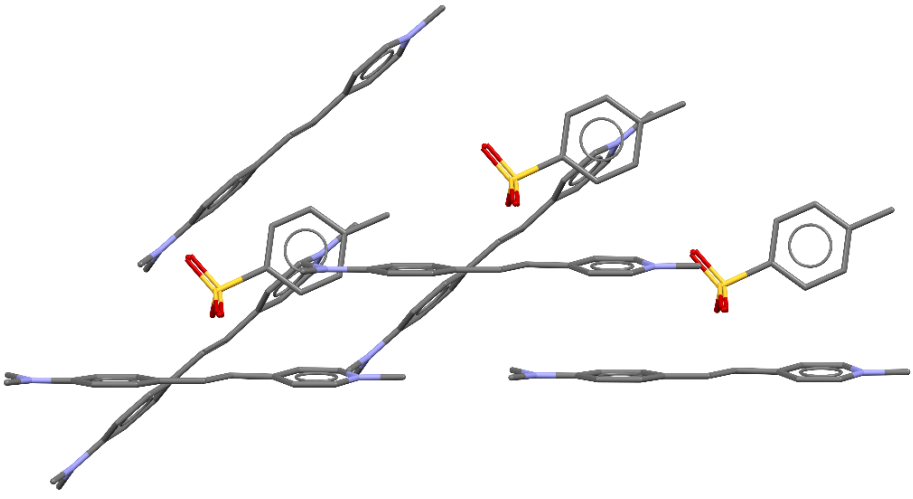

FIGURE 6 The packing of DAST[39]. Cations are arranged in strands, which form stacks with the help of π-π-interactions. Adjacent stacks are parallel despite being in a different plane. Hydrogens have been removed for clarity.

2.2.2 Hydrogen bonding

The chemical importance of the hydrogen bond is undeniable as it is responsible for many properties of water, as well as having a crucial role in a variety of biological systems. The interaction forms when a hydrogen atom, which is covalently bonded to a more electronegative atom (commonly oxygen or nitrogen) and is therefore slightly electron-deficient, is attracted to another atom's lone electron pair (Figure 7). The nature of the interaction leads to a predictable directionality of the contact, which makes hydrogen bonding a useful tool in crystal engineering.

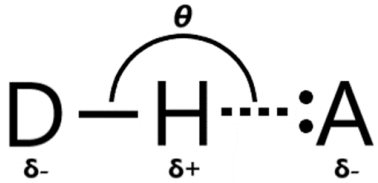

FIGURE 7 Schematic representation of the hydrogen bond. The bond angle θ is dependent on the nature of the donor (D) and acceptor (A) of the hydrogen bond. In general, the best donor forms a contact with the best acceptor.[40]

Nitroaniline derivatives were the first compounds where hydrogen bonds were utilized to gain non-centrosymmetric structures for nonlinear optics[41]. These compounds have been extensively studied and powder SHG efficiencies of up to 1000 times of urea have been reported.[42,43] Etter *et al.* studied the intermolecular NH⋯ O hydrogen bond in nitroanilines both experimentally[44] and via a structural database analysis[45]. They concluded that NH⋯ O is a rather predictable synthon, which leads to the formation of nitroaniline chains and an increased amount of non-centrosymmetric structures. Similar database analysis was also conducted on benzoic acids and it was observed that ortho-substitution of the acid could promote the non-centrosymmetry of the crystalline material, therefore being of potential interest to NLO studies.[46]

Charge-assisted hydrogen bonding (CAHB), an interaction variant possessing ionic character and often resulting from a reaction with a carboxylic acid, has been a common tool in the synthesis of NLO materials. Amino acids, whose SHG activity was found when the field of nonlinear optics was still young,[47] and their salts are some of the most intensively studied organo-ionic compounds exhibiting these interactions. The inherent chirality of amino acids, excluding the simplest compound glycine, ensures that the obtained crystals are non-centrosymmetric and therefore able to create SHG. Their nonlinear activities, however, have been much lower than the larger, more conjugated compounds generally display.[48–50] An exception to this trend have been the picrate salts, where the anion's conjugation enhances the compounds' nonlinearity and has led to reports of powder SHG intensities of over 10 times of urea.[51,52] Various other hydrogen-bonded salts like ammonium dihydrogen phosphates, chiral L-tartrates, and hydroxybenzoates have also been studied, but they haven't been able to reach the SHG efficiency of the larger conjugated compounds either.[53–55]

Owing to its predictable nature, hydrogen bonding has been successfully utilized in rationalizing step-by-step syntheses of novel SHG active structures. Miyano[56] *et al.* prepared a dipolar conjugated compound 4-aminoazobenzene-4-sulfonic acid, which crystallized as sheets whose polarities cancelled each other due to the centrosymmetry resulting from the hydrogen bonding motif. Recrystallization of the acid with a chiral amine component afforded non-centrosymmetric salts with helical CAHBs but the sheet-like structure was lost, possibly due to molecular length discrepancy. This issue was solved by the inclusion of various guest molecules capable of hydrogen bonding with the amines. These guest molecules settled in the same layer with the chiral amines without exceptions, which allowed the reformation of the polar 4-aminoazobenzene-4-sulfonic acid sheets (Figure 8) and led to structures with SHG activity up to 59 times of urea when measured from powder at 1.5 μm.

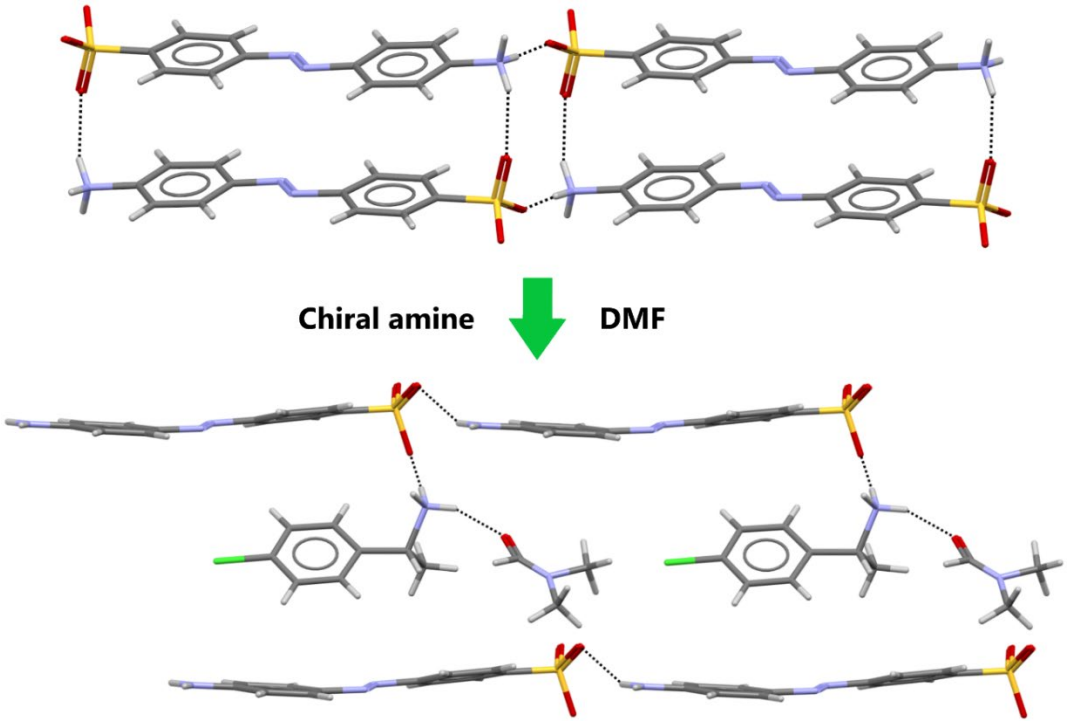

FIGURE 8 An example of the reactions performed by Miyano *et al.*[56] The initially centro-symmetric crystal structure of 4-aminoazobenzene-4-sulfonic acid (top) was re-ordered by hydrogen bonding interactions with (R)-1-(4-chlorophenyl) ethylamine and dimethylformamide (bottom).

In addition to steering the crystallization of structures, the hydrogen bond formation itself can affect the nonlinear optical properties of the system. Its effect on the NLO chromophore's hyperpolarizability has been studied both experimentally[57] and theoretically[58], and hydrogen bond formation has been proven to have a clear impact on the measured β of the compound. By comparing the results of Hyper-Rayleigh scattering measurements of para-nitroanilines in around 50 solvents, the hyperpolarizability was observed to double between certain solvents, and hydrogen bonding was found to consistently increase the values of β.[57] Even larger shifts caused by hydrogen bonding were obtained from

theoretical calculations of the hyperpolarizability β of highly solvatochromic aminobenzodifuranone.[58] It is therefore integral to take note of potential solvent-solute interactions upon solution-based measurements of molecular hyperpolarizability to prevent erroneous results.

2.2.3 Halogen bonding

Halogen bonding has only recently risen to prominence as one of the most studied interactions in crystal engineering despite being first observed over 150 years ago.[59] The force arises from the halogen atom's polarization within covalently bonded systems. Despite the halogens' high electronegativities, a small positively charged region is formed on the opposite side of the covalent bond. This so-called σ-hole is electrophilic and therefore attracted to nucleophilic regions of other atoms or molecules, forming the interaction known as the halogen bond. The σ-hole's relatively small size is also the main reason for the interaction's high directionality as θ_1 rarely deviates much from 180° (Figure 9). As the strength of this interaction heavily relies on the extent of the halogen atom's polarization, the larger and therefore more easily polarizable iodine and bromine tend to form stronger halogen bonds than the smaller chlorine and fluorine.

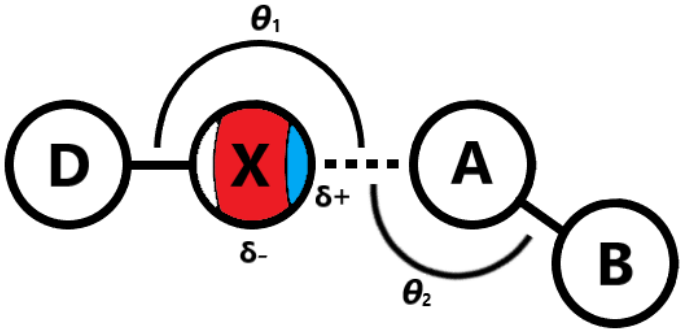

FIGURE 9 Schematic representation of halogen bonding showing the formation of the σ-hole (blue) on the halogen atom (X). Traditionally, halogen-halogen contacts have been divided into type I ($\theta_1 \approx \theta_2$) and type II ($\theta_1 \approx 180°$, $\theta_2 \approx 90°$), and only type II are considered as true halogen bonds.[60]

One of the supramolecular halogen bonding synthons that has been found useful in the design of nonlinearly active systems is the iodo ⋯ nitro contact. A couple of diaromatic systems containing these substituents have successfully been crystallized in non-centrosymmetric space groups. While para-disubstituted benzene utilizing the I ⋯ O_2N contacts crystallized with an inversion centre, a biphenyl structure with the same interaction was found to be non-centrosymmetric and SHG active.[61] The same synthon was successfully used in guiding the crystallization of N,N'-diphenyl urea derivatives. While all other halogen substituents were unable to prevent a centrosymmetric urea ⋯ nitro-synthon from forming, iodine's competition for the nitro contact was enough to make urea ⋯ urea the main hydrogen bonding synthon of the structure. This compound displayed SHG activity of over 13 times of urea, clearly

outperforming its few isostructural compounds with no possibility for halogen bonding.[62]

The use of halogen bonding in combination with hydrogen bonding has been explored in other studies as well. Halogen bonding in dipolar pyridine derivatives was found to be more prominent in the bromo- and iodo-substituted moieties, which were found to be rather consistent in forming non-centrosymmetric structures, whereas the chloro-derivatives had a more significant hydrogen bonding contribution.[63] This trend is in line with the general order of the polarization strength of the halogens and has been observed in other SHG studies as well.[64] Similar combinatory approach has been used with benzylammonium carboxylates, where hydrogen bonds and van der Waals interactions were responsible for forming polar two-dimensional layers which the halogen⋯ halogen interactions then stacked into three-dimensional structures. If type I halogen contacts were formed, the obtained crystals were centrosymmetric whereas type II halogen bonds afforded the desired non-centrosymmetric crystals (Figure 10).[65]

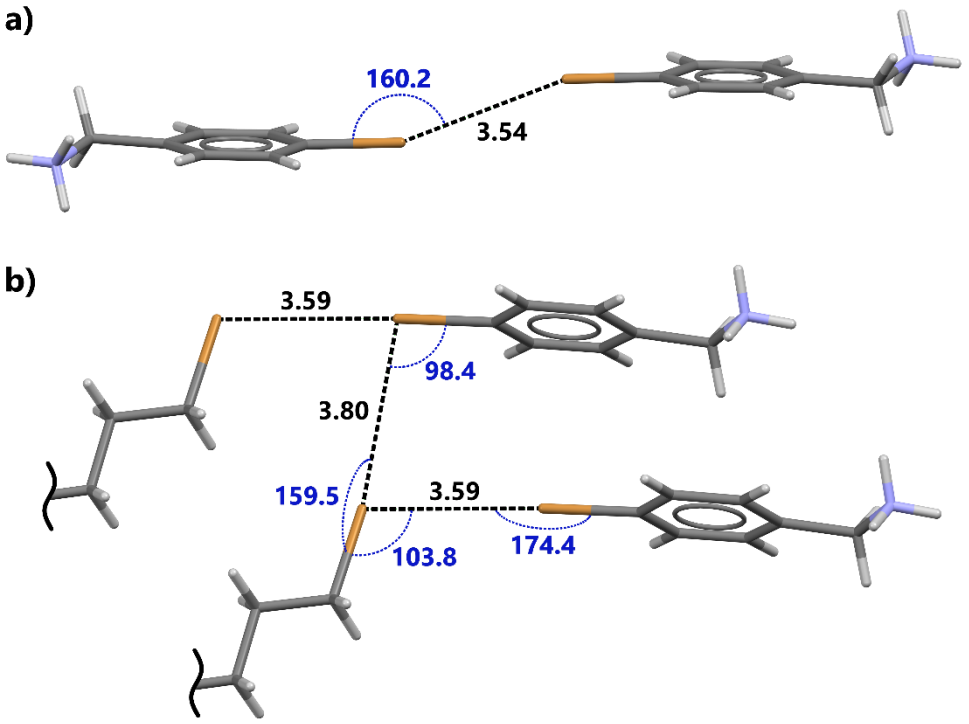

FIGURE 10 Contact lengths (in Å) and angles of a) type I halogen contacts in (4-bromophenyl)methaminium tridecanoate leading to centrosymmetric structure, and b) type II halogen bonds in (4-bromophenyl)methaminium 12-bromododecanoate giving rise to a non-centrosymmetric arrangement.[65]

Like in the case of hydrogen bond formation, the solvent's ability to interact with the solute via halogen bonding has been found to affect the generated SHG in solution both experimentally and theoretically.[66] Large shifts in the hyperpolarizabilities of the iodine-substituted diaromatic N,N-dimethylanilines' were observed based on the solvent selection for the EFISHG measurements. Changes of comparable extent were not observed with a structurally similar but

iodine-less NLO chromophore, which further underlines the vital role of the noncovalent interaction.

2.2.4 Metallo-organic materials

The search for metallo-organic NLO materials began in mid-1980s[67,68] with the aim of combining the strengths of both organic and inorganic materials. The discovery of a highly active ferrocene derivative[15] giving a second harmonic signal of 62 times of urea at 1907 nm showed the potential of metallo-organics, and the following interest in ferro- and other metallocenes have made them one of the most studied group of organometallic compounds for NLO applications.[69,70] Some of the best results so far have been achieved with (E)-1-ferrocenyl-2-(1-methylpyridinium-4-yl)ethylenes, which structurally resemble stilbazoliums with the exception of having a ferrocene on the place of the benzene ring (Figure 11). A series of reactions focusing on counteranion changes afforded several purple NLO active compounds, with the iodide salt reaching the highest powder SHG efficiency, up to 220 times of urea. Analogous ruthenocenyl compounds showed much more modest NLO activities, possibly due to centrosymmetric packing.[71]

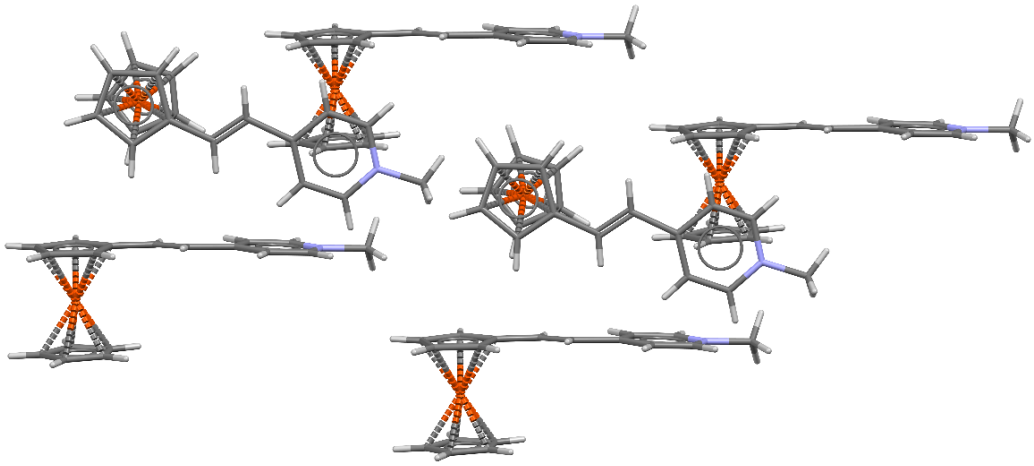

FIGURE 11 Packing of (E)-1-ferrocenyl-2-(1-methylpyridinium-4-yl)ethylene nitrate.[71] The molecules settle in two perpendicular, yet mostly parallel, planes to give rise to SHG activity of 120 times of urea. Nitrate anions have been removed for clarity.

The metal atoms within these compounds offer a unique way of switching their second-order nonlinear properties through reversible redox reactions of the metals. This ability has been observed in compounds involving metals such as iron and ruthenium, in which the alteration between the metal's oxidation states II and III causes clear changes in the complexes' hyperpolarizability β measured via Hyper-Rayleigh scattering.[72,73] The potential for NLO switches is especially pronounced with the ruthenium complex which essentially loses its SHG activity upon oxidation of the metal due to the polarity changes in the cation. While switching of the NLO properties has also been reported from purely organic

compounds e.g. photoswitching via cis-trans isomerization of the molecules, the extent of changes are often less complete and much slower.[74]

While the use of metals adds a new dimension to the modification of NLO compounds, the choice of the ligands remains as important, if not more, when considering the nonlinear properties. Just like with purely organic compounds, extensive conjugation remains a coveted property and consequently, the ligands used for metallo-organic systems have been predominantly aromatic. Bipyridines and their derivatives have been used with a variety of metals due to their good coordination abilities and intense low-energy charge transfer interactions. These usually bidentate ligands have been used to study octupolar metallo-organic complexes as an alternative for the traditional dipolar structures (Figure 12).[75–77] Compounds known to exhibit high nonlinearities have also seen use, like stilbazolium salts and their analogues, which have been utilized in bimetallic metal(II) chromium(III) oxalate complexes. Much like in the case of the stilbazolium derivatives in Chapter 2.2.1, high powder SHG intensities up to 100 times of urea (measured at 1.907 μm) have been observed from these ferromagnetic compounds.[78,79]

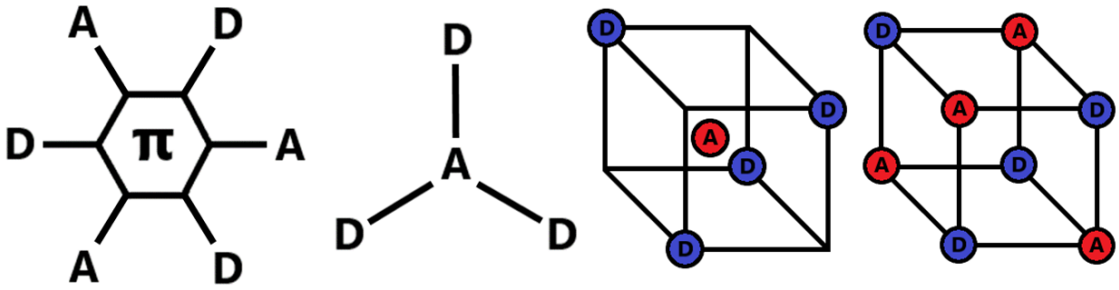

FIGURE 12 Schematic representation of different two- and three-dimensional octupolar arrangements of donor (D) and acceptor (A) moieties.

The rise of interest in the chemistry of metallo-organic frameworks (MOFs) has also seen them being explored for NLO applications.[80–82] The increasingly covalent and directional metal-ligand coordination bonds allow rational synthesis of multiple different geometries from 3D networks to 1D chains. The three-dimensional diamondoid motif has been found especially useful in forming non-centrosymmetric structures, particularly when using asymmetric ligands (Figure 13). While a variety of metal centres have been used in the reported MOF structures, d^{10} metals have been identified as especially useful due to their full d-orbitals preventing any unwanted absorptions arising from d-d transitions.[80] Divalent Zn^{2+} and Cd^{2+} have been the most frequently used d^{10} metals due to their stability and useful coordination geometries. These metals have formed some of the most efficient NLO MOFs to date in hydrothermal reactions with a benzo[e]indole ligand, as SHG activities of 50 and 80 times of urea have been reported for the 2D zinc and 1D cadmium structures, respectively. Both metals significantly enhanced the nonlinearity of the compound when compared with the pure organic ligand.[83,84]

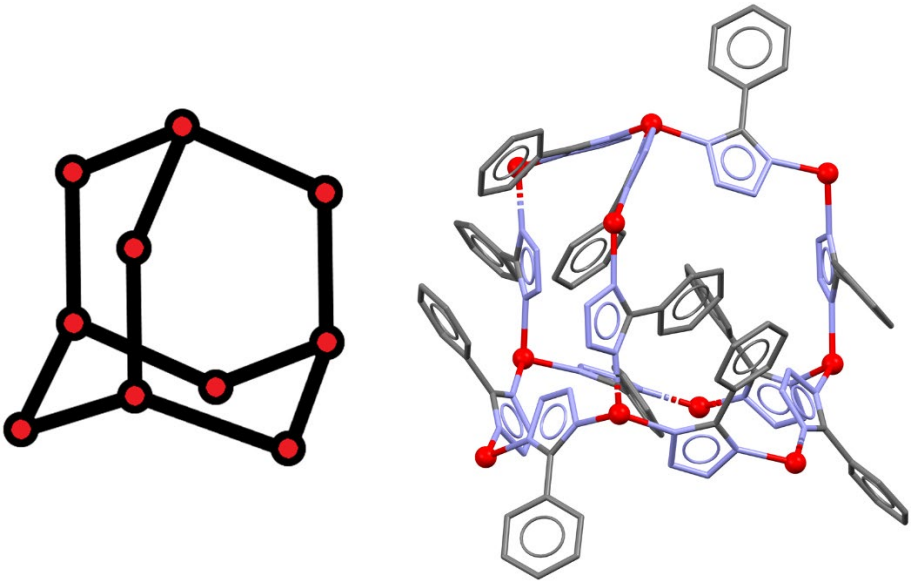

FIGURE 13 Three-dimensional diamondoid structure (left) in a SHG-active phenyltetrazole-zinc-MOF[83] (right). Hydrogens have been removed and zinc centres coloured red for clarity.

2.2.5 Van der Waals and π-interactions

Despite the improved structural control provided by the aforementioned interactions, some of the most efficient second-order NLO compounds are only interacting through weaker and non/less-directional van der Waals or π-interactions. As the outcomes of these interactions are more difficult to rationalize, the majority of the synthesis of these compounds has revolved around simply altering the molecules' substituents to cause changes in the molecular hyperpolarizability β and the crystal packing.

Among the most prominent groups of compounds taking advantage of this simple approach are substituted stilbenes. The extensive conjugation and donor-acceptor structure of these molecules has led to several compounds with large powder SHG efficiencies.[26,85,86] The most well-known stilbene, which continues to be the benchmark for SHG activity measured from powder with the laser wavelength of 1064 nm, is 3-methyl-4-methoxy-4'-nitrostilbene (MMONS), which has been reported to have the efficiency of up to 1250 times of urea.[85] Charge transfers excitons arising from the intermolecular π-π interactions have been suggested to be part of the reason behind the compound's high nonlinearity (Figure 14). An earlier study[26] before the discovery of MMONS had already presented a variety of stilbenes with high nonlinear activities, up to 300 times of urea, while also revealing the extensive polymorphism that the compounds tend to display.[26,87] As the weak dipole-dipole interactions are the main driving force behind the structures, any competing forces from e.g. crystallization solvents are more likely to make an impact. This can lead to an increase in the amount of different and potentially non-centrosymmetric structures.

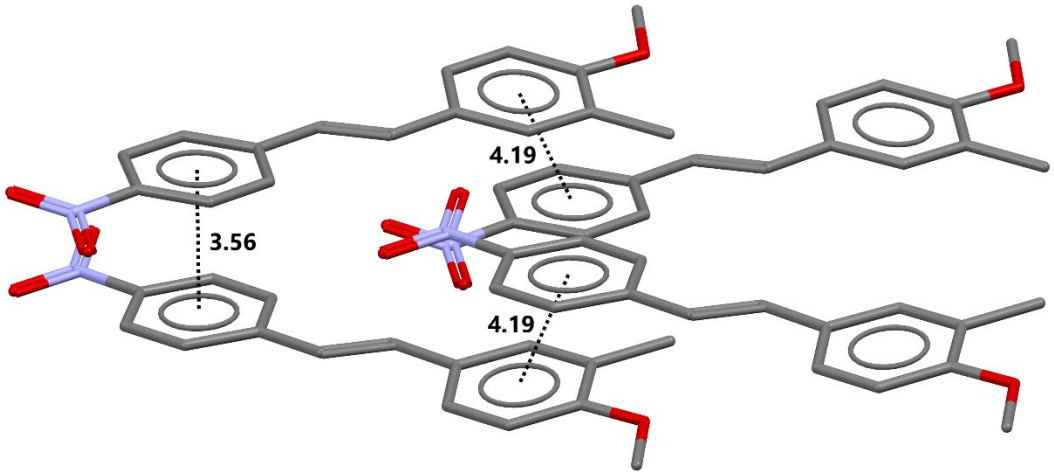

FIGURE 14 V-shaped packing of MMONS[87], showing the influence of π-π interactions (centroid-centroid distances in Å). Hydrogens have been removed for clarity.

Chalcones are another example of weakly interacting, diaromatic organic compounds that have been systematically studied[88–90] and found to exhibit notable SHG values. The compounds are structurally close to stilbenes, the only difference being an additional carbonyl group attached to the ethylene bridge between aromatic rings. The mid-chain oxygen can act as an electron acceptor of the whole molecule,[91] which is even more pronounced in certain long-chain 1,4-pentadiene-3-one derivatives.[92,93] The chalcones' strength is their wider transparency range compared to most conjugated organic compounds, which enables applications that require blue light transmittance of the material. In addition to mere substituent changes, greater structural modifications like switching one of the benzene rings into thiophene[89] or pyridine[94] as well as co-crystallization of different chalcones[95] have been reported as successful methods to synthesize novel compounds with increased second-order nonlinearity.

3 OPTICAL 3D PRINTING

Three-dimensional printing, sometimes called additive manufacturing, is a technique that has been commercially available for several decades. During that time, the variety of both different printing methods and their applications has kept growing. Traditionally, 3D printing has been used to create prototypes or objects for aesthetical or mechanical purposes, but recently researchers have discovered the unique possibilities it offers for scientific use. While most of the 3D printing materials do not have interesting chemical properties by nature, a variety of printing methods allow the inclusion of functional additives within the printing matrix and, consequently, the printed object. As a result, 3D printing techniques like powder-based Selective Laser Sintering (SLS) and extrusion-based Direct Ink Writing (DIW) have already found potential applications in e.g. metal scavenging[96,97] and electronics[98,99], respectively.

Stereolithography (SLA, Figure 15) is the oldest commercial 3D printing technique, first reported[100] in the early 1980s and eventually patented[101] in 1986. The method uses photopolymerizable resins, which are viscous liquids that usually consist of acrylate monomers, oligomers, and various additives. The building of the object begins when a UV laser beam excites the photoinitiator in the resin which, in turn, starts the polymerization reaction.[102] The object is then built in a layer-by-layer fashion, and the finished object is post-processed by washing the excess resin away before completing the interlayer polymerization by another UV light treatment. The main advantage of the stereolithographic method is the quality of printed objects, as it remains as one of the most accurate techniques in the market. Importantly, the method intrinsically allows the printing of transparent objects, which, combined with its high resolution, makes stereolithography a promising way of manufacturing objects for optical use.

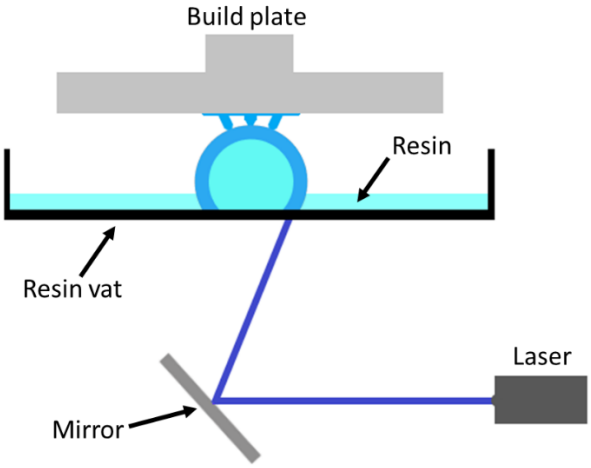

FIGURE 15 Schematic of a stereolithography 3D printing setup with "upside-down"-configuration, in which the build plate moves upwards after each printed layer.

Other techniques using transparent photopolymerizable resins have since been developed, e.g. digital light processing (DLP), which uses a digital light projector screen to cure an entire layer at a time, in contrast to the travelling laser beam in SLA. Another example of resin-based 3D printing are the various inkjet techniques, which in many ways operate similarly to extrusion-based printers but utilize UV-curable liquids instead of plastic filament.[103] The liquid resin is sprayed through a nozzle as hundreds of small droplets at a time and cured with a UV light source close to the printhead to form objects of high resolution and smooth surface finish.

3.1 3D printing of optical systems

Optical applications have been one of the more recent trends in the scientific use of 3D printing.[104,105] The near-limitless customizability offered by the techniques alongside the constantly improving quality of the printed objects has enabled the design of various optical objects from simple prisms and waveguides to more complex lens systems down to the micrometre scale.

The earliest 3D printed optical components were simple waveguides. Parker *et al.* used silk fibroin-based ink to print biocompatible waveguides via Direct Ink Writing (DIW). Although the ink wets and spreads on the substrate, leading to a non-circular cross-section, the printed objects were observed to function well.[106] Lorang *et al.* 3D printed waveguides with low optical loss by using the same printing method with UV-curable ink. The shape was kept ideal by using a custom printhead that allowed printing a fugitive hydrogel shell around the waveguide core, which successfully prevented it from wetting and spreading. After the core had been photopolymerized by a UV light source mounted next to the printhead, the supporting shell could be liquified and removed, allowing the repositioning of the printed waveguides (Figure 16).[107]

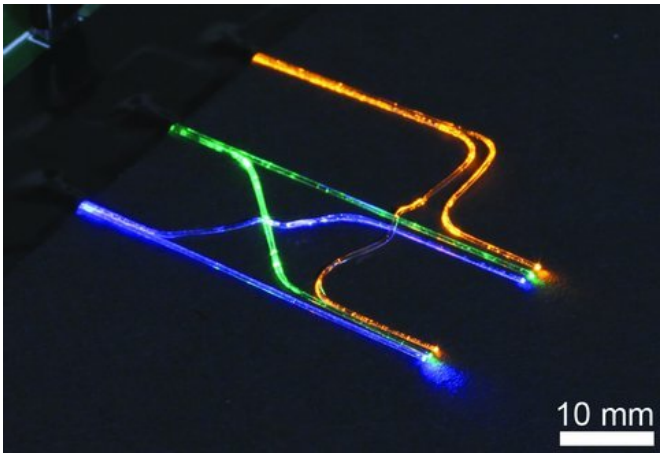

FIGURE 16 Optical waveguides printed from UV-curable ink, exhibiting minimal cross-talk between them. Reproduced from Lorang *et al.* with kind permission from John Wiley & Sons.[107]

Hinman *et al.* used the stereolithographic 3D printing method to fabricate custom prisms for biosensing of bacterial toxins. The surface roughness of the prisms after printing was highly variable, and therefore the objects were post-processed by wet sanding and polishing. One face of the smoothened prism was then coated with a thin layer of gold (50 nm) onto which a biomimetic lipid membrane was formed. The functionalized prism was successfully used in a cholera toxin biosensing experiment. To further prove the method's utility in optical detection, a dove prism was printed and the growth of gold nanoparticles on its surface was successfully monitored with UV-Vis spectroscopy.[108]

Direct laser writing (DLW) has been utilized as the 3D printing method to achieve micrometre-scale freeform optical systems.[109,110] The technique is based on two-photon absorption of photopolymerizable resins, which enables the exposure of extremely small volumes at a time and leads to the manufacturing of minuscule objects with unrivalled resolution. Other high-accuracy printing techniques based on photopolymerization have been reported by Sun *et al.*, who used micro-stereolithographic and micro-continuous liquid interface production (μCLIP) methods to print aspheric lenses.[111,112] While the techniques cannot quite reach DLW's sub-micrometre scale, they are significantly faster, with the latter technique allowing the printing of a 3 mm high lens in mere minutes.

3D printing has already found commercial success in the field of optics as ophthalmic lenses are being printed by using inkjet technology alongside photocurable resins. The patented process[113,114] deposits thousands of microdroplets of resin at the same time and allows them to spread and merge before UV curing, leading to exceptionally smooth surfaces.[115] The resulting lenses do not need additional post-processing and are therefore much faster to produce than via traditional methods. The utilization of 3D printing also allows easier integration of technology within the lenses, which can help in designing smart glasses. The next ophthalmic advancement could be 3D printing of contact lenses, and an initial study on the topic by using Digital Light Processing (DLP) as the printing method has already been reported.[116]

3.2 3D printing of optically functional objects

As evidenced by the previous chapter, 3D printing is emerging as a valuable tool for manufacturing objects for optical use. Moreover, multiple techniques allow the production of optical objects with additional functionality via mixing additives into the printing material. This approach was already used in the printing of the aforementioned silk waveguides. The silk fibroin ink was doped with rhodamine 6G-dye, and the resulting waveguides were shown to produce a yellow fluorescence emission.[106] By using the same DIW-printing method, two-component glass where one of the used silica inks was doped with gold nanoparticles has also been manufactured. The resulting red colour in the printed object remained throughout the post-processing.[117] In another glass-printing study, lanthanide salts were mixed into the printing material to fabricate an object where a specific part of the 3D printed boro-phospho-silicate glass object showed photoluminescent properties. Upon excitation with 980 nm infrared beam, blue light was emitted from the object due to the erbium and ytterbium ions within the structure (Figure 17).[118]

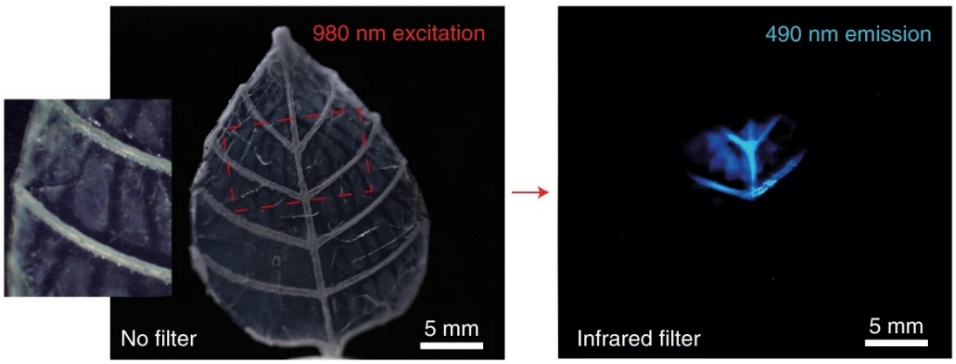

FIGURE 17 3D printed glass leaf with photoluminescent lanthanide-doped primary veins printed separately on top of the object. Adapted from Moore *et al.* with kind permission from Springer Nature.[118]

The aforementioned examples prove that the concept of optically functional additives within 3D printing materials works in practice, but is the method suited for nonlinear optics? Conventionally, the active components in NLO devices have been based on relatively large single crystals of the active material. However, as the Kurtz-Perry technique[16] demonstrates, it is possible to obtain nonlinear radiation from powderous materials despite their randomly oriented nature. Similarly, a more recent study[119,120] found that a polycrystalline material can create relatively efficient nonlinear radiation despite the random orientation of different crystalline regions, outperforming the phase-mismatched single crystals. The radiation was also found to grow in intensity with increasing thickness of the sample due to the random quasi-phase-matching of individual crystalline domains. These observations suggest a potential new way of designing NLO devices, as well as opening the door for the use of non-phase-

matchable materials which has not been possible with any single-crystal-based approach.

The concept of using powder-like NLO active materials as additives to give an object SHG properties has been proven to work in several distinct studies. Ferroelectric NLO active compounds have been used as nanocrystal additives with a hot press technique[121] as well as microparticles within aerogels and xerogels[122] to create composite materials with SHG properties. Optically active crystallites have also been precipitated within glass-ceramics with equal success.[123] These findings suggest that using microcrystalline NLO active materials as an additive in 3D printing is a tantalising prospect, which remains virtually unexplored to date.

All in all, 3D printing has shown real promise in the field of optics and a range of techniques have been successfully utilized to manufacture objects of varied size and complexity. The methods' undeniable strengths lie in the customizability of the objects as well as the printing material itself. Table 1 summarizes some of the key features of the different 3D printing methods used in the examples mentioned in Chapters 3.1 and 3.2.

TABLE 1 The main properties of different manufacturing techniques used in 3D printing of objects for optical use.

	Vat photo-polymerization	**Ink extrusion**	**Material jetting**	**Two-photon polymerization**
Techniques[A]	SLA, DLP, CLIP	DIW	MJM, DoD	DLW
Layer height (μm)	25-100[B] 5[C], 111	100-400[B] 5[C], 106	16-32[B] ~4.1[C], 115	Down to 0.1[B]
Use of multiple materials at once	Not possible	Inherently possible	Inherently possible	Possible
Additive introduction	Possible	Possible	Not possible	Not possible
Pros	Easy to use Inexpensive	Wide range of materials can be used	Excellent surface quality	Exceptional resolution
Cons	Limited to a single material	Needs optimization and post-processing	Expensive	Very expensive Slow for macroscopic printing

[A] SLA: Stereolithography, DLP: Direct Light Processing, CLIP: Continuous Liquid Interface Production, DIW: Direct Ink Writing, MJM: MultiJet Modeling, DoD: Drop-on-Demand, DLW: Direct Laser Writing
[B] Typical values for the technique
[C] Lowest reported values

4 RESULTS AND DISCUSSION

This section goes through the work reported in papers **I-III** and discusses the results, key findings, and their implications. The discussion begins with the noncovalent interaction studies with halogen bonding in paper **II**, continues with structural modification studies of highly NLO active materials in paper **III**, and concludes with a novel optical 3D printing application for NLO materials in paper **I**.

4.1 Halogen bonding interactions between 4-aminopyridine and di- or interhalogens[II]

The motivation for the study in paper **II** was to investigate the use of halogen bonding in building NLO active materials. The study consisted of a series of reactions between 4-aminopyridine, a compound capable of forming both hydrogen and halogen bonds, and four di- and interhalogens in a 1:1 molar ratio. The reaction with iodine was later repeated in a 2:1 ratio based on the products and analysis results of the initial reaction. All reactions were carried out in air at room temperature. In general, 1 mmol of each reactant was dissolved in dichloromethane, and the halogen solution was added dropwise in the 4-aminopyridine solution. The reaction mixtures were stirred for 2 hours, after which the solution was decanted off and the precipitates formed during the reactions were dried under vacuum. The resulting compounds are shown in Figure 18 below.

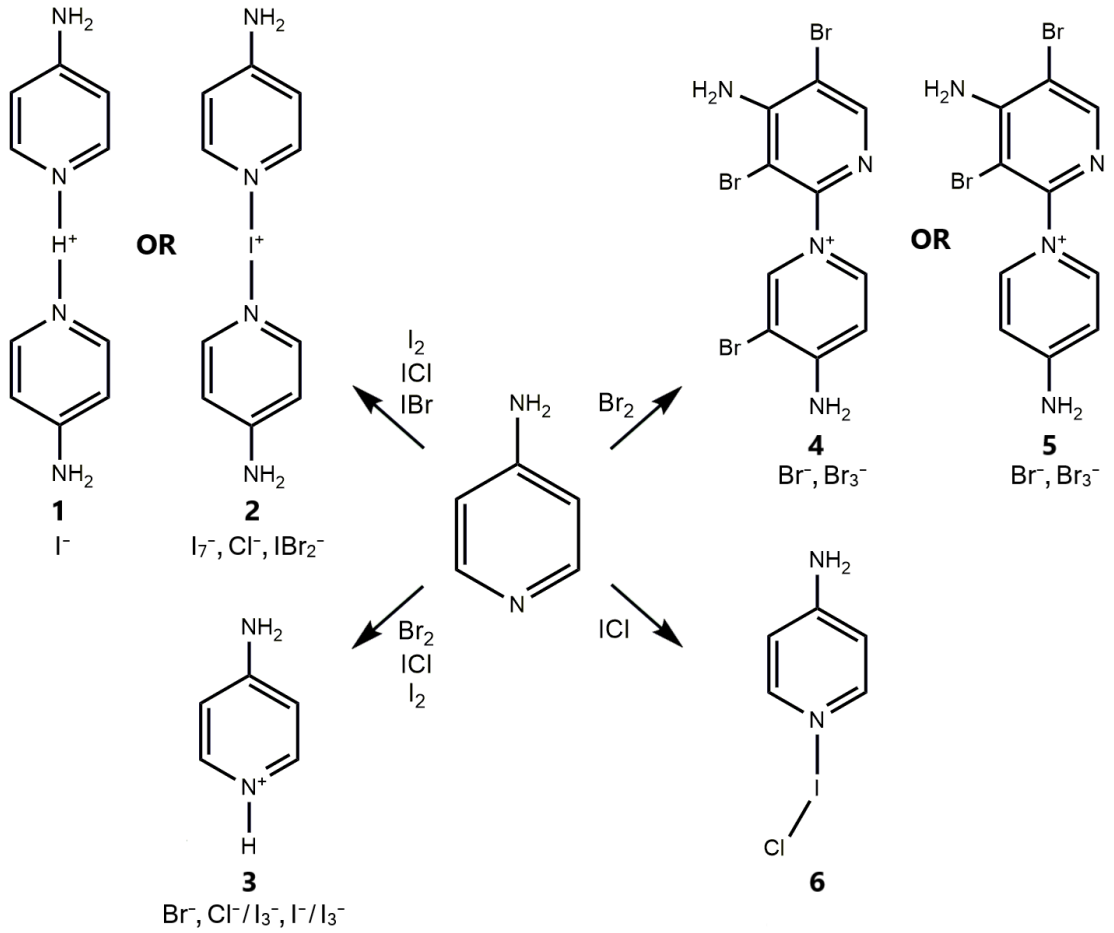

FIGURE 18 The cationic and neutral moieties **1-6** resulting from the 4-aminopyridine reactions with four di- and interhalogens.

Crystallizations from the two iodine reactions afforded three different structures (**1**-**3**), as did the iodine monochloride reaction (**2**, **3**, and **6**). Iodine monobromide formed only one structure (**2**) which crystallized in two different polymorphs, whereas bromine led to a total of four brominated pyridyl-pyridinium structures (**4**-**5**) in addition to a simple protonated pyridine structure (**3**). Expectedly, a variety of counteranions was observed.

In the reactions with iodine, both cation-bridged bis(pyridine) units **1** and **2** as well as protonated, single aminopyridine units **3** were observed as products. The protonated structures were obtained from crystallizations of the product of the reaction in 1:1 molar ratio, whereas the 2:1 ratio afforded the iodonium-bridged moiety **2**. The bridging hydrogen of **1** appears to be unequally shared between the pyridines, unlike the iodonium ions of **2** in virtually all studied compounds. The hydrogen bridge is also more bent compared to the iodine bridges in this study (Figure 19). Whereas hydrogen bonding between amines and iodides is strongly affecting the crystal structure in $\mathbf{1} \cdot I^-$, only much weaker hydrogen bonding is evident in $\mathbf{2} \cdot I_7^-$. The polyiodides of the latter structure form two-dimensional networks, and the bis(pyridine) units **2** are located at the cavities of these structures with a slight tilt in respect to the plane of anions that allows them to interact with two polyiodide layers. The bis(pyridine) units form

skewed stacks with long centroid ⋯ centroid distances (4.50 Å). The third compound $\mathbf{3_2} \cdot I^- \cdot I_3^-$, in turn, consists of protonated pyridines stacking with very short centroid ⋯ centroid distances (ranging from 3.48 to 3.68 Å). All four unique pyridines are oriented slightly differently, and the anions arrange vertically around the pyridine stacks in six chains with alternating I^- and I_3^- anions.[124]

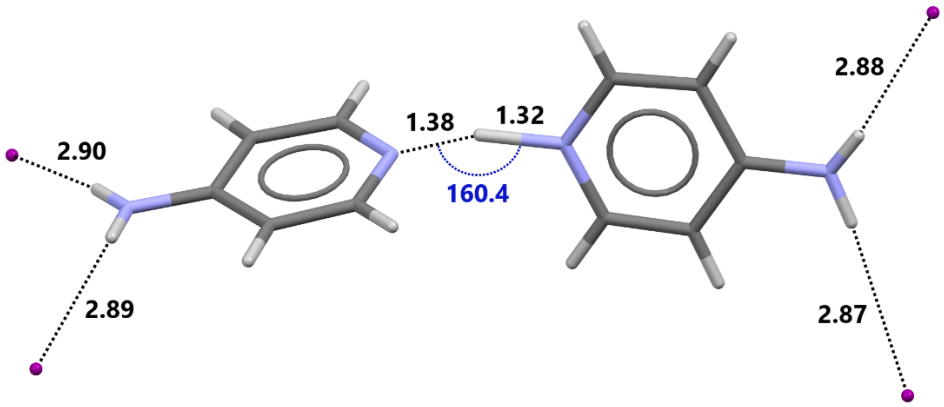

FIGURE 19 N ⋯ H⁺ ⋯ N contact parameters and hydrogen bonding distances (in Å) between amine groups and iodide anions in $\mathbf{1} \cdot I^-$.

In the reaction with iodine monochloride, the two-pyridine, N ⋯ I⁺ ⋯ N-bridged moiety with chlorine as the counterion ($\mathbf{2} \cdot Cl^-$) was expectedly observed as one of the products. However, another structure with a charge-transfer adduct of the reactants (**6**) in the same crystal lattice alongside the bridged moiety in equimolar ratio was also found. This curious compound is the first reported structure where the two different moieties coexist within the same crystal structure, and it is likely to be a reaction intermediate with pure $\mathbf{2} \cdot Cl^-$ as the final product. As a distinctive feature, the iodine-bridged pyridines (**2**) of the adduct-containing structure are nearly perpendicularly aligned, in stark contrast to the nearly planar alignment of pure $\mathbf{2} \cdot Cl^-$ (Figure 20). In addition to these two products, the crystallizations afforded a third structure with a protonated pyridine **3** where the interhalogen has broken apart to form chloride and triiodide counteranions. The compound $\mathbf{3_2} \cdot Cl^- \cdot I_3^-$ forms similar anion-surrounded pyridine stacks than $\mathbf{3_2} \cdot I^- \cdot I_3^-$ as could be expected from the analogous chemical composition. The packing of the pyridine units in $\mathbf{3_2} \cdot Cl^- \cdot I_3^-$ is even closer than in the iodine product (centroid-centroid distances ranging from 3.42 to 3.63 Å). As a common feature in all three ICl-structures, the amino groups of 4-aminopyridine interact with chloride anions via hydrogen bonding.

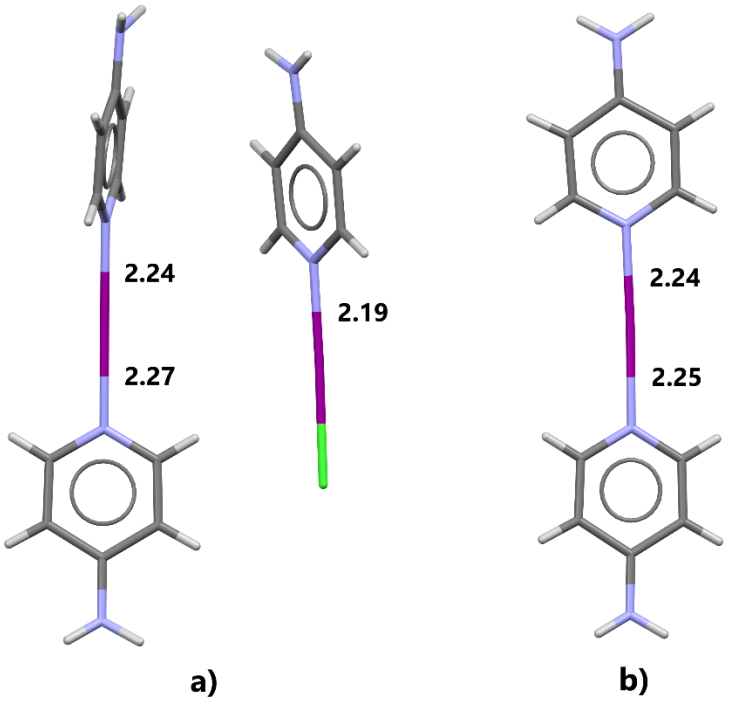

FIGURE 20 N···I⁺ contact lengths (in Å) and structural differences between the iodonium-bridged bis(pyridine) units in a) the adduct of **2** · Cl^- and **6**, and b) pure **2** · Cl^-. Counteranions have been omitted for clarity.

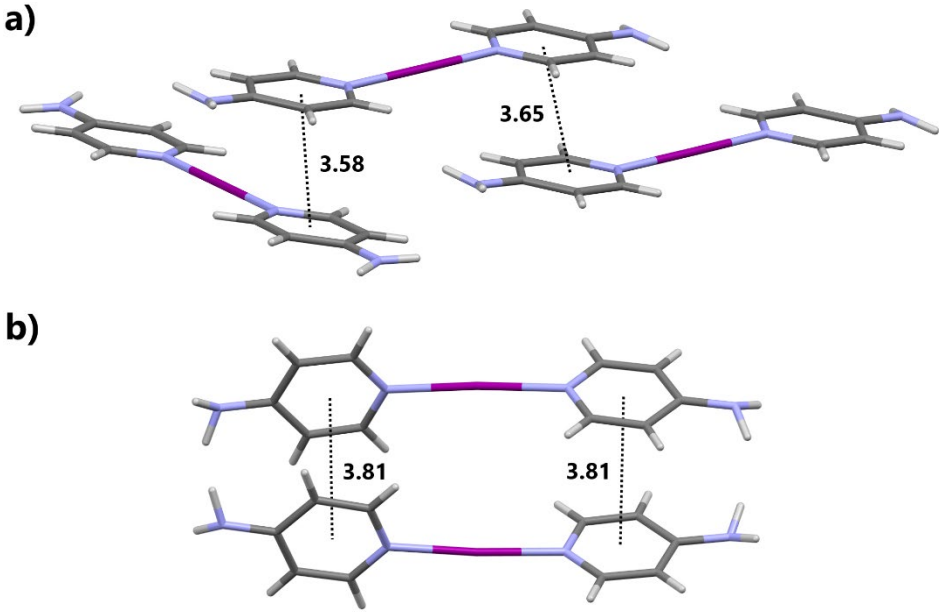

FIGURE 21 Stacking of the bis(pyridine) units (centroid-centroid distances in Å) in the a) monoclinic and b) orthorhombic polymorphs of **2** · IBr_2^-.

The reaction with iodine monobromide, despite the close relation to the aforementioned ICl, only produced two polymorphs of the iodonium-bridged bis(pyridine) **2** with IBr_2^- as the counteranion. The bridged moieties arrange very differently in their respective monoclinic and orthorhombic crystal lattices. The former has a layered structure with very planar units of **2**, whereas the latter

exhibits similar perpendicularity to **2** · Cl^- of the ICl-structure with adduct **6** (Figure 21). Both structures are also clearly influenced by π-π-interactions, with the planar monoclinic polymorph having a more significant contribution and the shortest centroid-centroid distance of all compounds which include the iodine-bridged bis(pyridine) cation **2**.

The reaction with bromine afforded the most products of all investigated halogens due to its unique behaviour compared to the other three reagents. In addition to forming a disordered dichloromethane solvate of a protonated pyridine structure (**3** · Br^-) much like the respective reactions with ICl and I_2 also afforded, Br_2 continued to brominate the product in a reaction which also formed a new covalent bond between two pyridines. All in all, this resulted in the formation of two tribrominated (**4**) and two dibrominated (**5**) pyridyl-pyridinium structures with either bromide or tribromide as the counteranion. All brominations took place at meta-positions of the pyridine rings, and all four compounds have a strong tilt between the aromatic rings (possibly) due to the additional steric factors caused by the bromines. Unlike all other structures in the study, **4** · Br^- includes water in its crystal lattice, forming an infinite amine ⋯ anion ⋯ water hydrogen bonding synthon. Its tribromide congener **4** · Br_3^-, in turn, has the most halogen bonding interactions of the structures with all three bromines of the pyridyl-pyridine unit in close contact with another bromine (Figure 22). The structure **5** · Br^- is affected by multiple interactions, including C-H ⋯ C_π contacts which are less pronounced or not present in the other three structures. **5** · Br_3^- displays the smallest tilt between the pyridyl-pyridinium's rings as well as the strongest π-π interactions between the molecules.

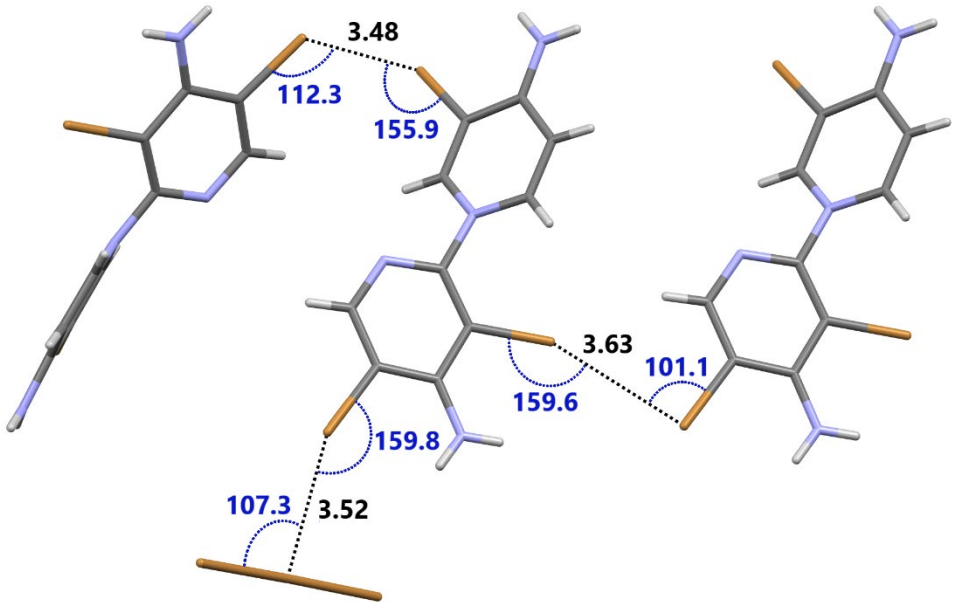

FIGURE 22 The three unique halogen ⋯ halogen contacts of **4** · Br_3^- (in Å).

In summary, all reactions with iodine-containing di- and interhalogens led to the formation of iodonium-bridged bis(pyridine) compounds. Protonated 4-

aminopyridine units were also obtained from multiple reactions, with one of them leading to the formation of an asymmetric N···H$^+$···N bridge. In contrast to all other halogen reactants, the reaction with bromine resulted in a variety of complex bromination-dimerization products, indicating greater reactivity towards pyridine derivatives. Iodine monochloride was the sole reactant to form a neutral charge-transfer adduct (**6**), although the structure also contained the iodonium-bridged **2**$\cdot$ Cl$^-$ in its crystal lattice which suggests that the peculiar product could be a reaction intermediate of sorts.

In most structures obtained from the reactions, the amine··· pyridine hydrogen bond synthon prevalent in pure 4-aminopyridine was blocked by either protonation or iodination of the pyridine nitrogen. The exceptions to this trend were the bromine products, where the pyridyl-pyridiniums formed hydrogen bonds in three different structures. In all other structures, the amines formed hydrogen bonds with the anions, and these interactions in combination with π-π-stacking had a major role in the crystallization of the compounds. Nevertheless, all obtained structures were centrosymmetric and consequently, the compounds were unable to generate the second harmonic.

4.2 Nonlinear optical properties of diaromatic stilbene derivatives[III]

For paper **III**, a total of 11 stilbene derivatives were synthesized via Horner-Wadsworth-Emmons[125] reaction, where a phosphonate carbanion reacts with an aldehyde in the presence of a strong base to produce alkenes (Figure 23). All reactions were carried out in air at room temperature. In general, 1 mmol of each reactant (an aldehyde and diethyl(4-nitrobenzyl)phosphonate) was dissolved in ethanol, and 3 mL of 1.5 M sodium hydroxide solution was added. The addition of the strong base led to a change of the solutions' colour in every reaction, as well as to partial precipitation of the product. The mixtures were stirred overnight to verify the completeness of the reactions. The precipitates were then filtered, washed, and dried, and successful reactions were confirmed by NMR and single-crystal x-ray diffraction measurements.

Each synthesized molecule was designed to have a highly conjugated dipolar structure with 4-nitrobenzene acting as the electron acceptor for all eleven compounds. As computational studies on similar molecules had suggested an improvement in molecular nonlinearity with longer chain length between the aromatic moieties[126] or the inclusion of thiophene[127], these structural modifications were investigated with compounds **8a**-**8c** and **9a**-**9c**, respectively (Figure 23).

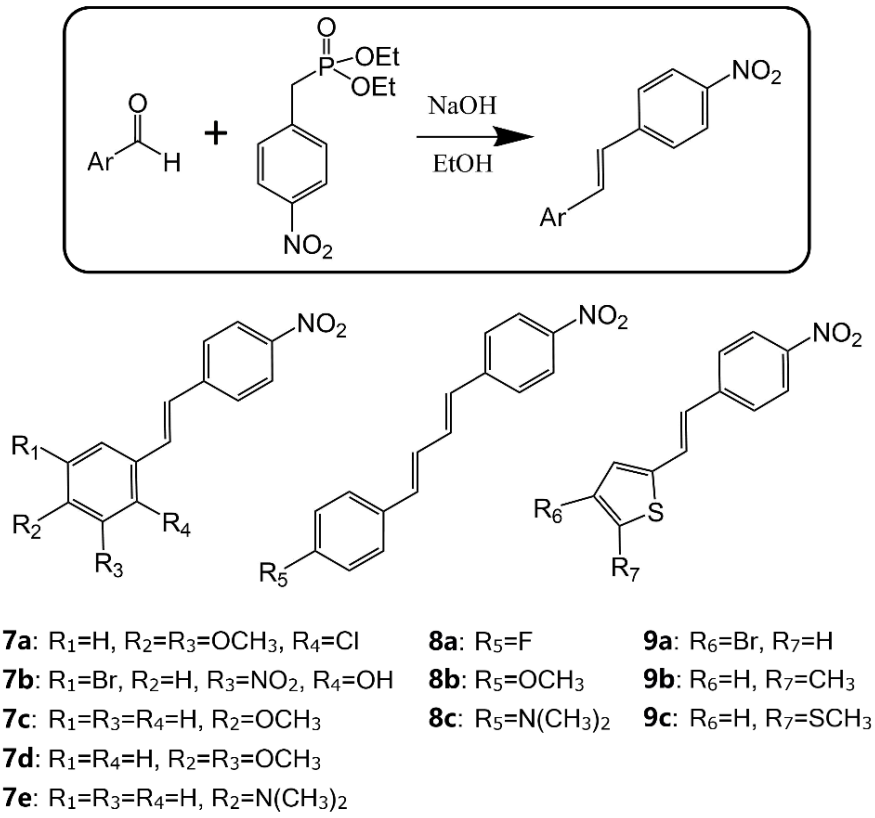

7a: R_1=H, R_2=R_3=OCH_3, R_4=Cl
7b: R_1=Br, R_2=H, R_3=NO_2, R_4=OH
7c: R_1=R_3=R_4=H, R_2=OCH_3
7d: R_1=R_4=H, R_2=R_3=OCH_3
7e: R_1=R_3=R_4=H, R_2=$N(CH_3)_2$

8a: R_5=F
8b: R_5=OCH_3
8c: R_5=$N(CH_3)_2$

9a: R_6=Br, R_7=H
9b: R_6=H, R_7=CH_3
9c: R_6=H, R_7=SCH_3

FIGURE 23 The general Horner-Wadsworth-Emmons[125] reaction used in the syntheses of substituted stilbenes, and the eleven obtained products **7**-**9**.

The synthesized compounds included five 4′-nitrostilbenes with variable substituents on the electron donor end of the molecule (**7a**-**7e**). Compound **7a** proved to be the most interesting of them as it afforded various crystal structures. In addition to non-centrosymmetric and centrosymmetric polymorphs of **7a**, the compound's presumed photodimerization during crystallization led to the formation of a cyclobutane derivative. Both polymorphs of the main product form herringbone layers through π-π interactions, with the centrosymmetric variant displaying a significantly shorter centroid-centroid distance. The crystal structure of compound **7b** bears resemblance to the non-centrosymmetric polymorph of **7a** (Figure 24), but with a stronger tilt between the aromatic rings. While the aforementioned structures were clearly influenced by π-π-interactions, their role in the methoxy-substituted **7c** and **7d** is far less evident. The former compound is instead mostly held together with weak C-H ⋯ O contacts, while the latter displays slightly stronger dimeric $OCH_3 \cdots OCH_3$ contacts as its main synthon. The methoxy-substituted **7c** is very planar whereas the dimethoxy-substituted **7d** has a more heavily tilted structure. The intensively red and disordered **7e** also lacked π-π contacts as it displays no overlap of the aromatic rings due to the different orientations of adjacent planes. Instead, the structure's main synthon is the weak cyclic $N(CH_3)_2 \cdots O_2N$ contact.

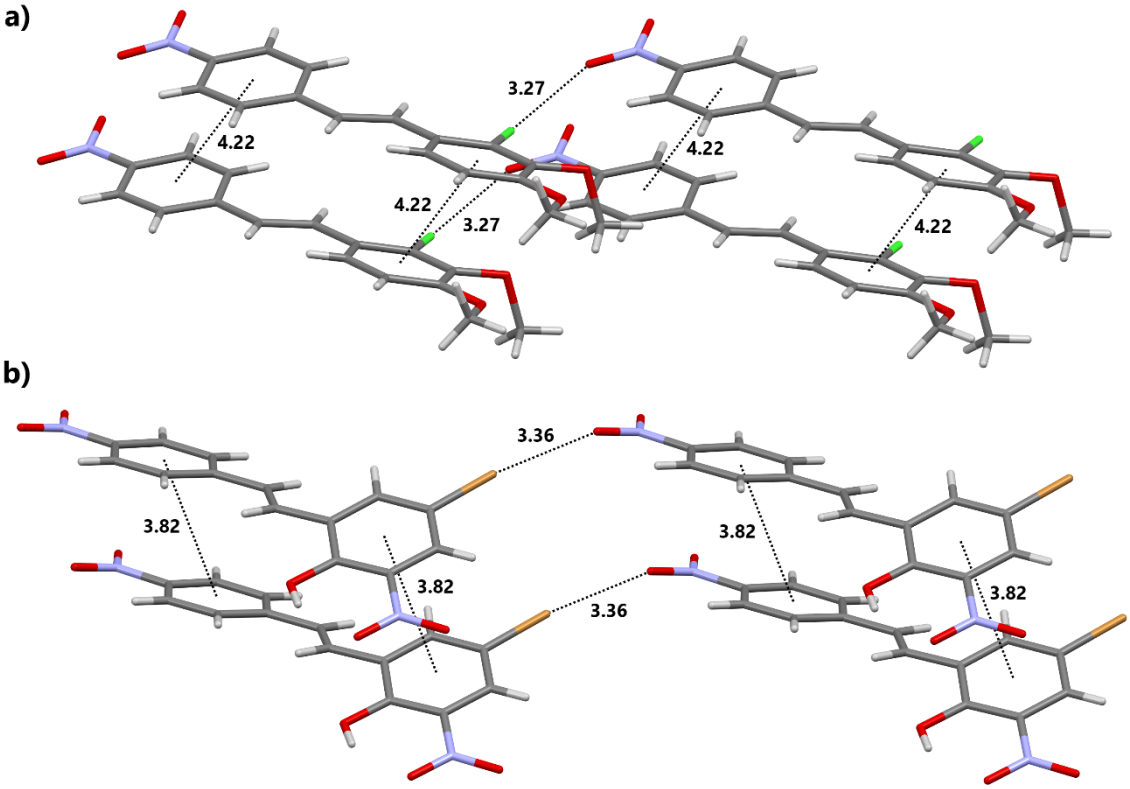

FIGURE 24 Weak ONO···X contacts and π-π interactions (in Å) in the crystal structures of a) non-centrosymmetric polymorph of **7a** and b) **7b**. The centrosymmetric polymorph of **7a** does not exhibit the same halogen contact but displays even shorter centroid-centroid distances.

The first tested structural alteration on the stilbene core was the elongation of the ethylene bridge between the aromatic rings, leading to three diphenylbutadienes **8a**-**8c**. The crystal structure determined for **8a** was heavily disordered despite several crystallizations and data collections, but indication of noncovalent interactions can still be seen from the structure, nonetheless. The compound displays V-shaped stacks, formed by weak C-H···O contacts and π-π interactions (Figure 25), which arrange into herringbone layers despite seemingly having no interactions between adjacent stacks. The previously reported[128,129] compounds **8b** and **8c** were synthesized to compare them with the similarly substituted stilbenes **7c** and **7e**. From the two compound pairs, the dimethylamino-substituted **8c** and **7e** exhibit rather similar features like the dimeric weak $N(CH_3)_2 \cdots O_2N$ contacts and the apparent lack of π-π-interactions. On the contrary, the differences between **8b** and **7c** are more pronounced. Although both structures exhibit $OCH_3 \cdots O_2N$ contacts, **8b** forms a planar sheet-like structure which has clear contributions from π-π interactions whereas **7c** crystallizes in two almost perpendicular planes with a lesser amount of π-π contribution.

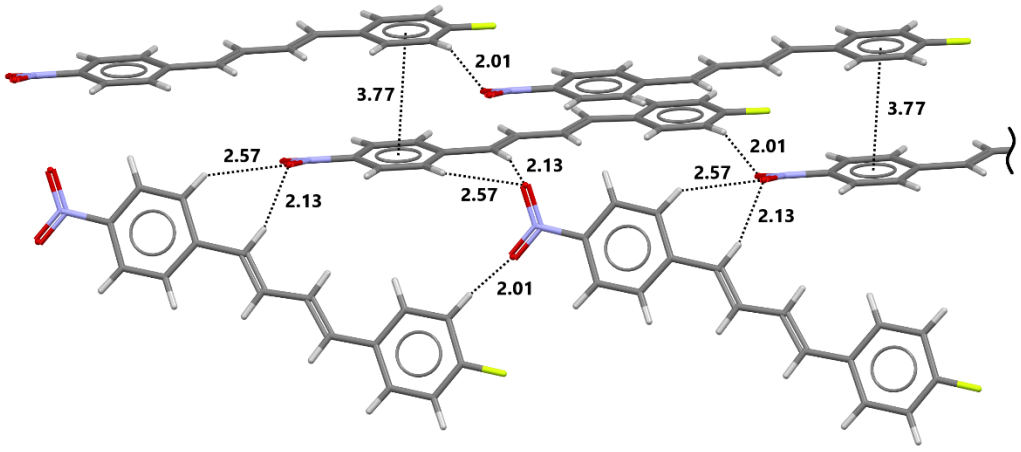

FIGURE 25 The weak C-H ⋯ O contacts and π-π interactions (in Å) in the crystal structure of the non-centrosymmetric **8a**. Disorder has been removed for clarity.

The second modification to the stilbene core was switching one of the benzene rings into thiophene, leading to three phenylethenylthiophenes **9a-9c**. Compound **9a** crystallized in two centrosymmetric polymorphs. The monoclinic variant forms a rather planar, sheet-like structure whereas the orthorhombic polymorph is more complex with molecules located in four different planes. Both polymorphs display a bromine ⋯ nitro halogen bond (Figure 26), with the orthorhombic contact being slightly shorter and its angle closer to 180°. Both structures also show π-π interactions between thiophene and benzene rings. Compound **9b** forms non-planar chains through weak $CH_3 \cdots O_2N$ contacts and lacks any real π-π interactions due to the alternating orientation of molecules, instead showing signs of C-H ⋯ C_π contacts. Analogously, compound **9c** forms herringbone chains through weak $SCH_3 \cdots O_2N$ contacts. These chains form two-dimensional buckled sheets, which interact with each other via π-π interactions.

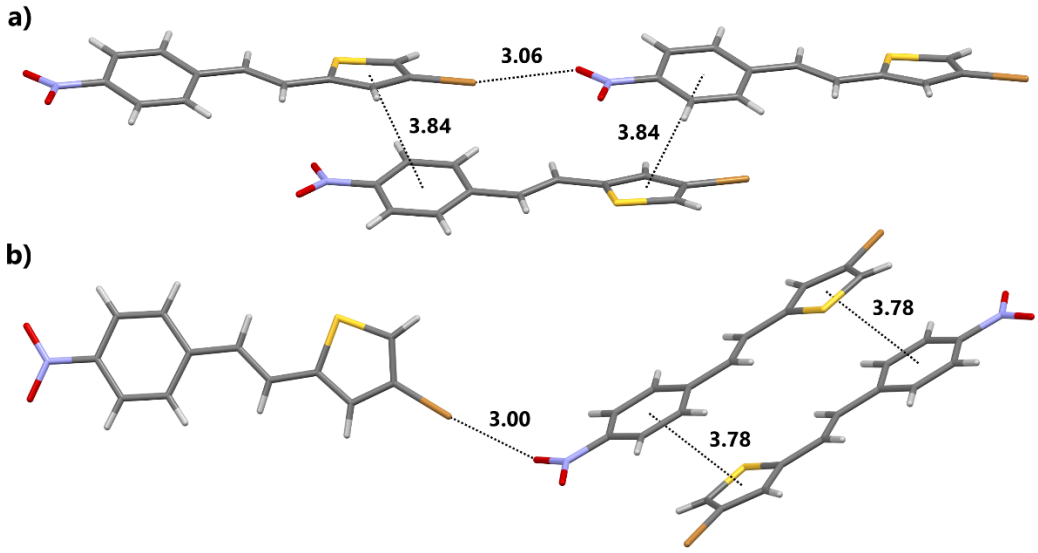

FIGURE 26 The ONO ⋯Br contacts and π-π interactions (in Å) in the crystal structures of a) monoclinic **9a** and b) orthorhombic **9a**.

Before the nonlinear optical measurements using the Kurtz-Perry technique, the crystalline samples were ground and sieved to a specific powder size, usually <125 µm. The powder samples were then packed within thin glass capillary tubes which had been sealed from the bottom with wax. A laser beam was focused on the capillaries, and the second harmonic generated by each respective sample was collected with a CCD detector. The intensities were then compared with similarly prepared and measured reference samples from urea and 3-methyl-4-methoxy-4'-nitrostilbene (MMONS), to get the relative SHG efficiencies of each compound.

Only some of the synthesized compounds proved to be useful for SHG as most compounds crystallized in centrosymmetric space groups, preventing the possibility for second-order nonlinear properties. All in all, three compounds displayed detectable SHG activity. Stilbene **7b** and the heavily disordered diphenylbutadiene **8a** produced SHG signals that were noticeably weaker than that of the reference urea sample, whereas the signal from the non-centrosymmetric polymorph of **7a** was significantly more intensive than urea's (Table 2).

Due to the weakness of MMONS's second harmonic signal compared to the literature values[85] as well as potential fluorescence of **7a** in the measurements with a femtosecond laser at 1030 nm, the experiment was repeated with a nanosecond laser at both 1030 nm and 1060 nm. For **7a**, the respective measurements using 1030 nm wavelength produced similar intensities, up to almost 8 times higher second harmonic efficiency than urea, whereas the switch to 1060 nm more than quadrupled the efficiency (Figure 27). MMONS, in turn, did not show such drastic changes with the alteration of measurement wavelength, but instead with the switch from femtosecond to nanosecond laser.

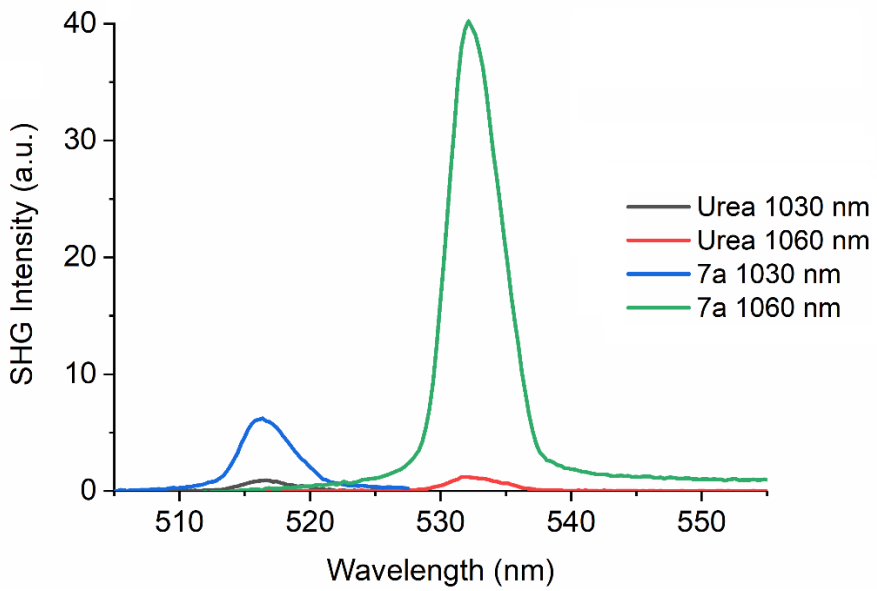

FIGURE 27 Kurtz-Perry SHG measurement results of the non-centrosymmetric polymorph of **7a** and the urea reference with 1030 nm fundamental laser wavelength compared to the same samples measured with 1060 nm wavelength.

TABLE 2 Kurtz-Perry SHG measurement results for all stilbene derivatives from which nonlinear optical activity was observed.

Sample	Laser wavelength (nm)	SHG activity (x urea)
MMONS	1030[a]	61.0
	1030[b]	205
	1060[b]	210
7a-nc	1030[a]	5.5
	1030[b]	7.7
	1060[b]	32.4
7b	1030[a]	0.04
8a	1030[a]	0.18

a femtosecond laser
b nanosecond laser

In addition to the NLO properties, the absorption and fluorescence spectra of the synthesized compounds were also measured. In the absorption studies with UV/Vis spectroscopy, most products displayed two absorption maxima in dichloromethane, with stilbene **7b** being the only compound to have three maxima instead. The strongest absorption maximum of each compound was generally found between 350-400 nm. Dimethylamino-substituted **7e** and **8c** were the clear outliers of the series as both of them had a maximum at around 450 nm. The donor's effect on the transparency of the crystal was evident as the absorption maxima showed a general red shift with the increasing electron donor nature of the substituents. Similar shifting can also be observed from the results of the fluorescence measurements, where every synthesized compound apart from **7b** exhibited fluorescence in dichloromethane.

As a summary, several of the eleven synthesized diaromatic compounds crystallized only in centrosymmetric structures which are fundamentally unable to exhibit the second-order nonlinearity. These included most of the compounds where modifications to the stilbene core were made (**8b**-**9c**), and therefore the changes' impact on the compounds' nonlinearity could not be properly evaluated with Kurtz-Perry measurements. Nevertheless, the study also afforded three novel SHG active compounds, the best of which (**7a**) reached a high powder SHG efficiency of over 32 times of urea.

4.3 3D printing of NLO active lenses with stereolithography[I]

Lastly, the possibility for using optically active materials as functional additives within a 3D printed polyacrylate matrix was investigated in paper **I**. Stereolithography was selected as the printing technique due to the possibility of producing transparent objects, a natural prerequisite for optical use, as well as the ease of additive introduction to the printing material.

Before printing, five round and flat lenses with a diameter of 2 cm were modelled using a CAD (computer-aided design) program. The thicknesses of the lenses were evenly spaced, ranging from 300 to 1500 µm. The CAD design file was then further processed with a slicer program to cut the modelled object into layers of determined height (50 µm) and give G-Code files that are readable by the 3D printer. This general workflow is visualized in Figure 28.

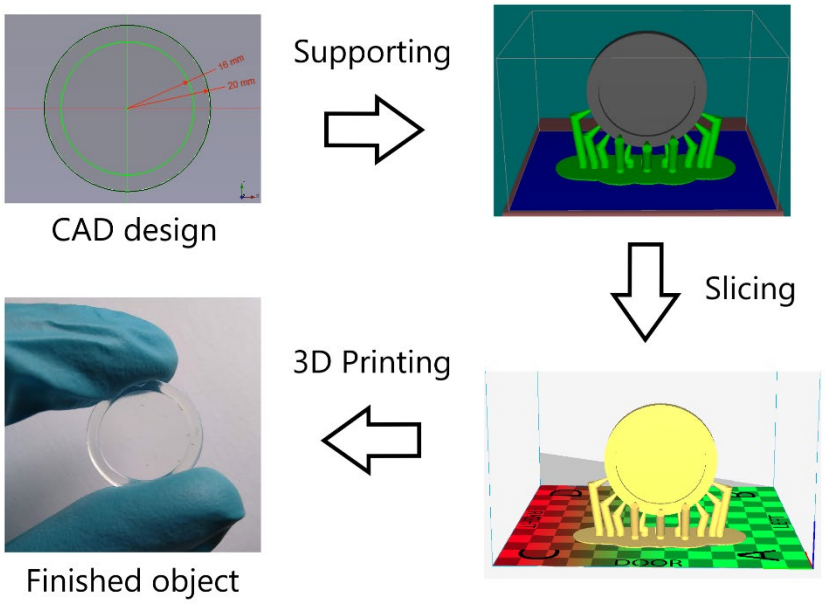

FIGURE 28 Schematic of the general workflow of 3D printing.

Urea and potassium dihydrogen phosphate (KDP), both commonly used as reference materials in Kurtz-Perry SHG measurements, were selected as the NLO active materials to be used in the lenses. The crystalline materials were ground and sieved to a crystal size of <125 µm as in the case of Kurtz-Perry measurements. The powdered material was then weighed and mixed with a predetermined amount (usually around 55 mL in volume) of polyacrylate-based resin meant for stereolithographic 3D printing to give mixtures containing a known weight percentage of the active materials. After some initial testing with varied amounts of the SHG active materials as additives in the resin, 5 w-% mixtures of both additives were chosen for 3D printing experiments. The respective mixtures were carefully stirred until a homogeneous blend was obtained, poured into a resin vat, and used to print the lenses. To eliminate all additional variables, all five lenses of each series were printed simultaneously.

After the printing had finished, the objects were still covered in unpolymerized resin mixture which was washed away with a series of rinses with ethanol and water. After the objects had been washed and dried, the polymerization between the objects' layers was completed by another UV light treatment. Finally, a layer of sprayed lacquer was added onto the lenses to improve their transparency.

Uniform spread and crystallinity of the NLO active materials within the lenses were confirmed by an optical microscope (Figure 29). To confirm the

resin's suitability for optical printing, the printed polymer's transparency was studied with UV/Vis spectroscopy. The resulting cut-off wavelength of around 420 nm suggests that while the material is not suitable for deep UV applications, most organic compounds have higher transparency limits due to their inherent absorption and thus the 3D printed polymer matrix would not negatively affect their optical usability.

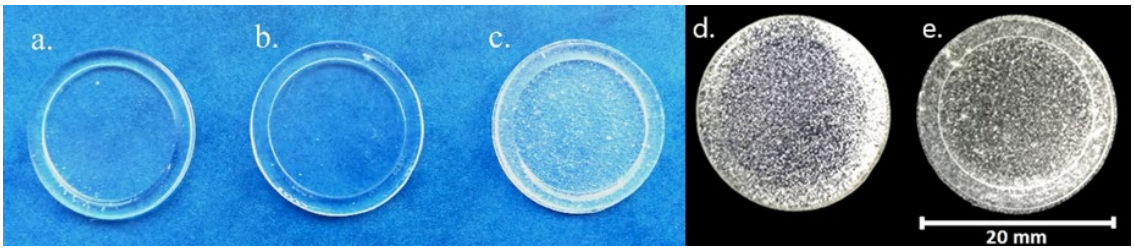

FIGURE 29 Image of the 300 µm thick 3D printed lenses (blue background) and as seen through an optical microscope (black background). Lens a. is a reference without any NLO component, b. and d. contain KDP, and c. and e. were printed with urea. Reproduced with kind permission from the American Chemical Society.[I]

For the measurements of the lenses' nonlinear activity, a setup similar to the Kurtz-Perry method was used, but instead of the powder sample, the laser was now aimed at the centre of the lens. In addition, a relatively wide laser beam size was used to get an average over a larger area of the lens to avoid misleading results by merely hitting individual crystals within the printed object. The SHG intensities were measured as an accumulation of 10 consecutive pulses, and a ten times longer exposure time was used for KDP lenses due to its inherent weakness compared to urea. In both KDP and urea's case, the SHG intensity produced by the lenses increased with the increasing thickness of the object (Figure 30). Especially KDP displays a very linear growth of second harmonic intensity. The results suggest that the additional amount of active material within the printed objects is enough to overcome the decreasing transparency and other issues caused by the increasing thickness of the lens, although urea shows signs of starting to even out at 1500 µm. However, the results cannot be generalized outside this particular additive weight percentage and further investigations would be required to draw broader conclusions.

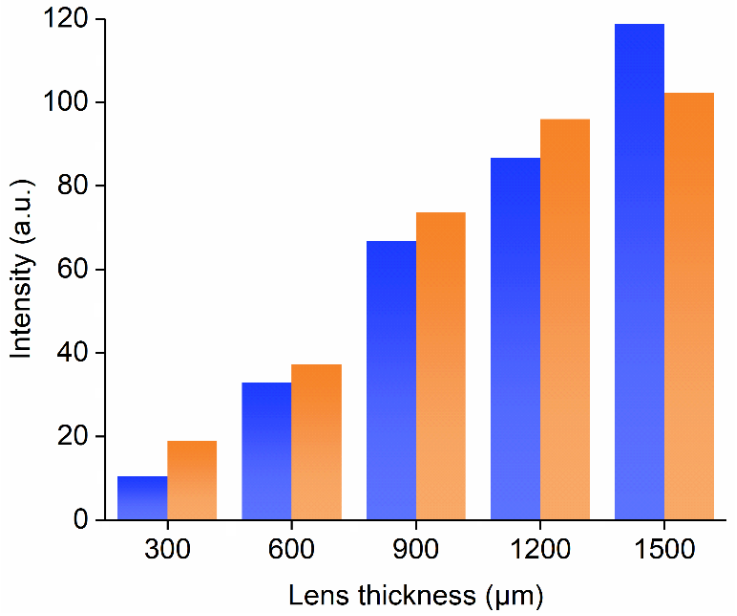

FIGURE 30 SHG measurement results of KDP (blue) and urea (orange) containing lenses. A laser wavelength of 1195 nm was used throughout the measurements.

Nevertheless, the results show that stereolithography can be used as an alternative way of manufacturing optically active lenses from materials that are tedious to crystallize in larger sizes or sparingly available. The technique also allows the design of shapes which would be near impossible to manufacture with conventional optical methods. Furthermore, the technique comes with inherent protection of the active materials from potentially disadvantageous environmental factors like moisture.

SUMMARY

The work in this thesis consists of series of studies with the common goal of synthesizing novel nonlinearly optically active compounds for second harmonic generation applications. Weak interactions were studied as a potential tool for obtaining non-centrosymmetric crystal structures, and novel ways of utilizing already existing NLO active materials with 3D printing were explored.

Firstly, several di- and interhalogens' ability to guide 4-aminopyridines towards non-centrosymmetric structures by halogen bonding was investigated. The studied compounds were observed to show a tendency towards the formation of iodonium-bridged bis(pyridine) cations or protonation of the pyridine nitrogen. Bromine was observed to have unique reactivity among the studied halogen compounds as it formed several dimerized and brominated structures. All in all, only centrosymmetric structures guided by hydrogen bonding and π-π interactions were observed. The chemistry of the di- and interhalogens was found to be versatile but poorly predictable, and as such, they are not the best choice to use for the synthesis of NLO active materials.

Substituted stilbenes have provided some of the highest second-order nonlinearities measured to date and therefore remain as one of the compound groups of interest in the field of nonlinear optics. In this work, the impact of both substituent changes and larger structural modifications on the stilbenes' nonlinear optical properties were investigated. While the synthesized diphenylbutadiene and phenylethenylthiophene derivatives did not show considerable SHG activity due to their mostly centrosymmetric crystal structures, a novel stilbene compound reached the second harmonic intensity of over 32 times of urea at 1060 nm. Overall, the results further evidenced that the stilbenes' molecular orientations within their crystal structures are hard to predict or control due to the weaker noncovalent van der Waals and π-π interactions acting as the primary driving force of these structures. In the future, having better structural control over the highly conjugated molecules through stronger and directional noncovalent interactions could result in the rationalized synthesis of NLO materials with even greater nonlinearities.

In the past decade, the scientific use of 3D printing has evolved from a mere curiosity into a high-potential and versatile method for numerous research areas. While the ever-increasing precision of the techniques has opened various possibilities for optical applications, studies on the inclusion of functional additives within the printed objects are still scarce. Therefore, a novel method of utilizing microcrystalline NLO active compounds as additives in photopolymerizable 3D printing resins was developed. Series of flat lenses containing NLO active urea and KDP, respectively, were manufactured by stereolithography. The printed lenses were shown to generate the second harmonic upon laser irradiation, and its intensity was found to increase as a function of lens thickness with both additives. These results confirm that the basic concept works well and suggest that further studies on the usability of other compounds as well as the optimization of the lenses' properties should be carried

out. In general, the ease of use and relatively low cost of the 3D printing method could well see stereolithography getting more widespread attention in manufacturing optically functional objects for nonlinear optics and beyond.

In conclusion, this thesis covers a range of topics around the synthesis of new nonlinear optical materials and their subsequent use in applications like NLO active lenses. The research presented provides further insight into the chemistry of di- and interhalogens as well as stilbenes and their derivatives, while also laying the groundwork for the utilization of 3D printing in the manufacturing of optically active objects.

REFERENCES

(1) Yao, J.; Wang, Y. Theory and Technology of Frequency Doubling and Frequency Mixing Lasers. In *Nonlinear Optics and Solid-State Lasers*; Springer, Berlin, Heidelberg, 2012; Vol. 164, pp 179–243.

(2) Campagnola, P. Second Harmonic Generation Imaging Microscopy: Applications to Diseases Diagnostics. *Anal. Chem.* **2011**, *83* (9), 3224–3231.

(3) Zumsteg, F. C.; Bierlein, J. D.; Gier, T. E. $K_xRb_{1-x}TiOPO_4$: A New Nonlinear Optical Material. *J. Appl. Phys.* **1976**, *47* (11), 4980–4985.

(4) Chen, C.; Wu, B.; Jiang, A.; You, G. A New-Type Ultraviolet SHG Crystal — β-BaB_2O_4. *Sci. China Ser. B-Chemistry, Biol. Agric. Med. Earth Sci.* **1985**, *28* (3), 235–243.

(5) Chen, C.; Wu, Y.; Jiang, A.; Wu, B.; You, G.; Li, R.; Lin, S. New Nonlinear-Optical Crystal: LiB_3O_5. *J. Opt. Soc. Am. B* **1989**, *6* (4), 616.

(6) Nicoud, J. F.; Twieg, R. J. Design and Synthesis of Organic Molecular Compounds for Efficient Second-Harmonic Generation. In *Nonlinear Optical Properties of Organic Molecules and Crystals*; Elsevier, 1987; pp 227–296.

(7) Maiman, T. H. Stimulated Optical Radiation in Ruby. *Nature* **1960**, *187* (4736), 493–494.

(8) Franken, P. A.; Hill, A. E.; Peters, C. W.; Weinreich, G. Generation of Optical Harmonics. *Phys. Rev. Lett.* **1961**, *7* (4), 118–119.

(9) Boyd, R. W. *Nonlinear Optics*, 3rd ed.; Academic Press, 2008.

(10) Oudar, J. L.; Chemla, D. S. Hyperpolarizabilities of the Nitroanilines and Their Relations to the Excited State Dipole Moment. *J. Chem. Phys.* **1977**, *66* (6), 2664–2668.

(11) Hobden, M. V.; Warner, J. The Temperature Dependence of the Refractive Indices of Pure Lithium Niobate. *Phys. Lett.* **1966**, *22* (3), 243–244.

(12) Houé, M.; Townsend, P. D. An Introduction to Methods of Periodic Poling for Second-Harmonic Generation. *J. Phys. D. Appl. Phys.* **1995**, *28* (9), 1747–1763.

(13) Meredith, G. R. Design and Characterization of Molecular and Polymeric Nonlinear Optical Materials: Successes and Pitfalls. In *Nonlinear Optical Properties of Organic and Polymeric Materials, ACS Symposium Series*; Williams, D. J., Ed.; ACS, 1983; pp 27–56.

(14) Marder, S. R.; Perry, J. W.; Schaefer, W. P. Synthesis of Organic Salts with Large Second-Order Optical Nonlinearities. *Science (80-.).* **1989**, *245* (4918), 626–628.

(15) Green, M. L. H.; Marder, S. R.; Thompson, M. E.; Bandy, J. A.; Bloor, D.; Kolinsky, P. V.; Jones, R. J. Synthesis and Structure of (Cis)-[1-Ferrocenyl-2-(4-Nitrophenyl)Ethylene], an Organotransition Metal Compound with a Large Second-Order Optical Nonlinearity. *Nature* **1987**, *330* (6146), 360–362.

(16) Kurtz, S. K.; Perry, T. T. A Powder Technique for the Evaluation of Nonlinear Optical Materials. *J. Appl. Phys.* **1968**, *39* (8), 3798.

(17) Levine, B. F.; Bethea, C. G. Second and Third Order Hyperpolarizabilities

of Organic Molecules. *J. Chem. Phys.* **1975**, *63* (6), 2666–2682.
(18) Levine, B. F.; Bethea, C. G. Effects on Hyperpolarizabilities of Molecular Interactions in Associating Liquid Mixtures. *J. Chem. Phys.* **1976**, *65* (6), 2429–2438.
(19) Clays, K.; Persoons, A. Hyper-Rayleigh Scattering in Solution. *Phys. Rev. Lett.* **1991**, *66* (23), 2980–2983.
(20) Clays, K.; Persoons, A. Hyper-Rayleigh Scattering in Solution. *Rev. Sci. Instrum.* **1992**, *63* (6), 3285–3289.
(21) Flipse, M. C.; de Jonge, R.; Woudenberg, R. H.; Marsman, A. W.; van Walree, C. A.; Jenneskens, L. W. The Determination of First Hyperpolarizabilities β Using Hyper-Rayleigh Scattering: A Caveat. *Chem. Phys. Lett.* **1995**, *245* (2–3), 297–303.
(22) Maker, P. D.; Terhune, R. W.; Nisenoff, M.; Savage, C. M. Effects of Dispersion and Focusing on the Production of Optical Harmonics. *Phys. Rev. Lett.* **1962**, *8* (1), 21–22.
(23) Jerphagnon, J.; Kurtz, S. K. Maker Fringes: A Detailed Comparison of Theory and Experiment for Isotropic and Uniaxial Crystals. *J. Appl. Phys.* **1970**, *41* (4), 1667–1681.
(24) Oudar, J. L. Optical Nonlinearities of Conjugated Molecules. Stilbene Derivatives and Highly Polar Aromatic Compounds. *J. Chem. Phys.* **1977**, *67* (2), 446–457.
(25) Zhao, B.; Lu, W. Q.; Zhou, Z. H.; Wu, Y. The Important Role of the Bromo Group in Improving the Properties of Organic Nonlinear Optical Materials. *J. Mater. Chem.* **2000**, *10* (7), 1513–1517.
(26) Wang, Y.; Tam, W.; Stevenson, S. H.; Clement, R. A.; Calabrese, J. New Organic Non-Linear Optical Materials of Stilbene and Diphenylacetylene Derivatives. *Chem. Phys. Lett.* **1988**, *148* (2–3), 136–141.
(27) Arunan, E.; Desiraju, G. R.; Klein, R. A.; Sadlej, J.; Scheiner, S.; Alkorta, I.; Clary, D. C.; Crabtree, R. H.; Dannenber, J. J.; Hobza, P.; et al. Definition of the Hydrogen Bond (IUPAC Recommendations 2011). *Pure Appl. Chem.* **2011**, *83* (8), 1637–1641.
(28) Desiraju, G. R.; Shing Ho, P.; Kloo, L.; Legon, A. C.; Marquardt, R.; Metrangolo, P.; Politzer, P.; Resnati, G.; Rissanen, K. Definition of the Halogen Bond (IUPAC Recommendations 2013). *Pure Appl. Chem.* **2013**, *85* (8), 1711–1713.
(29) Chen, C.; Sasaki, T.; Li, R.; Wu, Y.; Lin, Z.; Mori, Y.; Hu, Z.; Wang, J.; Uda, S.; Yoshimura, M.; et al. *Nonlinear Optical Borate Crystals*; Wiley-VCH Verlag GmbH & Co. KGaA: Weinheim, Germany, 2012.
(30) Wu, C.; Yang, G.; Humphrey, M. G.; Zhang, C. Recent Advances in Ultraviolet and Deep-Ultraviolet Second-Order Nonlinear Optical Crystals. *Coord. Chem. Rev.* **2018**, *375*, 459–488.
(31) Liang, F.; Kang, L.; Lin, Z.; Wu, Y. Mid-Infrared Nonlinear Optical Materials Based on Metal Chalcogenides: Structure–Property Relationship. *Cryst. Growth Des.* **2017**, *17* (4), 2254–2289.
(32) Guo, S.-P.; Chi, Y.; Guo, G.-C. Recent Achievements on Middle and Far-

Infrared Second-Order Nonlinear Optical Materials. *Coord. Chem. Rev.* **2017**, *335*, 44–57.
(33) Dey, A.; Desiraju, G. R. Correlation between Molecular Dipole Moment and Centrosymmetry in Some Crystalline Diphenyl Ethers. *Chem. Commun.* **2005**, No. 19, 2486–2488.
(34) Coe, B. J.; Harris, J. A.; Asselberghs, I.; Clays, K.; Olbrechts, G.; Persoons, A.; Hupp, J. T.; Johnson, R. C.; Coles, S. J.; Hursthouse, M. B.; et al. Quadratic Nonlinear Optical Properties of N-Aryl Stilbazolium Dyes. *Adv. Funct. Mater.* **2002**, *12* (2), 110–116.
(35) Ruiz, B.; Yang, Z.; Gramlich, V.; Jazbinsek, M.; Günter, P. Synthesis and Crystal Structure of a New Stilbazolium Salt with Large Second-Order Optical Nonlinearity. *J. Mater. Chem.* **2006**, *16* (27), 2839–2842.
(36) Yang, Z.; Jazbinsek, M.; Ruiz, B.; Aravazhi, S.; Gramlich, V.; Günter, P. Molecular Engineering of Stilbazolium Derivatives for Second-Order Nonlinear Optics. *Chem. Mater.* **2007**, *19* (14), 3512–3518.
(37) Yin, J.; Li, L.; Yang, Z.; Jazbinsek, M.; Tao, X.; Günter, P.; Yang, H. A New Stilbazolium Salt with Perfectly Aligned Chromophores for Second-Order Nonlinear Optics: 4-N,N-Dimethylamino-4′-N′-Methyl- Stilbazolium 3-Carboxy-4-Hydroxybenzenesulfonate. *Dye. Pigment.* **2012**, *94* (1), 120–126.
(38) Tonouchi, M. Cutting-Edge Terahertz Technology. *Nat. Photonics* **2007**, *1* (2), 97–105.
(39) Marder, S. R.; Perry, J. W.; Yakymyshyn, C. P. Organic Salts with Large Second-Order Optical Nonlinearities. *Chem. Mater.* **1994**, *6* (8), 1137–1147.
(40) Etter, M. C. Encoding and Decoding Hydrogen-Bond Patterns of Organic Compounds. *Acc. Chem. Res.* **1990**, *23* (4), 120–126.
(41) Zyss, J.; Nicoud, J. F.; Coquillay, M. Chirality and Hydrogen Bonding in Molecular Crystals for Phase-Matched Second-Harmonic Generation: N-(4-Nitrophenyl)-(L)-Prolinol (NPP). *J. Chem. Phys.* **1984**, *81* (9), 4160–4167.
(42) Okamoto, N.; Abe, T.; Chen, D.; Fujimura, H.; Matsushima, R. Large Second Harmonic Generation from Mixtures of Para-Nitroaniline and Its N-Alkyl Derivatives. *Opt. Commun.* **1990**, *74* (6), 421–424.
(43) Matsushima, R.; Hiramatsu, K.; Okamoto, N. Second-Harmonic Generation from Mixed Crystals of p-Nitroaniline. *J. Mater. Chem.* **1993**, *3* (10), 1045–1048.
(44) Panunto, T. W.; Urbanczyk-Lipkowska, Z.; Johnson, R.; Etter, M. C. Hydrogen-Bond Formation in Nitroanilines: The First Step in Designing Acentric Materials. *J. Am. Chem. Soc.* **1987**, *109* (25), 7786–7797.
(45) Etter, M. C.; Huang, K. S. Induction of Noncentrosymmetry by Polar Hydrogen-Bonded Chains in Nitroaniline Crystals. *Chem. Mater.* **1992**, *4* (4), 824–827.
(46) Frankenbach, G. M.; Etter, M. C. Relationship between Symmetry in Hydrogen-Bonded Benzoic Acids and the Formation of Acentric Crystal Structures. *Chem. Mater.* **1992**, *4* (2), 272–278.
(47) Rieckhoff, K. E.; Peticolas, W. L. Optical Second-Harmonic Generation in Crystalline Amino Acids. *Science (80-.).* **1965**, *147* (3658), 610–611.

(48) Monaco, S. B.; Davis, L. E.; Velsko, S. P.; Wang, F. T.; Eimerl, D.; Zalkin, A. Synthesis and Characterization of Chemical Analogs of L-Arginine Phosphate. *J. Cryst. Growth* **1987**, *85* (1–2), 252–255.
(49) Petrosyan, H. A.; Karapetyan, H. A.; Antipin, M. Y.; Petrosyan, A. M. Nonlinear Optical Crystals of L-Histidine Salts. *J. Cryst. Growth* **2005**, *275* (1–2), e1919–e1925.
(50) Fleck, M.; Petrosyan, A. M. Reactions of Amino Acids with Acids. In *Salts of Amino Acids*; Springer International Publishing, 2014; pp 207–571.
(51) Srinivasan, P.; Kanagasekaran, T.; Gopalakrishnan, R.; Bhagavannarayana, G.; Ramasamy, P. Studies on the Growth and Characterization of L-Asparaginium Picrate (LASP) - A Novel Nonlinear Optical Crystal. *Cryst. Growth Des.* **2006**, *6* (7), 1663–1670.
(52) Srinivasan, P.; Kanagasekaran, T.; Gopalakrishnan, R. A Highly Efficient Organic Nonlinear Optical Donor-Acceptor Single Crystal: L-Valinium Picrate. *Cryst. Growth Des.* **2008**, *8* (7), 2340–2345.
(53) Aakeröy, C. B.; Hitchcock, P. B.; Moyle, B. D.; Seddon, K. R. A Novel Class of Salts for Second Harmonic Generation. *J. Chem. Soc., Chem. Commun.* **1989**, No. 23, 1856–1859.
(54) Aakeröy, C. B.; Hitchcock, P. B.; Seddon, K. R. Organic Salts of L-Tartaric Acid: Materials for Second Harmonic Generation with a Crystal Structure Governed by an Anionic Hydrogen-Bonded Network. *J. Chem. Soc., Chem. Commun.* **1992**, No. 7, 553–555.
(55) Aakeröy, C. B.; Bahra, G. S.; Hitchcock, P. B.; Patell, Y.; Seddon, K. R. Crystal Engineering: Hydrogen-Bonded Salts of Hydroxybenzoic Acids for Second Harmonic Generation. *J. Chem. Soc., Chem. Commun.* **1993**, No. 2, 152–156.
(56) Miyano, T.; Sakai, T.; Hisaki, I.; Ichida, H.; Kanematsu, Y.; Tohnai, N. Hierarchical Construction of SHG-Active Polar Crystals by Using Multi-Component Crystals. *Chem. Commun.* **2016**, *52* (94), 13710–13713.
(57) Huyskens, F. L.; Huyskens, P. L.; Persoons, A. P. Solvent Dependence of the First Hyperpolarizability of P-Nitroanilines: Differences between Nonspecific Dipole-Dipole Interactions and Solute-Solvent H-Bonds. *J. Chem. Phys.* **1998**, *108* (19), 8161–8171.
(58) Bartkowiak, W.; Lipkowski, P. Hydrogen-Bond Effects on the Electronic Absorption Spectrum and Evaluation of Nonlinear Optical Properties of an Aminobenzodifuranone Derivative That Exhibits the Largest Positive Solvatochromism. *J. Mol. Model.* **2005**, *11* (4–5), 317–322.
(59) Guthrie, F. XXVIII.—On the Iodide of Iodammonium. *J. Chem. Soc.* **1863**, *16*, 239–244.
(60) Cavallo, G.; Metrangolo, P.; Milani, R.; Pilati, T.; Priimagi, A.; Resnati, G.; Terraneo, G. The Halogen Bond. *Chem. Rev.* **2016**, *116* (4), 2478–2601.
(61) Sarma, J. A. R. P.; Allen, F. H.; Hoy, V. J.; Howard, J. A. K.; Thaimattam, R.; Biradha, K.; Desiraju, G. R. Design of an SHG-Active Crystal, 4-Iodo-4′-Nitrobiphenyl: The Role of Supramolecular Synthons. *Chem. Commun.* **1997**, No. 1, 101–102.

(62) George, S.; Nangia, A.; Lam, C.-K.; Mak, T. C. W.; Nicoud, J.-F. Crystal Engineering of Urea α-Network via I···O_2N Synthon and Design of SHG Active Crystal N-4-Iodophenyl-N′-4′-Nitrophenylurea. *Chem. Commun.* **2004**, *412* (10), 1202–1203.
(63) Saha, B. K.; Nangia, A.; Nicoud, J.-F. Using Halogen···halogen Interactions to Direct Noncentrosymmetric Crystal Packing in Dipolar Organic Molecules. *Cryst. Growth Des.* **2006**, *6* (6), 1278–1281.
(64) Bond, A. D.; Griffiths, J.; Rawson, J. M.; Hulliger, J. Inducing Structural Polarity Using Fluorinated Organics: X-Ray Crystal Structures of p-XC_6F_4CN (X = Cl, Br, I). *Chem. Commun.* **2001**, *1* (23), 2488–2489.
(65) Sasaki, T.; Ida, Y.; Hisaki, I.; Tsuzuki, S.; Tohnai, N.; Coquerel, G.; Sato, H.; Miyata, M. Construction of Chiral Polar Crystals from Achiral Molecules by Stacking Control of Hydrogen-Bonded Layers Using Type II Halogen Bonds. *Cryst. Growth Des.* **2016**, *16* (3), 1626–1635.
(66) Cariati, E.; Forni, A.; Biella, S.; Metrangolo, P.; Meyer, F.; Resnati, G.; Righetto, S.; Tordin, E.; Ugo, R. Tuning Second-Order NLO Responses through Halogen Bonding. *Chem. Commun.* **2007**, No. 25, 2590–2592.
(67) Frazier, C. C.; Harvey, M. A.; Cockerham, M. P.; Hand, H. M.; Chauchard, E. A.; Lee, C. H. Second-Harmonic Generation in Transition-Metal-Organic Compounds. *J. Phys. Chem.* **1986**, *90* (22), 5703–5706.
(68) Calabrese, J. C.; Tam, W. Organometallics for Non-Linear Optics: Metal-Pyridine and Bipyridine Complexes. *Chem. Phys. Lett.* **1987**, *133* (3), 244–245.
(69) Thompson, M. E.; Djurovich, P. E.; Barlow, S.; Marder, S. Organometallic Complexes for Optoelectronic Applications. In *Comprehensive Organometallic Chemistry III*; Elsevier Ltd, 2007; Vol. 12, pp 101–194.
(70) Di Bella, S.; Dragonetti, C.; Pizzotti, M.; Roberto, D.; Tessore, F.; Ugo, R. Coordination and Organometallic Complexes as Second-Order Nonlinear Optical Molecular Materials. In *Topics in Organometallic Chemistry*; Springer Verlag, 2010; Vol. 28, pp 1–55.
(71) Marder, S. R.; Perry, J. W.; Tiemann, B. G.; Schaefer, W. P. Organometallic Salts with Large Second-Harmonic-Generation Powder Efficiencies: (E)-1-Ferrocenyl-2-(1-Methyl-4-Pyridiniumyl)Ethylene Salts. *Organometallics* **1991**, *10* (6), 1896–1901.
(72) Coe, B. J.; Houbrechts, S.; Asselberghs, I.; Persoons, A. Efficient, Reversible Redox-Switching of Molecular First Hyperpolarizabilities in Ruthenium(II) Complexes Possessing Large Quadratic Optical Nonlinearities. *Angew. Chemie Int. Ed.* **1999**, *38* (3), 366–369.
(73) Weyland, T.; Ledoux, I.; Brasselet, S.; Zyss, J.; Lapinte, C. Nonlinear Optical Properties of Redox-Active Mono-, Bi-, and Trimetallic σ-Acetylide Complexes Connected through a Phenyl Ring in the Cp*(Dppe)Fe Series. An Example of Electro-Switchable NLO Response. *Organometallics* **2000**, *19* (24), 5235–5237.
(74) Coe, B. J. Molecular Materials Possessing Switchable Quadratic Nonlinear Optical Properties. *Chem. - A Eur. J.* **1999**, *5* (9), 2464–2471.

(75) Maury, O.; Viau, L.; Sénéchal, K.; Corre, B.; Guégan, J. P.; Renouard, T.; Ledoux, I.; Zyss, J.; Le Bozec, H. Synthesis, Linear, and Quadratic-Nonlinear Optical Properties of Octupolar D_3 and D_{2d} Bipyridyl Metal Complexes. *Chem. - A Eur. J.* **2004**, *10* (18), 4454–4466.
(76) Maury, O.; Le Bozec, H. Molecular Engineering of Octupolar NLO Molecules and Materials Based on Bipyridyl Metal Complexes. *Acc. Chem. Res.* **2005**, *38* (9), 691–704.
(77) Le Bozec, H.; Renouard, T. Dipolar and Non-Dipolar Pyridine and Bipyridine Metal Complexes for Nonlinear Optics. *Eur. J. Inorg. Chem.* **2000**, *2000* (2), 229–239.
(78) Bénard, S.; Yu, P.; Coradin, T.; Rivière, E.; Nakatani, K.; Clément, R. Design of Strongly NLO-Active Molecularly-Based Ferromagnets. *Adv. Mater.* **1997**, *9* (12), 981–984.
(79) Bénard, S.; Yu, P.; Audière, J. P.; Rivière, E.; Clément, R.; Guilhem, J.; Tchertanov, L.; Nakatani, K. Structure and NLO Properties of Layered Bimetallic Oxalato-Bridged Ferromagnetic Networks Containing Stilbazolium-Shaped Chromophores. *J. Am. Chem. Soc.* **2000**, *122* (39), 9444–9454.
(80) Wang, C.; Zhang, T.; Lin, W. Rational Synthesis of Noncentrosymmetric Metal–Organic Frameworks for Second-Order Nonlinear Optics. *Chem. Rev.* **2012**, *112* (2), 1084–1104.
(81) Du, S.; Zhang, H. Metal–Organic Frameworks for Second-Order Nonlinear Optics. In *Metal-Organic Frameworks for Photonics Applications*; Chen, B., Qian, G., Eds.; Springer Verlag, 2013; Vol. 157, pp 145–165.
(82) Mingabudinova, L. R.; Vinogradov, V. V.; Milichko, V. A.; Hey-Hawkins, E.; Vinogradov, A. V. Metal-Organic Frameworks as Competitive Materials for Non-Linear Optics. *Chem. Soc. Rev.* **2016**, *45* (19), 5408–5431.
(83) Ye, Q.; Li, Y.-H.; Song, Y.-M.; Huang, X.-F.; Xiong, R.-G.; Xue, Z. A Second-Order Nonlinear Optical Material Prepared through In Situ Hydrothermal Ligand Synthesis. *Inorg. Chem.* **2005**, *44* (10), 3618–3625.
(84) Ye, Q.; Tang, Y.-Z.; Wang, X.-S.; Xiong, R.-G. Strong Enhancement of Second-Harmonic Generation (SHG) Response through Multi-Chiral Centers and Metal-Coordination. *Dalt. Trans.* **2005**, No. 9, 1570.
(85) Tam, W.; Guerin, B.; Calabrese, J. C.; Stevenson, S. H. 3-Methyl-4-Methoxy-4′-Nitrostilbene (MMONS): Crystal Structure of a Highly Efficient Material for Second-Harmonic Generation. *Chem. Phys. Lett.* **1989**, *154* (2), 93–96.
(86) Grubbs, R. B.; Marder, S. R.; Perry, J. W.; Schaefer, W. P. Second-Order Nonlinearities and Crystal Structure of 2-Methoxy-4′-Nitro-(E)-Stilbene. *Chem. Mater.* **1991**, *3* (1), 3–4.
(87) Munshi, P.; Skelton, B. W.; McKinnon, J. J.; Spackman, M. A. Polymorphism in 3-Methyl-4-Methoxy-4′-Nitrostilbene (MMONS), a Highly Active NLO Material. *CrystEngComm* **2008**, *10* (2), 197–206.
(88) Fichou, D.; Watanabe, T.; Takeda, T.; Miyata, S.; Goto, Y.; Nakayama, M. Influence of the Ring-Substitution on the Second Harmonic Generation of Chalcone Derivatives. *Jpn. J. Appl. Phys.* **1988**, *27* (3A), L429–L430.

(89) Goto, Y.; Hayashi, A.; Kimura, Y.; Nakayama, M. Second Harmonic Generation and Crystal Growth of Substituted Thienyl Chalcone. *J. Cryst. Growth* **1991**, *108* (3–4), 688–698.
(90) Uchida, T.; Kozawa, K.; Sakai, T.; Aoki, M.; Yoguchi, H.; Abdureyim, A.; Watanabe, Y. Novel Organic SHG Materials. *Mol. Cryst. Liq. Cryst. Sci. Technol. Sect. A Mol. Cryst. Liq. Cryst.* **1998**, *314*, 437–442.
(91) Zhang, G.; Kinoshita, T.; Sasaki, K.; Goto, Y.; Nakayama, M. Crystal Growth of 4-Br-4′-Methoxychalcone and Its Characterization. *J. Cryst. Growth* **1990**, *100* (3), 411–416.
(92) Ravindra, H. J.; Kiran, A. J.; Dharmaprakash, S. M.; Satheesh Rai, N.; Chandrasekharan, K.; Kalluraya, B.; Rotermund, F. Growth and Characterization of an Efficient Nonlinear Optical D–π–A–π–D Type Chalcone Single Crystal. *J. Cryst. Growth* **2008**, *310* (18), 4169–4176.
(93) Wu, D.; Zhao, B.; Zhou, Z. An Ab Initio Study on the Polarizabilities of 1,5-Diphenylpenta-2,4-Dien-1- Ones. *J. Mol. Struct. THEOCHEM* **2004**, *682* (1–3), 83–88.
(94) Jayarama, A.; Ravindra, H. J.; Menezes, A. P.; Dharmaprakash, S. M.; Ng, S. W. Synthesis, Growth, and Characterization of 3-(4-Methoxyphenyl)-1-(Pyridin- 2-Yl) Prop-2-En-1-One Single Crystal: A Potential NLO Material. *J. Mol. Struct.* **2013**, *1051*, 285–291.
(95) D'Silva, E. D.; Podagatlapalli, G. K.; Rao, S. V.; Rao, D. N.; Dharmaprakash, S. M. New, High Efficiency Nonlinear Optical Chalcone Co-Crystal and Structure-Property Relationship. *Cryst. Growth Des.* **2011**, *11* (12), 5362–5369.
(96) Lahtinen, E.; Kivijärvi, L.; Tatikonda, R.; Väisänen, A.; Rissanen, K.; Haukka, M. Selective Recovery of Gold from Electronic Waste Using 3D-Printed Scavenger. *ACS Omega* **2017**, *2* (10), 7299–7304.
(97) Lahtinen, E.; Hänninen, M. M.; Kinnunen, K.; Tuononen, H. M.; Väisänen, A.; Rissanen, K.; Haukka, M. Porous 3D Printed Scavenger Filters for Selective Recovery of Precious Metals from Electronic Waste. *Adv. Sustain. Syst.* **2018**, *2* (10), 1800048.
(98) Zhang, Y.; Shi, G.; Qin, J.; Lowe, S. E.; Zhang, S.; Zhao, H.; Zhong, Y. L. Recent Progress of Direct Ink Writing of Electronic Components for Advanced Wearable Devices. *ACS Appl. Electron. Mater.* **2019**, *1* (9), 1718–1734.
(99) Hou, Z.; Lu, H.; Li, Y.; Yang, L.; Gao, Y. Direct Ink Writing of Materials for Electronics-Related Applications: A Mini Review. *Front. Mater.* **2021**, *8*, 647229.
(100) Kodama, H. Automatic Method for Fabricating a Three-Dimensional Plastic Model with Photo-Hardening Polymer. *Rev. Sci. Instrum.* **1981**, *52* (11), 1770–1773.
(101) Hull, C. W. Apparatus for Production of Three-Dimensional Objects by Stereolithography. US4575330A, 1986.
(102) Bagheri, A.; Jin, J. Photopolymerization in 3D Printing. *ACS Appl. Polym. Mater.* **2019**, *1* (4), 593–611.

(103) Quan, H.; Zhang, T.; Xu, H.; Luo, S.; Nie, J.; Zhu, X. Photo-Curing 3D Printing Technique and Its Challenges. *Bioact. Mater.* **2020**, *5* (1), 110–115.
(104) Heinrich, A.; Rank, M.; Maillard, P.; Suckow, A.; Bauckhage, Y.; Rößler, P.; Lang, J.; Shariff, F.; Pekrul, S. Additive Manufacturing of Optical Components. *Adv. Opt. Technol.* **2016**, *5* (4), 293–301.
(105) Camposeo, A.; Persano, L.; Farsari, M.; Pisignano, D. Additive Manufacturing: Applications and Directions in Photonics and Optoelectronics. *Adv. Opt. Mater.* **2019**, *7* (1), 1800419.
(106) Parker, S. T.; Domachuk, P.; Amsden, J.; Bressner, J.; Lewis, J. A.; Kaplan, D. L.; Omenetto, F. C. Biocompatible Silk Printed Optical Waveguides. *Adv. Mater.* **2009**, *21* (23), 2411–2415.
(107) Lorang, D. J.; Tanaka, D.; Spadaccini, C. M.; Rose, K. A.; Cherepy, N. J.; Lewis, J. A. Photocurable Liquid Core-Fugitive Shell Printing of Optical Waveguides. *Adv. Mater.* **2011**, *23* (43), 5055–5058.
(108) Hinman, S. S.; McKeating, K. S.; Cheng, Q. Plasmonic Sensing with 3D Printed Optics. *Anal. Chem.* **2017**, *89* (23), 12626–12630.
(109) Thiele, S.; Arzenbacher, K.; Gissibl, T.; Giessen, H.; Herkommer, A. M. 3D-Printed Eagle Eye: Compound Microlens System for Foveated Imaging. *Sci. Adv.* **2017**, *3* (2), e1602655.
(110) Gissibl, T.; Thiele, S.; Herkommer, A.; Giessen, H. Sub-Micrometre Accurate Free-Form Optics by Three-Dimensional Printing on Single-Mode Fibres. *Nat. Commun.* **2016**, *7* (1), 1–9.
(111) Chen, X.; Liu, W.; Dong, B.; Lee, J.; Ware, H. O. T.; Zhang, H. F.; Sun, C. High-Speed 3D Printing of Millimeter-Size Customized Aspheric Imaging Lenses with Sub 7 Nm Surface Roughness. *Adv. Mater.* **2018**, *30* (18), 1705683.
(112) Shao, G.; Hai, R.; Sun, C. 3D Printing Customized Optical Lens in Minutes. *Adv. Opt. Mater.* **2020**, *8* (4), 1901646.
(113) Blessing, K.; van de Vrie, R. Print Head, Upgrade Kit for a Conventional Inkjet Printer, Printer and Method for Printing Optical Structures. US9592690B2, 2017.
(114) van de Vrie, R.; Biskop, J. Method for Printing a Three-Dimensional Structure with Smooth Surfaces. US9662837B2, 2017.
(115) Assefa, B. G.; Pekkarinen, M.; Partanen, H.; Biskop, J.; Turunen, J.; Saarinen, J. Imaging-Quality 3D-Printed Centimeter-Scale Lens. *Opt. Express* **2019**, *27* (9), 12630.
(116) Alam, F.; Elsherif, M.; Alqattan, B.; Salih, A.; Lee, S. M.; Yetisen, A. K.; Park, S.; Butt, H. 3D Printed Contact Lenses. *ACS Biomater. Sci. Eng.* **2021**, *7* (2), 794–803.
(117) Nguyen, D. T.; Meyers, C.; Yee, T. D.; Dudukovic, N. A.; Destino, J. F.; Zhu, C.; Duoss, E. B.; Baumann, T. F.; Suratwala, T.; Smay, J. E.; et al. 3D-Printed Transparent Glass. *Adv. Mater.* **2017**, *29* (26), 1701181.
(118) Moore, D. G.; Barbera, L.; Masania, K.; Studart, A. R. Three-Dimensional Printing of Multicomponent Glasses Using Phase-Separating Resins. *Nat. Mater.* **2020**, *19* (2), 212–217.

(119) Baudrier-Raybaut, M.; Haïdar, R.; Kupecek, P.; Lemasson, P.; Rosencher, E. Random Quasi-Phase-Matching in Bulk Polycrystalline Isotropic Nonlinear Materials. *Nature* **2004**, *432* (7015), 374–376.
(120) Skipetrov, S. E. Disorder Is the New Order. *Nature* **2004**, *432* (7015), 285–286.
(121) Li, A. D.; Liu, W. C. Optical Properties of Ferroelectric Nanocrystal/Polymer Composites. In *Physical Properties and Applications of Polymer Nanocomposites*; Elsevier Ltd, 2010; pp 108–158.
(122) Lisinski, S.; Schaniel, D.; Ratke, L.; Woike, T. Second-Harmonic Generation by Ferroelectric Microparticles in Aerogels. *Chem. Mater.* **2006**, *18* (6), 1534–1538.
(123) Liu, X.; Zhou, J.; Zhou, S.; Yue, Y.; Qiu, J. Transparent Glass-Ceramics Functionalized by Dispersed Crystals. *Prog. Mater. Sci.* **2018**, *97*, 38–96.
(124) Reiss, G. J.; Leske, P. B. The Twinned Crystal Structure of Bis((4-Aminopyridin-1-Ium) Iodide Triiodide, $C_{20}H_{28}I_8N_8$. *Zeitschrift für Krist. - New Cryst. Struct.* **2014**, *229* (4), 452–454.
(125) Wadsworth, W. S.; Emmons, W. D. The Utility of Phosphonate Carbanions in Olefin Synthesis. *J. Am. Chem. Soc.* **1961**, *83* (7), 1733–1738.
(126) Cheng, L. T.; Tam, W.; Marder, S. R.; Stiegman, A. E.; Rikken, G.; Spangler, C. W. Experimental Investigations of Organic Molecular Nonlinear Optical Polarizabilities. 2. A Study of Conjugation Dependences. *J. Phys. Chem.* **1991**, *95* (26), 10643–10652.
(127) Varanasi, P. R.; Jen, A. K.-Y.; Chandrasekhar, J.; Namboothiri, I. N. N.; Rathna, A. The Important Role of Heteroaromatics in the Design of Efficient Second-Order Nonlinear Optical Molecules: Theoretical Investigation on Push−Pull Heteroaromatic Stilbenes. *J. Am. Chem. Soc.* **1996**, *118* (49), 12443–12448.
(128) Kelley, S. P.; Yang, K.; Corretjer, N.; Gadban, S.; Glaser, R.; Kozak, M. M.; Hathaway, B. A. CCDC 1879519. *CSD Commun.* **2018**.
(129) Rawal, M.; Garrett, K. E.; Johnson, L. E.; Kaminsky, W.; Jucov, E.; Shelton, D. P.; Timofeeva, T.; Eichinger, B. E.; Tillack, A. F.; Robinson, B. H.; et al. Alternative Bridging Architectures in Organic Nonlinear Optical Materials: Comparison of π- and χ-Type Structures. *J. Opt. Soc. Am. B* **2016**, *33* (12), E160.

ORIGINAL PAPERS

I

THREE-DIMENSIONAL PRINTING OF NONLINEAR OPTICAL LENSES

by

Esa Kukkonen, Elmeri Lahtinen, Pasi Myllyperkiö, Jari Konu
and Matti Haukka 2018

ACS Omega, 3 (9), 11558-11561

DOI: 10.1021/acsomega.8b01659

ACS OMEGA

Article

Cite This: ACS Omega 2018, 3, 11558−11561

http://pubs.acs.org/journal/acsodf

Three-Dimensional Printing of Nonlinear Optical Lenses

Esa Kukkonen,[†] Elmeri Lahtinen,[†] Pasi Myllyperkiö,[‡] Jari Konu,[†] and Matti Haukka*[,†]

[†]Department of Chemistry and [‡]Nanoscience Center, University of Jyväskylä, P.O. Box 35, FI-40014 Jyväskylä, Finland

Supporting Information

ABSTRACT: In the current paper, a series of nonlinear optical (NLO) active devices was prepared by utilizing stereolithographic three-dimensional printing technique. Microcrystalline NLO active component, urea, or potassium dihydrogen phosphate was dispersed in a simple photopolymerizable polyacrylate-based resin and used as the printing material to fabricate highly efficient transparent NLO lenses. The nonlinear activity of the printed lenses was confirmed by second-harmonic generation measurements using a femtosecond laser-pumped optical parametric amplifier operating at a wavelength of 1195 nm. The three-dimensional printing provides a simple method to utilize a range of NLO active compounds without tedious crystal growing and processing steps. Furthermore, introducing NLO additives in the printing material provides an easy and cost-efficient way to manufacture lenses with NLO functionality.

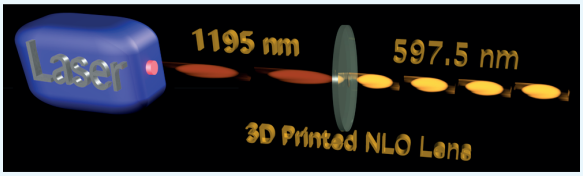

INTRODUCTION

The research on nonlinear optical (NLO) materials dates back to the early days of lasers. Franken et al. reported the observation of second-harmonic generation (SHG) phenomenon already in 1961.[1] In SHG, two photons having the same frequency are combined in a medium generating radiation that has twice the frequency ("frequency doubling") and thus half the wavelength of the original photons. Half a century later, SHG still remains as one of the most investigated NLO property owing to its potential applications in laser technology and optoelectronics.[2,3] Especially, the growing interest in processes such as optical signal processing and electro-optical switches[4] has been fueling the research in the field of NLO materials and devices.[5,6]

Most commonly used NLO devices contain large single crystals of the active material. Although a variety of NLO active materials, both inorganic and organic, are known, only a limited number of these are commercially used. The advantages of the most commonly used inorganic compounds, such as β-barium borate[7] and potassium titanyl phosphate,[8,9] arise from the wide-transparency regions, wide phase matching range, and high conversion efficiency, as well as high physical and chemical stability and durability. Due to these reasons, the selection of commercial materials has remained nearly unchanged for decades even though numerous new inorganic and organic materials have shown superior NLO properties.[10−12] Especially, various organic compounds have displayed a number of NLO properties that clearly exceed that of the commercial inorganic crystals.[10−14] Unfortunately, many of these organic NLO components suffer from inferior stability and malleability, which has hindered their utilization in optical devices. However, the stability problems of certain NLO films have been successfully tackled by using specific preparation techniques based on self-assembly of the NLO compounds.[15,16] Despite the steps taken forward, assembling molecules or the need to grow single crystals of high quality and substantial size have still limited the use of wider selection of organic compounds. Crystallization techniques such as top-seeded solution growth technique, Czochralski technique, and hydrothermal methods, commonly used for inorganic compounds, are often less suitable for organic materials.[17,18] Furthermore, the mechanical processing of NLO crystals, required to meet the demands of optical components, may be inapplicable for organic crystals. One way around these problems is to fabricate thin films by the poling technique where the organic NLO chromophore is mixed with a polymer matrix. In this technique, the dipoles of the NLO components are aligned by an external electric field.[19,20] Again, this method is not suitable for all organic NLO compounds. Another potential solution would be utilization of microcrystalline materials, instead of large single crystals, as in the Kurtz−Perry technique, which is used for measuring SHG properties.[21] However, the powdery material is difficult to handle and therefore poorly applicable for practical NLO use as it is.

In this paper, we present a method for manufacturing NLO active devices from microcrystalline NLO components by three-dimensional (3D) printing. In this method, the chromophore microcrystals, such as urea or potassium dihydrogen phosphate (KDP), are mixed with photopolymerizable polyacrylate-based resin, commonly used as printing material in stereolithographic (SLA) 3D printing technique. The 3D printing opens possibilities of tailor-made size, shape and, optical properties of the printed objects. The 3D printing has already been successfully used for printing high-quality lenses.[22] By using an NLO additive in the printing material, it is possible to prepare lenses with NLO properties. Use of

Received: July 14, 2018
Accepted: September 10, 2018
Published: September 21, 2018

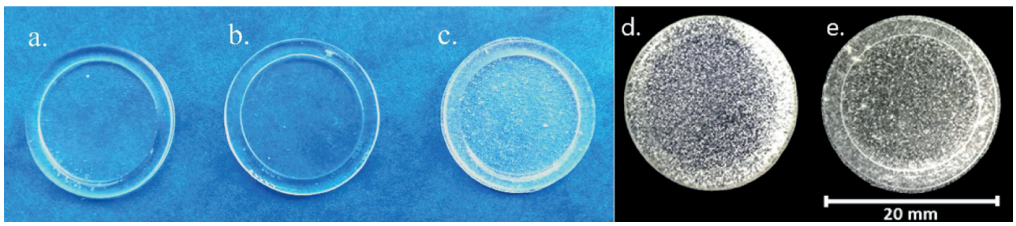

Figure 1. Photographs (blue background) and optical microscope images (black background) of the printed lenses. (a) The 300 μm thick reference lens without the NLO component. (b, d) The 300 μm thick NLO lens with 5 wt % KDP. (c, e) The 300 μm thick NLO lens with 5 wt % urea.

polymer matrix also serves as a protecting media for the NLO component. This makes it possible to utilize a whole range of less stable organic compounds as NLO chromophores.

RESULTS AND DISCUSSION

The 3D printing experiments were conducted by adding microcrystalline urea or potassium dihydrogen phosphate (KDP) as the NLO active component in the printable photopolymer matrix. Both of these highly effective NLO chromophores are commonly used reference materials in the SHG measurements carried out by the Kurtz–Perry powder method.[21,23,24] A series of round NLO lenses with 5 wt % urea or KDP were printed by SLA technique. The diameter of the printed objects was 2 cm, and the thicknesses 300, 600, 900, 1200, and 1500 μm (Figure 1). As can be seen in Figure 1, both additives were uniformly dispersed throughout the objects. Furthermore, the additives retained their original microcrystalline structure even after the printing process.

The 3D printed NLO lenses' ability to generate the second-harmonic signal was confirmed by measurements with an amplified femtosecond laser (Integra-C, Quantronix)-pumped tunable optical parametric amplifier (TOPAS, Light Conversion Ltd.) operating at 1195 nm. A laser beam of 3 mm (full width at half maximum, FWHM), a 130 fs pulse width, and 8 μJ of pulse energy was aimed at the middle of each object, and the intensity of the second-harmonic wavelength generated was measured through the accumulation of 10 consecutive pulses. Relatively wide laser beam was used to obtain an average result covering the whole lens.

With both urea and KDP lenses, the intensity of the SHG signal increased with the increasing thickness of the object (Figures S1, S2 and Table S1). The intensities of the SHG signals relative to the thickness of the lens are shown in Figure 2. With KDP, the intensity grew nearly linearly. The small deviations from the linear growth are likely due to inherently random orientations of the microcrystals inside the NLO lens. In the case of urea, the linear growth started to level after 1200 μm thickness. After certain thickness, the increased amount of microcrystals, crystal-to-crystal interactions, and decreasing transparency effectively reduce the intensity more than the new microcrystals increase it.

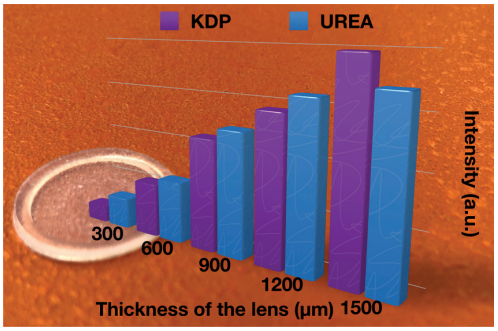

Figure 2. SHG intensities based on the integrated surface areas of the SHG signals for KDP and urea lenses as the function of lens thickness.

Organic polymers typically absorb UV radiation. Depending on the material, the absorption cutoff point can be reached already in the visible region. This must be kept in mind when choosing the matrix polymer. Therefore, the UV/vis spectrum of the printed acrylate polymer was measured in the range of 890–300 nm (Figures S3 and S4). Significant absorption started at ca. 420 nm, indicating the apparent cutoff wavelength for this material. Although the absorption of the polymer sets the limit for the usable wavelengths, it does not necessarily set additional limitations in the case of objects with organic NLO chromophores. It should be noted that also the organic NLO components tend to absorb strongly in the UV region.[25,26] Consequently, a similar cutoff would occur even without the polymer matrix.

The results show that stereolithography 3D printing can be utilized to produce highly efficient NLO lenses by using simple and readily available materials. Both urea- and KDP-based objects displayed significant ability to generate second-harmonic signal. The 3D printing method introduced here provides a way to considerably extend the selection of NLO active compounds that can be used for practical NLO devices. One of the main advantages of this novel approach is that there is no need for tedious preprocessing steps usually required when conventional NLO crystals are manufactured. Use of polymer matrix can also protect the highly efficient but less stable organic NLO compounds, which makes also those materials available for NLO applications. The ability to design the shape and size of the NLO lenses makes 3D printing a powerful tool for both research and manufacturing of new and improved electro-optical devices. It is already well established that 3D printing can be used to produce lenses with high-quality optical properties. We believe that by combining the choice of efficient NLO compounds with the optical design of the object can open up a whole new era in manufacturing NLO lenses.

METHODS

Materials. The acrylate-based resin used in 3D printing was purchased from PeoPoly. Urea was purchased from Sigma-Aldrich (ACS Reagent, 99.0–100.5%) and potassium dihydrogen phosphate (KDP) from Merck (≥99.5%). All chemicals were used as received. High-purity water of 18.2 MΩ cm resistivity was used throughout the experiments.

DOI: 10.1021/acsomega.8b01659
ACS Omega 2018, 3, 11558–11561

Preparation of the NLO Lenses. Approximately, 55 mL of a commercial acrylate-based resin was weighed in a beaker and mixed with 5 wt % urea or KDP. The NLO components had been sifted through 125 μm sieve to obtain uniform crystal sizes. The mixtures were carefully stirred before printing until a homogeneous printing material was obtained. The mixture was used for SLA 3D printing immediately after the preparation. After the 3D printing, the objects were first washed thoroughly with ethanol and water and then cured using 405 nm UV lamp for 10 min to make sure that the polymerization was complete. The fully cured printed objects were coated with sprayed lacquer to improve the transparency.

Three-Dimensional Printing. The models of the NLO lenses were designed by FreeCad v.0.16 software. The PeoPoly version of the Cura 2.6.2.-14 and B9Creator v.1.1.0. was used for preparing the models for printing. All objects were printed with the PeoPoly Moai SLA 3D printer operating with a 150 mW 405 nm laser. The layer height used for preparation of the objects was 50 μm.

NLO Measurements. The SHG measurements were conducted using a widely tunable optical parametric amplifier (TOPAS, Light Conversion Ltd.) pumped by an amplified femtosecond laser (Integra-C, Quantronix). OPA signal beam output at 1195 nm was used to generate second harmonic on the samples. The beam size at the sample was 3 mm (FWHM). The pulse duration was ∼130 fs, and pulse energy was 8 μJ. Exposure time of 0.217 s was used for urea lenses, whereas 2.17 s was used for KDP lenses.

UV/Vis Measurements. UV/vis spectrum of the printed polymer was measured from 890 to 300 nm using a PerkinElmer Lambda 25 UV/vis spectrophotometer. The analyzed NLO lens used as a sample was placed in front of the sample cuvette holder, and the reference cuvette holder was left empty as air was used as reference. A slit of 1.0 nm was used, with a scan speed of 240 nm/min and a data interval of 5.0 nm.

■ ASSOCIATED CONTENT

Supporting Information

The Supporting Information is available free of charge on the ACS Publications website at DOI: 10.1021/acsomega.8b01659.

Observed SHG intensities of the 3D printed lenses and UV/vis absorbance spectra of the lenses (PDF)

■ AUTHOR INFORMATION

Corresponding Author

*E-mail: matti.o.haukka@jyu.fi.

ORCID

Pasi Myllyperkiö: 0000-0003-1651-1676

Jari Konu: 0000-0002-7408-8995

Matti Haukka: 0000-0002-6744-7208

Author Contributions

M.H. and J.K. conceptualized the utilization of 3D printing for nonlinear optics and supervised the work. E.K. and E.L. printed and processed the objects. E.L. did the three-dimensional modeling. P.M. conducted the SHG measurements with E.K. and E.L. The paper was written jointly by E.K., E.L., J.K., and M.H.

Notes

The authors declare no competing financial interest.

■ ACKNOWLEDGMENTS

Financial support received from the Centennial Foundation of Technology Industries of Finland and Jane and Aatos Erkko foundation as a part of The Future Makers program is greatly appreciated.

■ REFERENCES

(1) Franken, P. A.; Hill, A.; Peters, C.; Weinreich, G. Generation of optical harmonics. *Phys. Rev. Lett.* **1961**, 118.

(2) Wang, Y.; Pan, S. Recent development of metal borate halides: Crystal chemistry and application in second-order NLO materials. *Coord. Chem. Rev.* **2016**, *323*, 15−35.

(3) Cho, M. J.; Choi, D. H.; Sullivan, P. A.; Akelaitis, A. J. P.; Dalton, L. R. Recent progress in second-order nonlinear optical polymers and dendrimers. *Prog. Polym. Sci.* **2008**, *33*, 1013−1058.

(4) Garmire, E. Nonlinear optics in daily life. *Opt. Express* **2013**, *21*, No. 30532.

(5) Mutailipu, M.; et al. Chemical Cosubstitution-Oriented Design of Rare-Earth Borates as Potential Ultraviolet Nonlinear Optical Materials. *J. Am. Chem. Soc.* **2017**, *139*, 18397−18405.

(6) Mutailipu, M.; et al. $SrB_5O_7F_3$ Functionalized with $[B_5O_9F_3]^{6-}$ Chromophores: Accelerating the Rational Design of Deep-Ultraviolet Nonlinear Optical Materials. *Angew. Chem., Int. Ed.* **2018**, *57*, 6095−6099.

(7) Chuantian, C.; Bochang, W.; Aidong, J.; Guiming, Y. A New-Type Ultraviolet SHG Crystal — β-BaB_2O_4. *Sci. Sin., Ser. B* **1985**, *28*, 235−243.

(8) Zumsteg, F. C.; Bierlein, J. D.; Gier, T. E. $K_xRb_{1-x}TiOPO_4$: A new nonlinear optical material. *J. Appl. Phys.* **1976**, *47*, 4980−4985.

(9) Bierlein, J. D.; Vanherzeele, H. Potassium titanyl phosphate: properties and new applications. *J. Opt. Soc. Am. B* **1989**, *6*, 622.

(10) Tam, W.; Guerin, B.; Calabrese, J. C.; Stevenson, S. H. 3-Methyl-4-methoxy-4′-nitrostilbene (MMONS): Crystal structure of a highly efficient material for second-harmonic generation. *Chem. Phys. Lett.* **1989**, *154*, 93−96.

(11) Pan, F.; Wong, M. S.; Bosshard, C.; Günter, P. Crystal growth and characterization of the organic salt 4-N, N-dimethylamino-4′-N-methyl-stilbazolium tosylate (dast). *Adv. Mater.* **1996**, *8*, 592−595.

(12) Marder, S. R.; Perry, J. W.; Yakymyshyn, C. P. Organic Salts with Large Second-Order Optical Nonlinearities. *Chem. Mater.* **1994**, *6*, 1137−1147.

(13) Ledoux, I.; Lepers, C.; Périgaud, A.; Badan, J.; Zyss, J. Linear and nonlinear optical properties of N-4-nitrophenyl L-prolinol single crystals. *Opt. Commun.* **1990**, *80*, 149−154.

(14) Marder, S. R. Organic nonlinear optical materials: where we have been and where we are going. *Chem. Commun.* **2006**, 131−134.

(15) Heflin, J. R.; et al. Efficient, Thermally Stable, Second Order Nonlinear Optical Response in Organic Hybrid Covalent/Ionic Self-Assembled Films. *Langmuir* **2006**, *22*, 5723−5727.

(16) Zhu, P.; et al. Realization of Expeditious Layer-by-Layer Siloxane-Based Self-assembly as an Efficient Route to Structurally Regular Acentric Superlattices with Large Electro-optic Responses. *Chem. Mater.* **2002**, *14*, 4982−4989.

(17) Dhanaraj, G.; Byrappa, K.; Prasad, V.; Dudley, M. *Springer Handbook of Crystal Growth*; Springer, 2010.

(18) Czochralski, J. Ein neues Verfahren zur Messung der Kristallisationsgeschwindigkeit der Metalle. *Z. Phys. Chem.* **1918**, *92U*, 219−221.

(19) Lee, H. S.; et al. Ellipsometric study of the poling effect on nonlinear-optical side-chain polymers containing disperse red 1. *J. Appl. Phys.* **2007**, *102*, No. 013514.

(20) Gaidukovs, S.; Kampars, V.; Rutkis, M.; Nitis, E.; Tokmakovs, A. Poled nonlinear polymeric material, Patent EP2824509A1, 2013.

(21) Kurtz, S. K.; Perry, T. T. A Powder Technique for the Evaluation of Nonlinear Optical Materials. *J. Appl. Phys.* **1968**, *39*, 3798.

DOI: 10.1021/acsomega.8b01659
ACS Omega 2018, 3, 11558−11561

(22) Gawedzinski, J.; Pawlowski, M. E.; Tkaczyk, T. S. Quantitative evaluation of performance of three-dimensional printed lenses. *Opt. Eng.* **2017**, *56*, No. 084110.
(23) Jerphagnon, J.; Kurtz, S. K. Optical Nonlinear Susceptibilities: Accurate Relative Values for Quartz, Ammonium Dihydrogen Phosphate, and Potassium Dihydrogen Phosphate. *Phys. Rev. B* **1970**, *1*, 1739−1744.
(24) Halbout, J.-M.; Blit, S.; Donaldson, W.; Chung, Tang Efficient phase-matched second-harmonic generation and sum-frequency mixing in urea. *IEEE J. Quantum Electron.* **1979**, *15*, 1176−1180.
(25) Uchida, T.; et al. Novel Organic SHG Materials. *Mol. Cryst. Liq. Cryst. Sci. Technol., Sect. A* **1998**, *315*, 135−140.
(26) Patil, P. S.; et al. Second harmonic generation and crystal growth of new chalcone derivatives. *J. Cryst. Growth* **2007**, *303*, 520−524.

DOI: 10.1021/acsomega.8b01659
ACS Omega 2018, 3, 11558−11561

II

REACTIVITY OF 4-AMINOPYRIDINE WITH HALOGENS AND INTERHALOGENS: WEAK INTERACTIONS SUPPORTED NETWORKS OF 4-AMINOPYRIDINE AND 4-AMINOPYRIDINIUM

by

Esa Kukkonen, Henri Malinen, Matti Haukka and Jari Konu 2019

Cryst. Growth Des., 19 (4), 2434-2445

DOI: 10.1021/acs.cgd.9b00119

CRYSTAL GROWTH & DESIGN

Article

Cite This: Cryst. Growth Des. 2019, 19, 2434−2445

pubs.acs.org/crystal

Reactivity of 4-Aminopyridine with Halogens and Interhalogens: Weak Interactions Supported Networks of 4-Aminopyridine and 4-Aminopyridinium

Esa Kukkonen, Henri Malinen, Matti Haukka, and Jari Konu*

Department of Chemistry, University vof Jyväskylä, P.O. Box 35, Jyväskylä FI-40014, Finland

Supporting Information

ABSTRACT: The reaction of 4-aminopyridine (4-AP) with ICl in a 1:1 molar ratio in CH_2Cl_2 produced the expected charge-transfer complex [4-NH_2-1λ^4-C_5H_4N-1-ICl] (**1**·ICl) and the ionic species [(4-NH_2-1λ^4-C_5H_4N)$_2$-1μ-I^+][Cl^-] (**2**·Cl^-) in a 2:1 relation, as indicated by ^{1}H NMR spectroscopy in solution. In contrast, only the ionic compound [(4-NH_2-1λ^4-C_5H_4N)$_2$-1μ-I^+][IBr_2^-] (**2**·IBr_2^-) was observed in the analogous reaction with IBr. The reaction between 4-AP and I_2 in a 1:1 molar ratio also afforded two components, one of which was identified as the congeneric cation in [(4-NH_2-1λ^4-C_5H_4N)$_2$-1μ-I^+][I_7^-] (**2**·I_7^-) that contains a polyiodide anion as a result of transformation in a 1:2 molar ratio between the starting materials. In all of these ionic products, the crystal structures feature an iodonium ion, I^+, trapped between two 4-AP rings through N···I^+···N contact. Surprisingly, the reaction of 4-AP with Br_2 in CH_2Cl_2 resulted in an immediate protonation of the 4-aminopyridine (^{1}H NMR) and [4-NH_2-1λ^4-C_5H_4N-1-H^+][Br^-] (**3**·Br^-) was characterized as the main product. A subsequent peculiar bromination−dimerization process afforded the novel pyridyl-pyridinium cations {3,3′,5′-Br_3-1λ^4-[1,2′-(C_5H_4N)$_2$]-4,4′-(NH_2)$_2$}$^+$[X^-] (**4**·Br^-, **4**·Br_3^-) and {3′,5′-Br_2-1λ^4-[1,2′-(C_5H_4N)$_2$]-4,4′-(NH_2)$_2$}$^+$[X^-] (**5**·Br^-, **5**·Br_3^-). Compounds **1**−**5** as well as two protonated species, [4-NH_2-1λ^4-C_5H_4N-1-H^+]$_2$[Cl^-][I_3^-] (**3**$_2$·Cl^-·I_3^-) and [(4-NH_2-1λ^4-C_5H_4N)$_2$-1μ-H^+][I^-] (**6**·I^-), all display extended 3D networks supported by halogen and hydrogen bonding in the solid state.

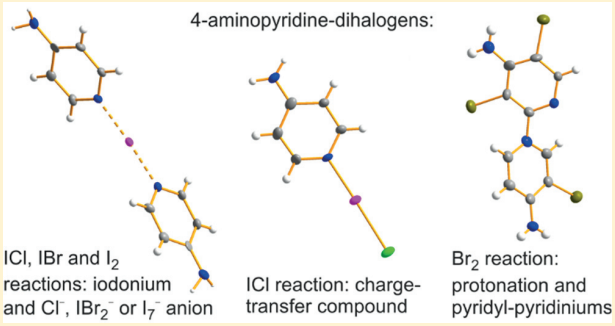

INTRODUCTION

The halogen bond (XB) was first discovered in 1863,[1] some 50 years before its conceptual congener, the hydrogen bond.[2] While the latter concept has drawn significantly more attention during the last century, the past few decades have also witnessed increasing interest toward both theoretical[3−10] and practical aspects of XB, especially through utilization of halogen bonds in building functional materials.[11−19] Accordingly, numerous applications in a variety of fields such as ion recognition,[20−26] optical materials,[27−30] organic synthesis and catalysis,[31] medicinal chemistry,[32−37] and crystal engineering and supramolecular chemistry[38−43] have been reported. It is evident that the halogen-bonding concept has grown from infancy to maturity. Owing to the versatility of adjustable properties, for example the directionality and strength of XB, halogen bonding has the potential to become as widely used a chemical tool as hydrogen bonding.

IUPAC's recent definition for the halogen bond describes it as an interaction between an electrophilic region of a polarized halogen atom (XB donor) and a nucleophilic region of another, or the same, molecular entity (XB acceptor).[44] Effectively this means that, somewhat counterintuitively, the XB donor (halogen atom) acts as the e^- acceptor and the XB acceptor is the e^- donor. Although the XB interaction is often considered to be primarily electrostatic in nature, the definition includes virtually all noncovalent electron donor−acceptor connections involving halogen atoms: for example, charge-transfer contacts and dispersion forces. Molecular properties of the XB components (electron delocalization, exchange repulsion, polarization, etc. of the XB donors and acceptors) are also contributing factors to the nature of halogen bonds.[7,45,46] Similarly to the perfluorohalocarbons, another widely used group of halogen compounds,[47] dihalogens (X_2) can act as halogen bond donors. In the case of X_2, the formation of a halogen bond is often understood as a charge-transfer process in which the XB acceptor donates electron density to the σ^* orbital of the X_2 molecule, providing the attractive electrostatic interaction between the XB components. At the very least the XB contact results in polarization and weakening in the X−X bond of dihalogen, but even heterolytic cleavage with the formation of ion pairs (X^+/X^- containing units) is commonly observed. Stabilization of the consequent halonium cation (X^+) typically requires the presence of two (or more) XB acceptors such as in the

Received: January 25, 2019
Revised: March 4, 2019
Published: March 8, 2019

Scheme 1. Reactions of 4-Aminopyridine (4-AP) with ICl, IBr, Br_2, and I_2 in CH_2Cl_2

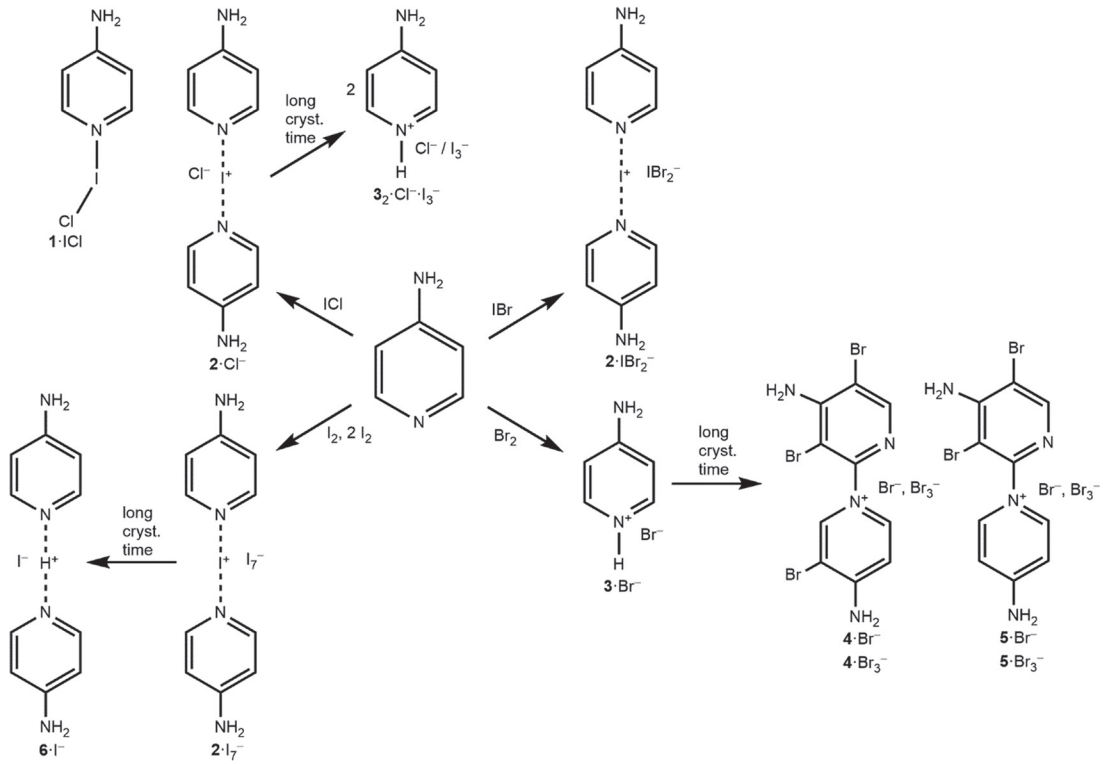

classical example of iodonium cation trapped between two pyridine nitrogen donors through N···I^+···N contacts.[48] Recent studies suggest that the N···X^+···N arrangement is comprised of a three-center–four-electron bond[49] that also can be utilized as useful XB donors.[38−43]

Halogen-bonded systems with X_2 molecules and charge distribution in X_2 and polyhalides have been extensively investigated.[50−57] However, to our knowledge systematic studies of the effect of charge distribution in dihalogens on the formation of halogen bonds are virtually nonexistent.[58] In this connection, we describe here our investigations of the reactions between 4-aminopyridine (4-AP) and heavier halogens and interhalogens, namely ICl, IBr, Br_2, and I_2, conducted in CH_2Cl_2. The reactions were monitored by ^{1}H NMR spectroscopy in solution, and the formation (Scheme 1) and single-crystal X-ray structures of [4-NH_2-1λ^4-C_5H_4N-1-ICl] (**1**·ICl), [(4-NH_2-1λ^4-C_5H_4N)$_2$-1μ-I^+][Cl^-] (**2**·Cl^-), [(4-NH_2-1λ^4-C_5H_4N)$_2$-1μ-I^+][IBr_2^-] (**2**·IBr_2^-), [(4-NH_2-1λ^4-C_5H_4N)$_2$-1μ-I^+][I_7^-] (**2**·I_7^-), [4-NH_2-1λ^4-C_5H_4N-1-H^+][Br^-] (**3**·Br^-), [4-NH_2-1λ^4-C_5H_4N-1-H^+]$_2$[Cl^-][I_3^-] (**3**$_2$·Cl^-·I_3^-), {3,3′,5′-Br_3-1λ^4-[1,2′-(C_5H_4N)$_2$]-4,4′-(NH_2)$_2$}$^+$[X^-] (**4**·Br^-, **4**·Br_3^-) and {3′,5′-Br_2-1λ^4-[1,2′-(C_5H_4N)$_2$]-4,4′-(NH_2)$_2$}$^+$[X^-] (**5**·Br^-, **5**·Br_3^-) and [(4-NH_2-1λ^4-C_5H_4N)$_2$-1μ-H^+][I^-] (**6**·I^-), as well as the main features of the halogen- and hydrogen-bonding-supported extended 3D networks, are discussed.

EXPERIMENTAL METHODS

Reagents and General Procedures. The reactions were carried out in air. All of the starting materials and solvents were purchased from commercial sources. Solvents were dried over 3 Å molecular sieves, and the remaining reagents were used without further purification: 4-aminopyridine (Aldrich, 98%), iodine monochloride (Aldrich, 98%), iodine monobromide (Aldrich, 98%), iodine (Merck, 99.999%), bromine (Fluka, >99%), MeCN (VWR Chemicals, 99.9%), Et_2O (Aldrich, >99.8%), CH_2Cl_2 (VWR Chemicals, 99%), hexanes (VWR Chemicals, 99%), THF (Aldrich, >99.9%), and toluene (Aldrich, >99.5%). Elemental analyses were performed by analytical services at the Department of Chemistry, University of Jyväskylä.

Spectroscopic Methods. The ^{1}H NMR spectra were obtained in CD_3CN at 30 °C and at −20 °C (ICl and IBr reactions only) on Bruker Avance III 300 and Bruker Avance III 500 spectrometers operating at 300.15 and 500.13 MHz, respectively. ^{1}H NMR spectra are referenced to the solvent signal, and the chemical shifts are reported relative to $(CH_3)_4Si$.

X-ray Crystallography. Crystallographic data for compounds **1**·ICl and **2**·Cl^-, **2**·Cl^-, **2**·IBr_2^-·mono, **2**·IBr_2^-·ortho, **3**$_2$·Cl^-·I_3^-, **3**·Br^-·CH_2Cl_2, **4**·Br^-, **4**·Br_3^-, **5**·Br^-, **5**·Br_3^-, and **6**·I^- are summarized in Tables S1 and S2 in the Supporting Information. Crystals were coated with FomblinY oil and mounted on a MiTeGen loop. Diffraction data were collected on an Agilent SuperNova Dual Source diffractometer equipped with Atlas CCD area detector using graphite-monochromatized Cu Kα radiation (λ = 1.54184 Å; **1**·ICl and **2**·Cl^-, **3**$_2$·Cl^-·I_3^-, **2**·IBr_2^-·mono, **2**·IBr_2^-·ortho, **3**·Br^-·CH_2Cl_2, **4**·Br^-, **4**·Br_3^-, **5**·Br^-, **5**·Br_3^-, and **6**·I^-) or Mo Kα radiation (λ = 0.71073 Å; **2**·Cl^- and **2**·I_7^-) at −150 °C. The data were processed by applying Gaussian absorption correction for compounds **2**·Cl^-, **2**·IBr_2^-·ortho, and **6**·I^- and by performing analytical numeric absorption correction for compounds **1**·ICl and **2**·Cl^-, **3**$_2$·Cl^-·I_3^-, **2**·IBr_2^-·mono, **4**·Br^-, **4**·Br_3^-, **5**·Br^-, **5**·Br_3^-, and **2**·I_7^- using a multifaceted crystal with the CrysAlisPro program.[59] All structures were solved by direct methods with SHELXS or SHELXT and refined by using SHELXL implemented in the Olex^2 program package.[60,61] After full-matrix least-squares refinement of the non-hydrogen atoms with anisotropic thermal parameters, the carbon-bound hydrogen atoms were placed in calculated positions (C−H = 0.93 Å). The nitrogen-bonded H atoms were located from the difference Fourier map for compounds **1**·ICl and **2**·Cl^-, **2**·Cl^-, **2**·IBr_2^-·mono, **2**·IBr_2^-·ortho, **4**·Br^-, **5**·Br_3^-, **2**·I_7^-, and **6**·I^-, while for compounds **3**$_2$·Cl^-·I_3^-, **4**·Br_3^-, and **5**·Br^- the −NH_2 hydrogens were calculated (N−H = 0.86 Å). The isotropic

DOI: 10.1021/acs.cgd.9b00119
Cryst. Growth Des. 2019, 19, 2434−2445

thermal parameters of the calculated hydrogen atoms were fixed at 1.2 times that of the corresponding carbon or nitrogen. In the final refinement, the calculated hydrogen atoms were riding on their respective carbon or nitrogen atoms, and the $-NH_2$ hydrogens located in the difference Fourier map were refined as isotropic with case-specific restrictions in the N−H bond distances.

Reaction of 4-AP with ICl in 1:1 Molar Ratio. A solution of ICl (0.162 g, 1.00 mmol) in 10 mL of CH_2Cl_2 was added dropwise to a solution of 4-AP (0.094 g, 1.00 mmol) in 10 mL of CH_2Cl_2 at 23 °C. The reaction mixture was stirred for 2 h, giving a red solution and a pale red precipitate. The solvent was decanted, and the solid product was dried under vacuum to afford 0.115 g of a red powder (45%, calculated as an equimolar mixture of the starting materials). The solvent portion was evaporated and dried under vacuum, giving a brown powder (0.051 g) that was shown by ^{1}H NMR spectroscopy to contain primarily only one of the products observed in the initial powder (^{1}H NMR of the solvent portion (CD_3CN, 30 °C): δ 8.04 [m, 2H, $-C_5H_4N$], δ 6.56 [m, 2H, $-C_5H_4N$], δ 5.76 [s, br, 2H, $-NH_2$]). Anal. Calcd for $C_{20}H_{24}N_8Cl_3I_3$ (calculated as a 2:1 mixture of [4-NH_2-1λ^4-C_5H_4N-1-ICl] (**1**·ICl) and [(4-NH_2-1λ^4-C_5H_4N)$_2$-1μ-I^+][Cl^-] (**2**·Cl^-)): C, 27.82; H, 2.80; N, 12.98. Found: C, 27.64; H, 2.83; N, 13.10. ^{1}H NMR of the initial powder (CD_3CN, 30 °C): δ 8.06 [m, 4H, $-C_5H_4N$], δ 6.58 [m, 4H, $-C_5H_4N$], δ 5.72 [s, br, 2H, $-NH_2$], δ 5.32 [s, br, 2H, $-NH_2$]. ^{1}H NMR of the initial powder (CD_3CN, −20 °C): δ 8.06 [m, 2H, $-C_5H_4N$], δ 7.98 [m, 2H, $-C_5H_4N$], δ 6.61 [m, 2H, $-C_5H_4N$], δ 6.52 [m, 2H, $-C_5H_4N$], δ 5.88 [s, br, 2H, $-NH_2$], δ 5.53 [s, br, 2H, $-NH_2$]. X-ray-quality crystals of cocrystalline [4-NH_2-1λ^4-C_5H_4N-1-ICl] (**1**·ICl) and [(4-NH_2-1λ^4-C_5H_4N)$_2$-1μ-I^+][Cl^-] (**2**·Cl^-) in a 1:1 molar ratio were obtained by slow evaporation of an MeCN solution at 23 °C. The crystals containing solely [(4-NH_2-1λ^4-C_5H_4N)$_2$-1μ-I^+][Cl^-] (**2**·Cl^-) were grown by diffusion from an MeCN solution layered with Et_2O. Extended crystallization time afforded protonation of the 4-aminopyridine; the crystals of [(4-NH_2-1λ^4-C_5H_4N-1-H)$^+$]$_2$[Cl^-][I_3^-] (**3**$_2$·Cl^-·I_3^-) were obtained by evaporation of a toluene solution at 23 °C.

Reaction of 4-AP with IBr in 1:1 Molar Ratio. A solution of IBr (0.207 g, 1.00 mmol) in 10 mL of CH_2Cl_2 was added dropwise to a solution of 4-AP (0.094 g, 1.00 mmol) in 5 mL of CH_2Cl_2 at 23 °C. The resulting orange reaction mixture was stirred for 2 h. The solvent was decanted, and the solid product was dried under vacuum to afford a pale orange powder. The solvent portion was allowed to evaporate under ambient conditions over a period of 3 days, giving an orange powder that was shown by NMR spectroscopy to be identical with that of the solution portion (combined yield 0.237 g, 79%, calculated as an equimolar mixture of the starting materials). Anal. Calcd for $C_5H_6N_2BrI$: C, 19.96; H, 2.01; N, 9.31. Found: C, 19.91; H, 2.13; N, 9.40. ^{1}H NMR (CD_3CN, 30 °C): δ 8.05 [s, br, 2H, $-C_5H_4N$], δ 6.57 [s, br, 2H, $-C_5H_4N$], δ 5.83 [s, br, 1H, $-NH_2$], δ 5.70 [s, br, 1H, $-NH_2$]. ^{1}H NMR (CD_3CN, −20 °C): δ 8.03 [m, 2H, $-C_5H_4N$], δ 6.54 [m, 2H, $-C_5H_4N$], δ 5.93 [s, br, 1H, $-NH_2$], δ 5.83 [s, br, 1H, $-NH_2$]. X-ray-quality crystals of two polymorphs of [(4-NH_2-1λ^4-C_5H_4N)$_2$-1μ-I^+][IBr_2^-] (**2**·IBr_2^-) (monoclinic and orthorhombic; **2**·IBr_2^-·mono, **2**·IBr_2^-·ortho) were both obtained by slow evaporation of a CH_2Cl_2 solution at 23 °C.

Reaction of 4-AP with Br_2 in 1:1 Molar Ratio. A solution of Br_2 (0.052 mL, 0.160 g, 1.00 mmol) in 5 mL of CH_2Cl_2 was added dropwise to a solution of 4-AP (0.094 g, 1.00 mmol) in 5 mL of CH_2Cl_2 at 23 °C. The reaction mixture was stirred for 2 h, giving an orange solution and a yellow precipitate. The solvent was decanted, and the solid product was dried under vacuum to afford an orange-yellow powder (0.187 g, 74%, calculated as a 1:1 adduct of the starting materials). Anal. Calcd for $C_{20}H_{28}N_8Br_{10}$: C, 20.37; H, 2.39; N, 9.50. Found: C, 19.99; H, 2.21; N, 9.67. ^{1}H NMR (CD_3CN, 30 °C): δ 11.29 [m, br, 1H, $C_5H_4NH^+$], δ 7.94 [m, 2H, $C_5H_4NH^+$], δ 6.85 [m, 2H, $C_5H_4NH^+$], δ 6.60 [s, br, 2H, $-NH_2$]. X-ray-quality crystals of the initial main product, [4-NH_2-1λ^4-C_5H_4N-1-H$^+$][Br^-] (**3**·Br^-), were obtained by slow diffusion from THF solution layered with CH_2Cl_2 at 23 °C. Longer crystallization times resulted in the formation of brominated pyridyl-pyridinium cations: tribromides {3,3′,5′-Br_3-1λ^4-[1,2′-(C_5H_4N)$_2$]-4,4′-(NH_2)$_2$}$^+$[X^-] (**4**·Br^-, **4**·Br_3^-) by slow evaporation of MeCN (**4**·Br^-) and CH_2Cl_2 (**4**·Br_3^-) solutions and dibromides {3′,5′-Br_2-1λ^4-[1,2′-(C_5H_4N)$_2$]-4,4′-(NH_2)$_2$}$^+$[X^-] (**5**·Br^-, **5**·Br_3^-) by slow diffusion from an MeCN solution layered with Et_2O (**5**·Br^-) and a CH_2Cl_2 solution layered with hexanes (**5**·Br_3^-) at 23 °C.

Reaction of 4-AP with I_2 in 1:1 Molar Ratio. A solution of I_2 (0.254 g, 1.00 mmol) in 10 mL of CH_2Cl_2 was added dropwise to a solution of 4-AP (0.094 g, 1.00 mmol) in 5 mL of CH_2Cl_2 at 23 °C. The reaction mixture was stirred for 2 h, giving a brownish yellow solution and a brown precipitate. The solvent was decanted, and the product was dried under vacuum to afford a brown powder (0.215 g, 62%, calculated as a 1:1 adduct of the starting materials). Anal. Calcd for $C_5H_6N_2I_2$: C, 17.26; H, 1.74; N, 8.05. Found: C, 17.03; H, 1.86; N, 8.07. ^{1}H NMR (CD_3CN, 30 °C): δ 8.05 [m, 2H, C_5H_4N], 8.01 [m, 2H, C_5H_4N], δ 6.57 [m, 4H, C_5H_4N], δ 5.83 [s, br, 2H, $-NH_2$], δ 5.51 [s, br, 2H, $-NH_2$]. Prolonged crystallization times resulted in the formation of protonated 4-aminopyridines that were not detectable in the initial product (^{1}H NMR). X-ray-quality crystals of [(4-NH_2-1λ^4-C_5H_4N)$_2$-1μ-H$^+$][I^-] (**6**·I^-) were obtained by slow evaporation (ca. 8 days) of a CH_2Cl_2 solution at 23 °C. Also, crystals of the previously determined salt of the 4-aminopyridinium species [4-NH_2-1λ^4-C_5H_4N-1-H$^+$]$_2$[I^-][I_3^-] (**3**$_2$·I^-·I_3^-; structure code WULTEE in the CSD database)[62] were detected on the basis of the unit cell measurements.

Reaction of 4-AP with I_2 in 1:2 Molar Ratio. Due to the apparent two products from the reaction of 4-AP and I_2 in a 1:1 molar ratio (as indicated by NMR spectroscopy), the reaction was repeated in a 1:2 molar ratio. A solution of 4-AP (0.047 g, 0.50 mmol) in 10 mL of CH_2Cl_2 was added dropwise to a solution of I_2 (0.254 g, 1.00 mmol) in 10 mL of CH_2Cl_2 at 23 °C. The reaction mixture was stirred for 2 h, giving a red solution and a dark brown precipitate. Solvent was evaporated under vacuum to afford a dark red powder (0.263 g, 87%). Anal. Calcd for $C_5H_6N_2I_4$: C, 9.98; H, 1.01; N, 4.66. Found: C, 10.72; H, 1.32; N, 4.98. ^{1}H NMR (CD_3CN, 30 °C): δ 8.04 [m, 2H, C_5H_4N], 6.59 [m, 2H, C_5H_4N], δ 5.82 [s, br, 2H, $-NH_2$]. X-ray-quality crystals of [(4-NH_2-1λ^4-C_5H_4N)$_2$-1μ-I^+][I_7^-] (**2**·I_7^-) were obtained by slow evaporation from a CH_2Cl_2 solution at 23 °C.

RESULTS AND DISCUSSION

Reaction of 4-AP with ICl: Formation and Structural Characterization of [4-NH_2-1λ^4-C_5H_4N-1-ICl] (1·ICl), [(4-NH_2-1λ^4-C_5H_4N)$_2$-1-μ-I^+][Cl^-] (2·Cl^-), and [(4-NH_2-1λ^4-C_5H_4N-1-H)$^+$]$_2$[Cl^-][I_3^-] (3$_2$·Cl^-·I_3^-). The reaction of 4-AP with 1 equiv of ICl was carried out in CH_2Cl_2 to afford a red solution and pale red precipitate. The ^{1}H NMR spectrum of the initial powder in CD_3CN at 30 °C displays two sets of multiplets arising from the pyridine hydrogens in the range of 6.58−8.06 ppm as well as two singlets at δ 5.32 and 5.72 for the amine groups in an approximate ratio of 4:4:2:2 (Figure S3). At −20 °C, the signals in the range of 6.58−8.06 ppm show further splitting into four multiplets, while the singlets arising from NH_2 groups remain unchanged, giving six signals in equal intensity altogether (Figure S4). Consequently, the ^{1}H NMR data suggest the presence of two independent 4-AP units in the initial reaction powder. Workup of the solution portion (see Experimental Methods) resulted in a brown solid which, on the basis of the ^{1}H NMR spectrum, contained primarily only one of the products observed in the powder portion.

Crystallization efforts of the initial pale red powder in various organic solvents (see Experimental Methods) afforded three different sets of crystals: (1) a structure consisting of a mixture of direct charge-transfer adduct between 4-AP and ICl, [4-NH_2-1λ^4-C_5H_4N-1-ICl] (**1**·ICl), *and* an ionic compound in which the I^+ cation is trapped between two 4-AP units through N···I^+···N contacts, [(4-NH_2-1λ^4-C_5H_4N)$_2$-1μ-I^+][Cl^-] (**2**·Cl^-), *both in the same crystal lattice* (Figure 1a,b), (2) a

DOI: 10.1021/acs.cgd.9b00119
Cryst. Growth Des. 2019, 19, 2434−2445

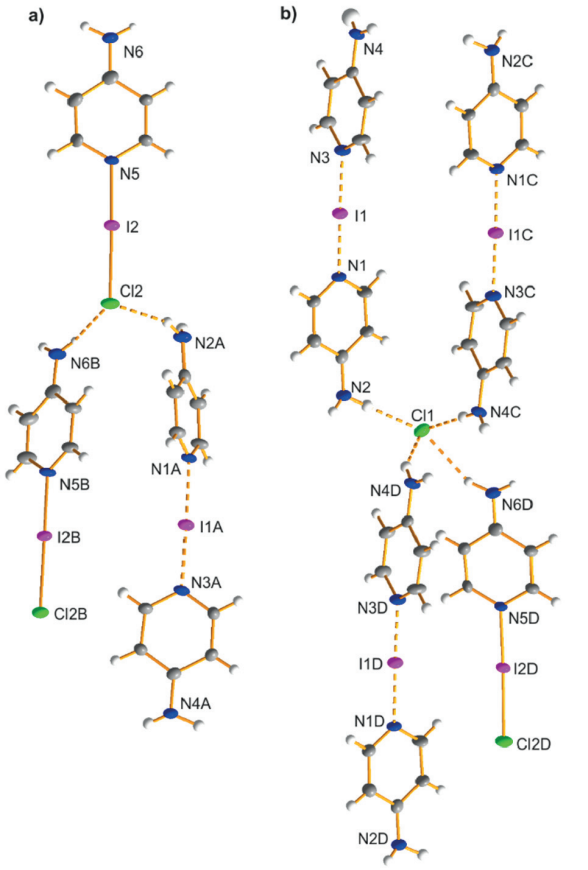

Figure 1. Crystal structure of the cocrystalline **1**·ICl and **2**·Cl^- showing NH···Cl contacts of (a) the charge-transfer unit and (b) the Cl^- anion. Symmetry operations: (A) $1 - x$, $0.5 + y$, $2.5 - z$; (B) $1 + x$, $0.5 - y$, $0.5 + z$; (C) $-x$, $-y$, $2 - z$; (D) $1 + x$, y, $1 + y$.

structure containing solely the I^+/Cl^- ion pair in **2**·Cl^- (Figure 2), and (3) a protonated 4-AP cation with Cl^- and I_3^- counterions in $[(4\text{-}NH_2\text{-}1\lambda^4\text{-}C_5H_4N\text{-}1\text{-}H)^+]_2[Cl^-][I_3^-]$ (**3**$_2$·Cl^-·I_3^-, Figure 3). While the formation of both **1**·ICl and **2**·Cl^- is consistent with the observed ^{1}H NMR spectrum of the pale red powder, no protonation of 4-AP is evident in the initial product. Therefore, the appearance of **3**$_2$·Cl^-·I_3^- is likely a result of the prolonged crystallization process (Scheme 1). Furthermore, elemental analysis suggests a 2:1 molar ratio between the adduct **1**·ICl and the ionic form **2**·Cl^-, which is in excellent correspondence with the NMR spectroscopic data; the ^{1}H NMR spectrum of the pale red powder displays a 1:1 intensity ratio for the two independent $-NH_2$ singlets arising from the 2:1 molar ratio of **1**·ICl and **2**·Cl^- due to the one 4-AP unit in the former compound and two 4-AP molecules in the latter compound. Taken together, these data indicate that the equimolar reaction between 4-AP and ICl in CH_2Cl_2 in fact takes place in a 3:2 molar ratio initially. However, as evidenced by the single crystals containing only the ionic form **2**·Cl^-, the reaction likely does eventually proceed to create the I^+/Cl^- ion pair and the compound **2**·Cl^- as the final product.

The unusual combination of the charge-transfer compound **1**·ICl and the N···I^+···N-bridged **2**·Cl^- crystallizes in the centrosymmetric space group $P2_1/c$ in an equimolar ratio of the two constituents (Figure 1). The two components are organized rather randomly in discrete strands of **1**·ICl and **2**·

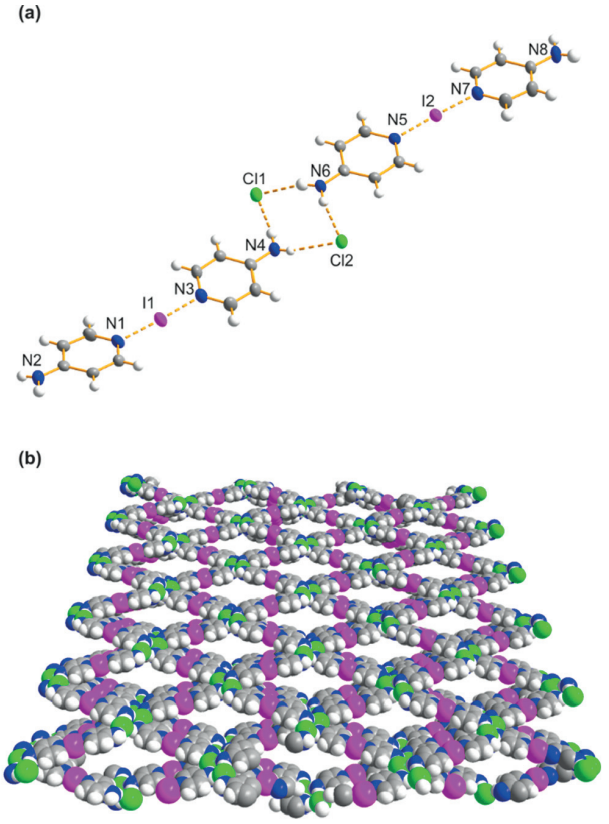

Figure 2. (a) Part of a single strand in **2**·Cl^- and (b) a space-filling depiction showing the perpendicular formation of strands through NH···Cl interactions (van der Waals radii used (in Å): I, 1.98; N, 1.55; C, 1.70; H, 1.20; Cl, 1.75).

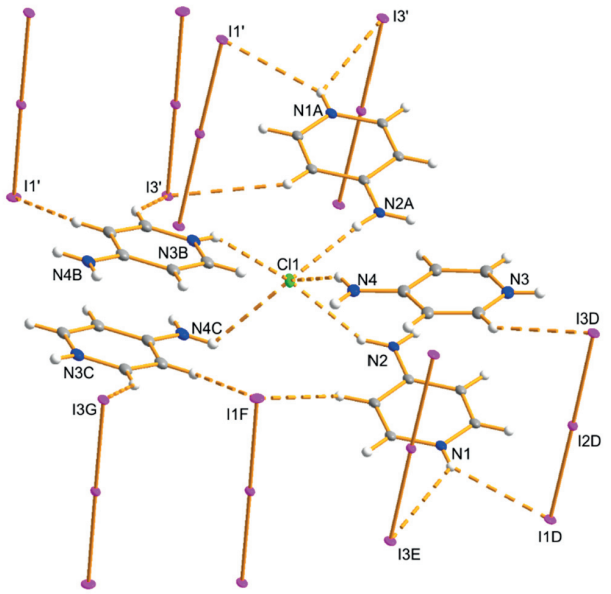

Figure 3. Crystal structure of **3**$_2$·Cl^-·I_3^- showing NH···Cl and NH···I contacts. Symmetry operations: (A) $-1 - x$, $-y$, $-z$; (B) $-1 - x$, $0.5 + y$, $-0.5 - z$; (C) x, $0.5 - y$, $0.5 + z$; (D) $-x$, $-y$, $-z$; (E) x, y, $-1 + z$, (F) x, $0.5 - y$, $-0.5 + z$; (G) $-x$, $0.5 + y$, $0.5 - z$.

DOI: 10.1021/acs.cgd.9b00119
Cryst. Growth Des. 2019, 19, 2434−2445

Table 1. Pertinent Bond Parameters and Close Contacts (in Å and deg) for the Cocrystalline [4-NH_2-1λ^4-C_5H_4N-1-ICl] (**1**·ICl), [(4-NH_2-1λ^4-C_5H_4N)$_2$-1μ-I^+][Cl^-] (**2**·Cl^-), [(4-NH_2-1λ^4-C_5H_4N)$_2$-1μ-I^+][Cl^-] (**2**·Cl^-), and [4-NH_2-1λ^4-C_5H_4N-1-H^+]$_2$[Cl^-][I_3^-] (**3**$_2$·Cl^-·I_3^-) from ICl Reaction[a]

1·ICl/**2**·Cl^- [b]		**2**·Cl^-		**3**$_2$·Cl^-·I_3^- [c]	
N1···I1	2.269(5) [*0.64*, 0.48]	N1···I1	2.250(3) [*0.64*, 0.51]	N1···I1D	3.690(5)
N3···I1	2.240(5) [*0.64*, 0.52]	N3···I1	2.246(3) [*0.64*, 0.51]	N1···I3E	3.782(5)
N5−I2	2.186(5) [*0.62*, 0.62]	N5···I2	2.254(2) [*0.64*, 0.50]	N2···Cl1	3.275(5)
I2−Cl2	2.634(1) [*0.71*, 0.36]	N7···I2	2.240(3) [*0.64*, 0.52]	N2A···Cl1	3.272(5)
N2···Cl1	3.284(5)	N4···Cl1	3.266(3)	N3B···Cl1	3.176(6)
N4C···Cl1	3.340(6)	N4···Cl2	3.279(3)	N4···Cl1	3.314(6)
N6D···Cl1	3.276(5)	N6···Cl1	3.230(3)	N4C···Cl1	3.393(5)
N2A···Cl2	3.349(6)	N6···Cl2	3.243(3)	I1−I2	2.9557(3)
N6B···Cl2	3.328(6)			I2−I3	2.9053(5)
N5−I2−Cl2	178.4(1)	N1···I1···N3	177.2(1)	I1−I2−I3	179.27(2)
N1···I1···N3	178.3(2)	N5···I2···N7	177.8(1)	N1···H···I1D	134.6
N2A···H2′···Cl2	158(7)	N4···H4···Cl1	166(3)	N1···H···I3E	130.7
N2···H2···Cl1	177(8)	N4···H4′···Cl2	171(3)	N2···H···Cl1	150.5
N4C···H4···Cl1	176(8)	N6···H6···Cl1	163(3)	N2A···H′···Cl1	161.9
N4D···H4′···Cl1	155(11)	N4···H6′···Cl2	170(3)	N3B···H···Cl1	125.7
N6B···H6···Cl2	163(6)			N4···H···Cl1	152.8
N6D···H6′···Cl1	156(7)			N4C···H′···Cl1	123.7

[a] R_{XB} values (in italics) to evaluate the strength of halogen bonds and calculated bond orders are shown in brackets. $R_{XB} = d_{XB}/(X_{vdW} + B_{vdW})$, where R_{XB} = strength of XB, d_{XB} = XB distance, and X_{vdW} and B_{vdW} = van der Waals radii of X and B, respectively.[67−69] Bond orders were calculated by the Pauling equation $N = 10^{(D-R)}/0.71$,[70] where R = the observed bond length (Å) and D = theoretical single-bond length estimated by the sums of appropriate covalent radii (Å):[71] N−I, 2.04; I−Cl, 2.32. [b] Symmetry operations: (A) $1 - x, 0.5 + y, 2.5 - z$, (B) $1 + x, 0.5 - y, 0.5 + z$; (C) $-x, -y, 2 - z$; (D) $1 + x, y, 1 + y$. [c] Symmetry operations: (A) $-1 - x, -y, -z$; (B) $-1 - x, 0.5 + y, -0.5 - z$; (C) $x, 0.5 - y, 0.5 + z$, (D) $-x, -y, -z$; (E) $x, y, -1 + z$.

Cl^-, respectively, with two orientations for both compounds. The two pyridine rings around the bridging N···I^+···N unit in **2**·Cl^- are hinged close to 90° with respect to each other (cf. Figure S1 in the Supporting Information). Overall, the crystal packing is primarily guided by six discrete NH_2···Cl hydrogen bonds averaging at ca. 2.43 Å (d(Cl···N) = 3.284(5)−3.349(6) Å, Table 1). The N···I^+···N distances of 2.269(5) and 2.240(5) Å in the ionic **2**·Cl^- are equal within the standard deviation and, expectedly, they are somewhat longer than the corresponding N5−I2 bond length of 2.186(5) Å in the charge-transfer component **1**·ICl (Table 1). The adjacent I2−Cl2 contact in **1**·ICl displays a distance of 2.634(1) Å. Both the N5−I2−Cl2 unit in **1**·ICl and the N1···I1···N3 portion of **2**·Cl^- are nearly linear at 178.4(1) and 178.3(2)°, respectively.

The ionic N···I^+···N bridging compound **2**·Cl^- was also obtained as an independent species in tetragonal space group $I4_1/a$ after an extended crystallization period (Figure 2). This centrosymmetric structure displays three discrete [(4-NH_2-1λ^4-C_5H_4N)$_2$-1μ-I^+][Cl^-] ion pairs, one of which is created by symmetry. The **2**·Cl^- units form a 2D network of cross-linking strands (Figure 2b) through 10 discrete hydrogen bonds with the amine NH_2···Cl distances between 2.36(4) and 2.58(3) Å (d(Cl···N) = 3.230(3)−3.352(3) Å, Table S4). In this instance, the pyridine rings in the [(4-NH_2-1λ^4-C_5H_4N)$_2$-1μ-I^+] cations are nearly coplanar and the almost linear N···I^+···N contacts (177.2(1)−180°) show distances of 2.240(3)−2.254(2) Å that are essentially equal with the corresponding contacts in the **2**·Cl^- component of the cocrystalline structure containing both **1**·ICl and **2**·Cl^- (Table 1). A search of the CSD database reveals 16 crystal structures of pyridine[39] and pyridine derivatives (including 2,4,6-Me_3-PY,[63,64] 2,6-Me_2-PY,[65] 4-Me_2N-PY,[66] 4-MeO-PY,[43] and 4-CF_3-PY[43]) with various counteranions containing the N···I^+···N bridging unit analogous to that in **2**·Cl^-. The pertinent bond parameters in **2**·Cl^- are essentially equal with those reported earlier and support the description of a three-center−four-electron bonding situation in the bridging N···I^+···N unit.[39,43,63−66]

In an effort to evaluate the relative strengths of the N···I and I···Cl contacts in **1**·ICl and **2**·Cl^-, the R_{XB} values for halogen bond strength[67−69] and the Pauling bond orders[70] were calculated (cf. selected values in square bracket in Table 1 and a more comprehensive list in Table S3). The N···I^+···N close contacts in **2**·Cl^- exhibit R_{XB} values of 0.64 and the Pauling bond order averages 0.50, while the analogous values in **1**·ICl are 0.62 (R_{XB}) and 0.62 (bo) for the N5−I2 bond and 0.71 (R_{XB}) and 0.39 (bo) for the I2−Cl2 contact. All these values are indicative of a bonding situation in which the (4-AP)N−I(Cl) bond in **1**·ICl is approaching a covalent single bond, resulting in significant weakening of the adjacent, highly polar I···Cl contact as is typical for a halogen bond.

Although the ionic compound **2**·Cl^- is likely the end product from the reaction between 4-AP and ICl, a prolonged crystallization time does result in protonation and formation of [4-NH_2-1λ^4-C_5H_4N-1-H^+]$_2$[Cl^-][I_3^-] (**3**$_2$·Cl^-·I_3^-, Figure 3). The crystal structure of **3**$_2$·Cl^-·I_3^- consists of two aminopyridinium cations and Cl^- and I_3^- counteranions. The ionic compound crystallizes in the monoclinic space group $P2_1/c$, and the extended 3D network is formed primarily through weak NH···Cl hydrogen bonds (d(N···Cl) = 3.176(6)−3.393(5) Å, Table S4) from both the $-NH_2$ unit and the protonated N atom of the pyridine ring. All of the NH···I close contacts to the I_3^- anion are relatively weak and likely mainly created by the crystal-packing forces.

DOI: 10.1021/acs.cgd.9b00119
Cryst. Growth Des. 2019, 19, 2434−2445

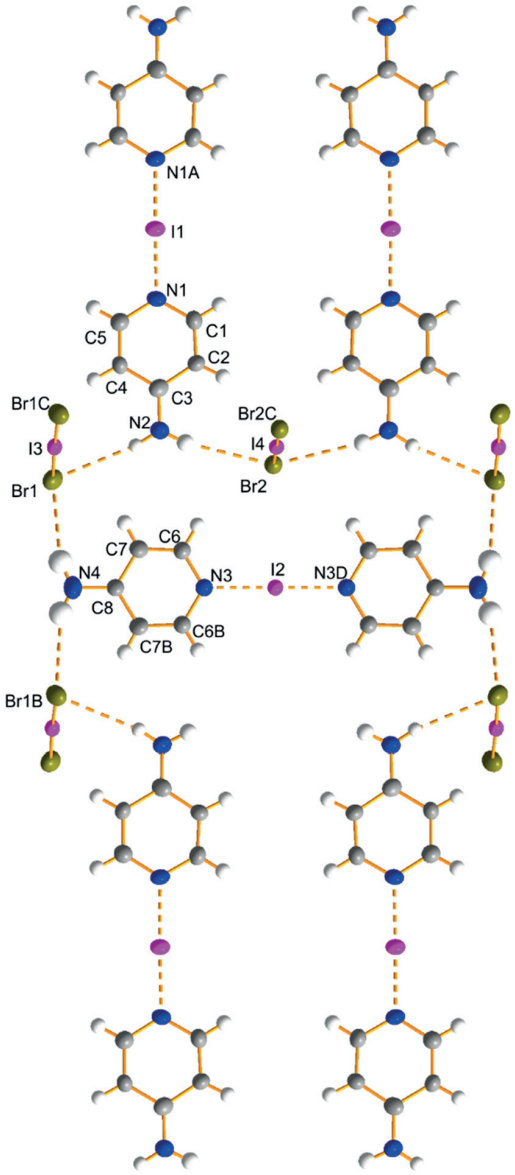

Figure 4. Crystal structure of the monoclinic **2**·IBr_2^-. Symmetry operations: (A) 1 − *x*, *y*, 1 − *z*; (B) 2 − *x*, *y*, −1 − *z*; (C) 2 − *x*, *y*, −*z*; (D) 2 − *x*,1 − *y*, −1 − *z*.

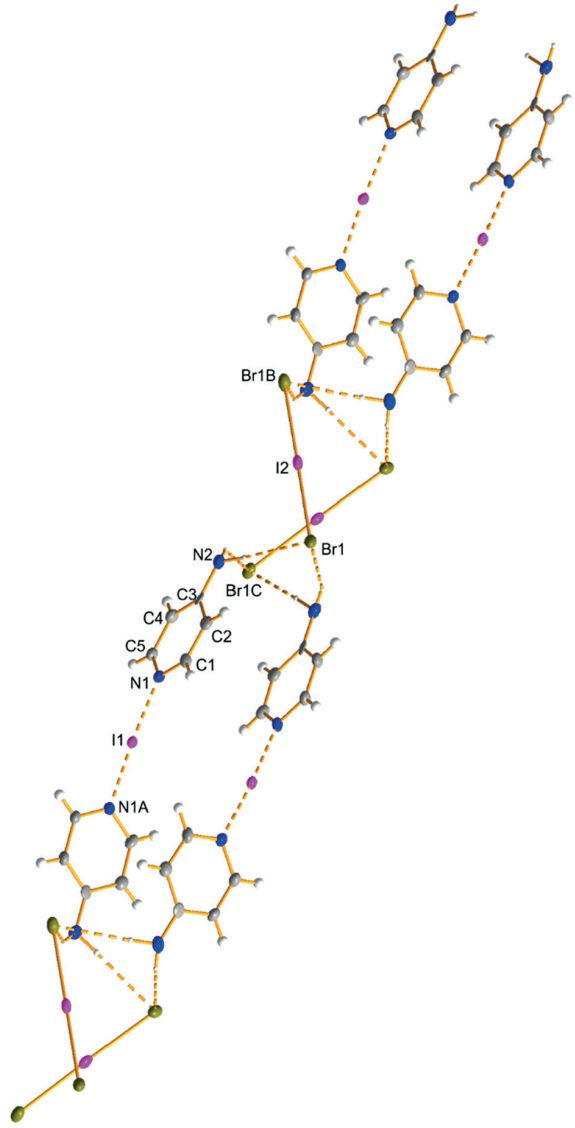

Figure 5. Crystal structure of the orthorhombic **2**·IBr_2^-. Symmetry operations: (A) 0.75 − *x*, 0.75 − *y*, *z*; (B) *x*, 1.75 − *y*, 0.75 − *z*; (C) 0.75 − *x*, *y*, 0.75 − *z*.

Reaction of 4-AP with IBr: Formation and Structural Characterization of Two Polymorphs of [(4-NH_2-1λ^4-C_5H_4N)$_2$-1μ-I^+][IBr_2^-] (2·IBr_2^-). The reaction of 4-AP and 1 equiv of IBr was carried out in CH_2Cl_2 to afford an orange precipitate in good yield (79%). The ^{1}H NMR spectrum of the product in CD_3CN at 30 °C displays two multiplets arising from the pyridine hydrogens at 6.57 and 8.05 ppm as well as two singlets at δ 5.70 and 5.83 for the amine groups in a 2:2:1:1 ratio (Figure S5). In contrast to the reaction with ICl, no further splitting of the signals is observed at −20 °C (Figure S6), therefore suggesting the formation of only one 4-AP ring with two inequivalent hydrogen atoms in the $-NH_2$ group on the NMR time scale.

Consistently with the formation of **2**·Cl^-, crystallization of the orange powder by slow evaporation of a CH_2Cl_2 solution revealed the existence of the congeneric N···I^+···N bridged cation with a polyhalide counteranion in [(4-NH_2-1λ^4-C_5H_4N)$_2$-1μ-I^+][IBr_2^-] (**2**·IBr_2^-, Figures 4 and 5). Two sets of crystals with different morphologies were obtained, yellow plates and orange block-shaped crystals, that were identified as monoclinic and orthorhombic polymorphs of **2**·IBr_2^-, respectively. In contrast to the reaction between 4-AP and ICl, no charge-transfer product analogous to **1**·ICl is observable in the reaction with IBr in the solid state or in solution (NMR spectroscopy). This is somewhat counterintuitive, given the higher polarity of ICl in comparison to IBr, but can, possibly, be contributed to the easier formation of the polyiodide anion IBr_2^- and therefore faster ionization process in the latter reaction (cf. Conclusions). Notably, recently reported experiments performed under similar conditions between the bare, unsubstituted pyridine and ICl or IBr resulted in the isolation of only the simple adducts [C_5H_4N-1-IX] (X = Cl, Br), without any evidence of ionization.[72] A

DOI: 10.1021/acs.cgd.9b00119
Cryst. Growth Des. 2019, 19, 2434−2445

Table 2. Pertinent Bond Parameters and Close Contacts (in Å and deg) for $[(4\text{-}NH_2\text{-}1\lambda^4\text{-}C_5H_4N)_2\text{-}1\mu\text{-}I^+][IBr_2^-]$ ($2\cdot IBr_2^-$·mono and $2\cdot IBr_2^-$·ortho), $[(4\text{-}NH_2\text{-}1\lambda^4\text{-}C_5H_4N)_2\text{-}1\mu\text{-}I^+][I_7^-]$ ($2\cdot I_7^-$), and $[(4\text{-}NH_2\text{-}1\lambda^4\text{-}C_5H_4N)_2\text{-}1\mu\text{-}H^+][I^-]$ ($6\cdot I^-$) from IBr and I_2 Reactions

$2\cdot IBr_2^-$·mono[a]		$2\cdot IBr_2^-$·ortho[b]		$2\cdot I_7^-$ [c]		$6\cdot I^-$ [d]	
N1···I1	2.242(7)	N1···I1	2.244(5)	N1···I1	2.243(5)	N1···H1	1.32(5)
N3···I2	2.228(9)	N2···Br1	3.589(6)	N2···I2	3.974(6)	N1···N3	2.662(5)
N2···Br1	3.693(7)	N2···Br1C	3.593(6)	N2···I3	3.711(6)	N2···I1	3.731(4)
N2···Br2	3.782(7)	Br1−I2	2.7309(6)	N2···I5	3.962(6)	N2···I1A	3.641(4)
N4···Br1	3.746(2)			I2−I3	2.7535(6)	N4···I1	3.667(4)
Br1−I3	2.710(1)			I4−I5	2.9273(4)	N4···I1A	3.684(4)
Br2−I4	2.753(1)			I3···I4	3.2804(6)		
N1···I1···N1A	179.0(3)	N1···I1···N1A	176.4(2)	N1···I1···N1A	180.0(2)	N1···H1···N3	160.7
N3···I2···N3A	180	Br1−I2−Br1B	176.54(3)	I4−I5−I4B	180.00(1)	N2···H···I1	174(5)
Br1−I3−Br1C	178.5(1)	N2···H···Br1	172(6)	N2···H···I2	155(7)	N2···H	165(5)
Br2−I4−Br2C	180.0(1)	N2···H′···Br1C	140(6)	N2···H···I3	131(8)	N4···H′···I1A···I1	166(4)
N2···H···Br1	170(8)			N2···H′···I5	152(6)	N4···H′···I1A	165(4)
N2···H′···Br2	169(10)			I3···I4−I5	90.61(1)		
				I2−I3···I4	171.58(2)		

[a]Symmetry operations: (A) $1-x, y, 1-z$; (B) $2-x, y, -1-z$; (C) $2-x, y, -z$; (D) $2-x, 1-y, -1-z$. [b]Symmetry operations: (A) $0.75-x, 0.75-y, z$; (B) $x, 1.75-y, 0.75-z$; (C) $0.75-x, y, 0.75-z$. [c]Symmetry operations: (A) $2-x, 1-y, 2-z$; (B) $-1-x, 1-y, 1-z$. [d]Symmetry operations: (A) $0.5-x, -1.5+y, 1.5-z$; (B) $0.5-x, 0.5+y, 1.5-z$.

further literature survey on the reactions of pyridine derivatives with dihalogens reveals a fine balance between charge-transfer adducts similar to **1**·ICl and the ionic species containing the cation **2**: while pyridine and pyridine derivatives 2,4,6-Me_3-PY, 3-Br-PY, and 4-Me_2N-PY prefer charge-transfer complexes, the 2,6-Me_2-PY congener forms ionic species with the N···I^+···N unit similarly to 4-AP.[72,73]

The centrosymmetric, monoclinic polymorph of $2\cdot IBr_2^-$ displays two parallel strands of the $[(4\text{-}NH_2\text{-}1\lambda^4\text{-}C_5H_4N)_2\text{-}1\mu\text{-}I^+]$ units which are separated by analogous, perpendicular cations (Figure 4). The spatial arrangement of the components takes place through weak NH···Br contacts (d(N···Br) = 3.693(7)−3.782(7) Å, Table 2) between the cations and IBr_2^- anions. Slight slippage of the layered strands prevents significant $\pi-\pi$ interactions between the 4-AP rings. The orthorhombic polymorph of $2\cdot IBr_2^-$ (Figure 5) also crystallizes in a centrosymmetric space group (*Fddd*). The NH···Br connections are somewhat stronger than in the monoclinic form with d(N···Br) = 3.589(6) and 3.593(6) Å. The N···I^+···N distances of 2.228(9)−2.244(5) Å as well as the linearity of this unit (176.2(4)−180°) are analogous to those in $2\cdot Cl^-$. Unsurprisingly, the I−Br bond lengths (2.7309(6)−2.753(1) Å) in both polymorphs of $2\cdot IBr_2^-$ show typical values for the polyhalide anion.[65]

Reaction of 4-AP with Br_2: Formation and Crystal Structures of $[4\text{-}NH_2\text{-}1\lambda^4\text{-}C_5H_4N\text{-}1\text{-}H^+][Br^-]$ ($3\cdot Br^-$), $\{3,3',5'\text{-}Br_3\text{-}1\lambda^4\text{-}[1,2'\text{-}(C_5H_4N)_2]\text{-}4,4'\text{-}(NH_2)_2\}^+[X^-]$ ($4\cdot Br^-$, $4\cdot Br_3^-$), and $\{3',5'\text{-}Br_2\text{-}1\lambda^4\text{-}[1,2'\text{-}(C_5H_4N)_2]\text{-}4,4'\text{-}(NH_2)_2\}^+[X^-]$ ($5\cdot Br^-$, $5\cdot Br_3^-$). The reaction of 4-AP with 1 equiv of Br_2 was carried out in CH_2Cl_2 to afford a yellow powder in good yield (74%, calculated as $3\cdot Br^-$). The ^{1}H NMR spectrum of the product in CD_3CN (Figure S7) displays typical signal patterns for the pyridine hydrogens at 6.85 and 7.94 ppm and a singlet at 6.60 ppm for the amine group. In addition, a broad multiplet at δ 11.29 with ca. half the intensity in comparison to the other signals was observable in the ^{1}H NMR spectrum, suggesting that protonation of 4-AP has occurred during the reaction.

Crystallization of the yellow product by slow diffusion of THF solution layered with CH_2Cl_2 confirmed that, in contrast to the reactions of 4-AP with interhalogens ICl and IBr, the analogous mixture with Br_2 results in an immediate protonation of the 4-AP unit and formation of $[4\text{-}NH_2\text{-}1\lambda^4\text{-}C_5H_4N\text{-}1\text{-}H^+][Br^-]$ ($3\cdot Br^-$) as the primary product.[74] The crystal structure of $3\cdot Br^-$ is comprised of five discrete $[4\text{-}NH_2\text{-}1\lambda^4\text{-}C_5H_4N\text{-}1\text{-}H^+][Br^-]$ ion pairs and two CH_2Cl_2 solvates (Figure S2) with an extensive hydrogen-bonding network. However, three of the cations **3** and both solvent molecules are disordered, and a detailed structural discussion is therefore ambiguous.

While the reason for the apparent propensity toward protonation in the reaction with Br_2 is not clear,[74] further reactivity of the 4-AP/Br_2 mixture is evidenced by multiple products obtained when the reaction mixture is left in solution for 12−14 h. The ^{1}H NMR spectra of the solution shows the appearance of numerous signal patterns, especially in the aromatic region. Subsequent crystallization efforts of the initial yellow product revealed additional chemical transformations to produce brominated pyridyl-pyridinium cations with either two or three bromine substituents in the pyridine rings (Scheme 1); single-crystal X-ray structures of $\{3,3',5'\text{-}Br_3\text{-}1\lambda^4\text{-}[1,2'\text{-}(C_5H_4N)_2]\text{-}4,4'\text{-}(NH_2)_2\}^+[X^-]$ ($4\cdot Br^-$, $4\cdot Br_3^-$) and $\{3',5'\text{-}Br_2\text{-}1\lambda^4\text{-}[1,2'\text{-}(C_5H_4N)_2]\text{-}4,4'\text{-}(NH_2)_2\}^+[X^-]$ ($5\cdot Br^-$, $5\cdot Br_3^-$) were determined (Figure 6). In all the structures of **4** and **5** (with Br^- and Br_3^- counterions) a covalent N^+-C^{ortho} bond has formed between two pyridine rings. The formally neutral pyridyl ring is disubstituted with Br atoms in meta positions in both ring systems **4** and **5**, whereas the cationic pyridinium unit is monobrominated in the meta position only in the structures of pyridyl-pyridinium **4**. The bond parameters in **4** and **5** (Table 3) are comparable with those of similar, although only monosubstituted (with -^{t}Bu, -NH_2 and -S groups), pyridyl-pyridinium cations reported previously.[75−79]

The previously reported $[4\text{-}R\text{-}1\lambda^4\text{-}1,2'\text{-}(C_5H_4N)_2]^+$ (R = ^{t}Bu, Me_2N) cations comparable to **4** and **5** have been prepared by a direct reaction between the appropriate pyridinium

DOI: 10.1021/acs.cgd.9b00119
Cryst. Growth Des. 2019, 19, 2434−2445

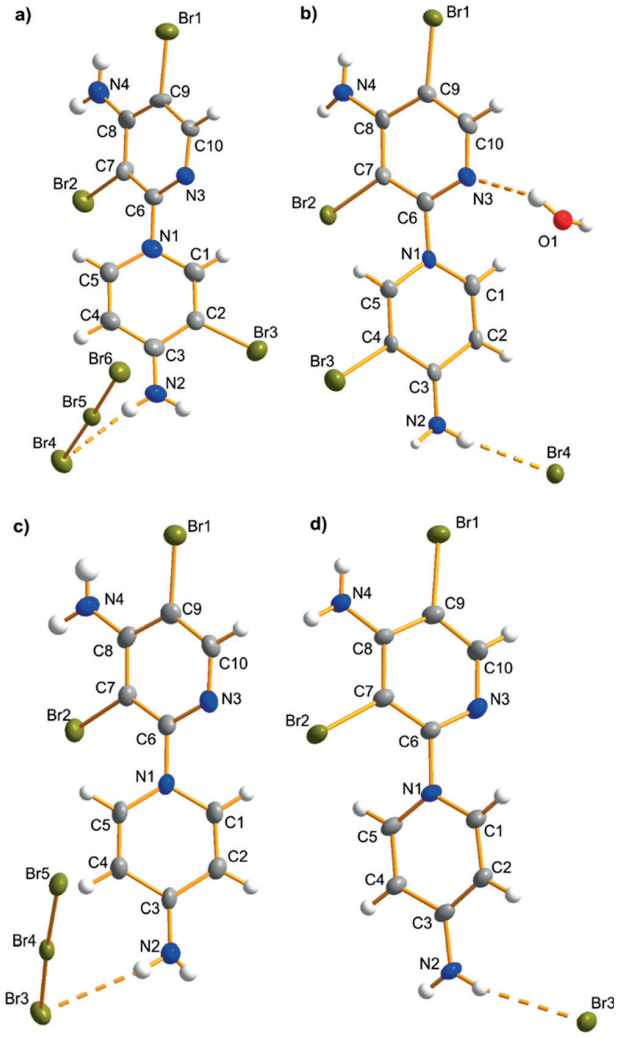

Figure 6. Crystal structures of (a) **4**·Br_3^-, (b) **4**·Br^-, (c) **5**·Br_3^-, and (d) **5**·Br^-.

derivative (triflate salt) and neutral pyridine under relatively harsh conditions: a sealed vial under vacuum at 150 °C.[76] It is therefore somewhat surprising that the protonated **3**·Br^- reacts further in CH_2Cl_2 at room temperature to produce pyridyl-pyridinium cations **4** and **5**. It is conceivable, however, that a partial cleavage of HBr acid in the solution of **3**·Br^- affords a mixture of both components, protonated and neutral 4-AP, required for the direct synthesis of substituted pyridyl-pyridinium cations. In addition, it has been reported that the equimolar reaction between 2-AP and Br_2 in the presence of acetic acid results in bromination of the pyridine ring.[80] In a similar vein, the acidic condition due to the presence of HBr could account for the bromination of 4-AP rings and formation of cations **4** and **5** during an extended period in solution.

Reactions of 4-AP with I_2: Formation and Structural Characterization of [(4-NH_2-1λ^4-C_5H_4N)$_2$-1μ-I^+][I_7^-] (2·I_7^-) and [(4-NH_2-1λ^4-C_5H_4N)$_2$-1μ-H^+][I^-] (6·I^-). The reaction of 4-AP with 1 equiv of I_2 was carried out in CH_2Cl_2, affording a brown precipitate. The ^{1}H NMR spectrum of the product in CD_3CN (Figure S8) displays four multiplets arising from the pyridine hydrogens in the range of 6.57−8.05 ppm and two singlets at δ 5.51 and 5.83 for the amine groups in approximately equal ratio indicating two inequivalent 4-AP components in solution. Owing to the two discrete 4-AP units and, especially, the well-known ability of iodine to form polyiodides, the reaction between 4-AP and I_2 was also performed in a 1:2 molar ratio under similar conditions. The reaction produced a dark red powder, which displays signals at 5.82, 6.59, and 8.04 ppm in a 1:1:1 ratio in the ^{1}H NMR spectrum in CD_3CN (Figure S9), suggesting the formation of only one of the two compounds observed in the reaction in a 1:1 molar ratio as a pure product in good yield (87%).

Slow evaporation of the CH_2Cl_2 solution of the product afforded dark red crystals that were determined as [(4-NH_2-1λ^4-C_5H_4N)$_2$-1μ-I^+][I_7^-] (**2**·I_7^-) by single-crystal X-ray crystallography (Figure 7). Similarly to the reactions with interhalogens ICl and IBr, the crystal structure of **2**·I_7^- exhibits an ionic compound with an I^+ cation trapped between two 4-AP units through N···I^+···N contacts and an I_7^- polyiodide counterion. The compound **2**·I_7^- displays symmetry centers both in the cation (N···I^+···N unit) and in the anion (central I_3^-). In the latter, the I2−I3 and I3−I4 bond lengths of

Table 3. Pertinent Bond Parameters and Close Contacts (in Å and deg) for {3,3′,5′-Br_3-1λ^4-[1,2′-(C_5H_4N)$_2$]-4,4′-(NH_2)$_2$}$^+$[X^-] (4·Br^-, 4·Br_3^-) and {3′,5′-Br_2-1λ^4-[1,2′-(C_5H_4N)$_2$]-4,4′-(NH_2)$_2$}$^+$[X^-] (5·Br^-, 5·Br_3^-) from Br_2 Reaction

4·Br^-		4·Br_3^-		5·Br^- [a]		5·Br_3^- [b]	
Br1−C9	1.894(6)	Br1−C9	1.910(9)	Br1−C9	1.898(5)	Br1−C9	1.893(6)
Br2−C7	1.890(6)	Br2−C7	1.920(9)	Br2−C7	1.892(5)	Br2−C7	1.901(6)
Br3−C4	1.873(6)	Br3−C2	1.890(9)	Br3···N2	3.388(4)	Br3···N2	3.542(6)
Br4···N2	3.339(5)	Br4···N2	3.404(9)	Br3A···N2	3.426(5)	Br5B···N2	3.461(6)
C3−C4−Br3	120.8(4)	C1−C2−Br3	116.8(7)				
C5−C4−Br3	117.1(4)	C3−C2−Br3	120.1(7)				
C6−C7−Br2	120.8(4)	C6−C7−Br2	122.8(7)	C6−C7−Br2	121.5(4)	C6−C7−Br2	122.4(4)
C8−C7−Br2	119.0(4)	C8−C7−Br2	115.5(7)	C8−C7−Br2	118.8(4)	C8−C7−Br2	117.5(4)
C8−C9−Br1	120.5(5)	C8−C9−Br1	118.1(7)	C8−C9−Br1	120.5(4)	C8−C9−Br1	118.5(5)
C10−C9−Br1	118.6(4)	C10−C9−Br1	118.4(7)	C10−C9−Br1	117.7(4)	C10−C9−Br1	120.6(5)
N2···H···Br4	167(8)	N2···H···Br4	168.0	N2···H···Br3	155.5	N2···H···Br3	164(8)
				N2···H′···Br3A	149.4	N2···H′···Br5B	139(10)

[a]Symmetry operations: (A) 1 − x, −0.5 + y, −0.5 − z (Br3A not shown in Figure 6d). [b]Symmetry operations: (B) 2 − x, 1 − y, 2 − z (Br5B not shown in Figure 6c).

DOI: 10.1021/acs.cgd.9b00119
Cryst. Growth Des. 2019, 19, 2434−2445

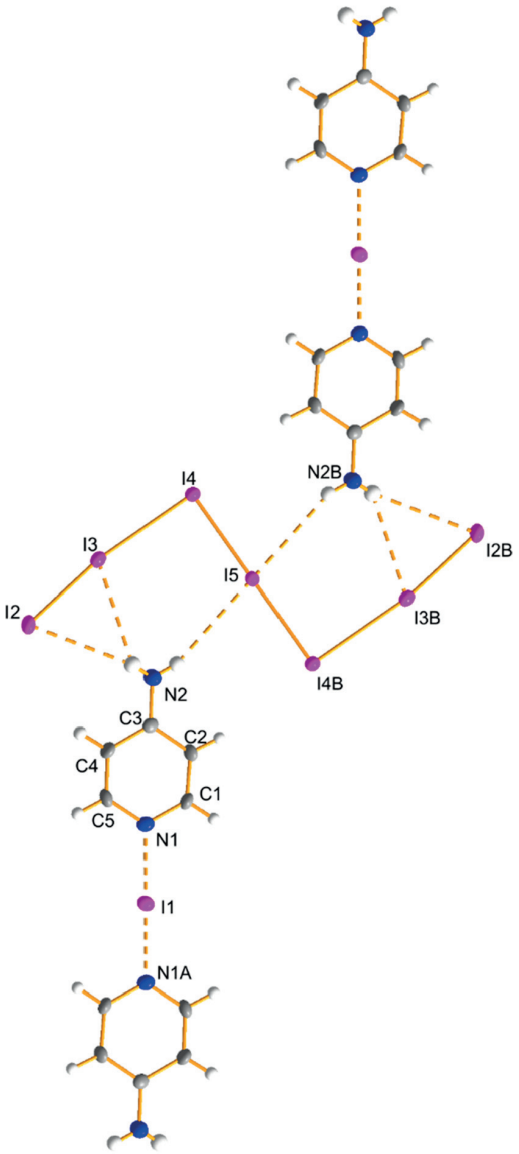

Figure 7. Crystal structure of **2**·I_7^-. Symmetry operations: (A) $2 - x$, $1 - y$, $2 - z$; (B) $-1 - x$, $1 - y$, $1 - z$.

2.7535(6) and 2.9273(4) Å, respectively (Table 2), along with the I3···I4 distance of 3.2804(6) Å are consistent with an I_7^- component comprised of two neutral I_2 units and one I_3^- anion. The ion pairs are connected to infinite strands through weak NH···I contacts (d(N···I) = 3.711(6) −3.974(6) Å, Table S5). The 4-AP rings around the I^+ cation are essentially coplanar, and the N···I^+···N distance of 2.244(5) Å is equal to those observed for **2**·Cl^- and **2**·IBr_2^-. The formation of **2**·I_7^- is consistent with the analogous reaction between unsubstituted pyridine and 2 equiv of I_2.[48]

Similarly to the Br_2 reaction, the proclivity for protonation of **2**·I_7^- is evident from the single-crystal structures of [(4-NH_2-1λ^4-C_5H_4N)$_2$-1μ-H^+][I^-] (**6**·I^-, Figure 8) and the previously reported [4-NH_2-1λ^4-C_5H_4N-1-H^+]$_2$[I^-][I_3^-] (CCDC 1403481)[62] obtained after long standing of the product in various solvents (Scheme 1). The centrosymmetric crystal structure of **6**·I^- is comprised of an H^+ cation trapped between

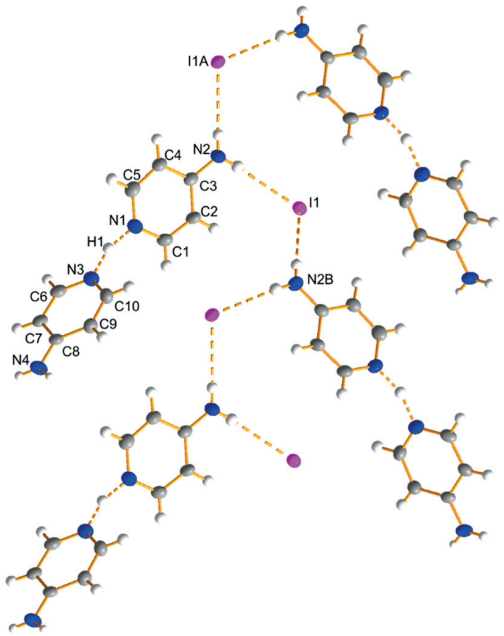

Figure 8. Crystal structure of **6**·I^-. Symmetry operations: (A) $0.5 - x$, $-1.5 + y$, $1.5 - z$; (B) $0.5 - x$, $0.5 + y$, $1.5 - z$.

two 4-AP rings by N···H^+···N contacts and an I^- counteranion (Figure 8). The ion pairs form cross-linking strands through four NH···I contacts of ca. 2.88 Å (d(N···I) = 3.641(4)−3.731(4) Å, Table S5). The CSD database contains 12 structures in which a proton is trapped between two pyridine or substituted pyridine units. Both coplanar and perpendicular arrangements of the pyridine rings exist with N···N distance of ca. 2.58−2.68 Å in the nearly linear N···H^+···N units (177−180°). While the N1···N3 distance of 2.662(5) Å in **6**·I^- falls within same range with the previously reported values, the distinctive tilting between the pyridines is clearly noticeable in the N1···H1···N3 angle of 160.7° (Table 2) in comparison to the value of 172°, representing the narrowest angle in the corresponding systems.[81]

CONCLUSIONS

The reactions of 4-aminopyridine (4-AP) with dihalogens (ICl, IBr, Br_2, and I_2) reveal versatile chemical and structural behavior. Intriguingly, the chemical transformation between 4-AP and ICl in a 1:1 molar ratio results in the formation of both the charge-transfer adduct **1**·ICl and the iodonium cation in **2**·Cl^-. Although the two basic units in these compounds, neutral C_5H_4N−ICl and C_5H_4N···I^+···NH_4C_5 cation, have been well-characterized in various pyridine derivates, this is the first time the coexistence of both components has been observed in solution (NMR) and as a cocrystalline material in the solid state. Moreover, to the best of our knowledge the unsubstituted pyridine (PY) is the only congener for which both the charge-transfer C_5H_4N−I_2[82] and ionic C_5H_4N···I^+···NH_4C_5[48] forms have been structurally characterized by X-ray crystallography in independent investigations.

Somewhat surprisingly, the analogous reaction between 4-AP and IBr affords *solely* the iodonium salt [(4-NH_2-1λ^4-C_5H_4N)$_2$-1μ-I^+][IBr_2^-] (**2**·IBr_2^-) with polyhalide as the counteranion despite the lower polarity of IBr in comparison to ICl. Consistently, 1 equiv of virtually nonpolar I_2 also reacts

DOI: 10.1021/acs.cgd.9b00119
Cryst. Growth Des. 2019, 19, 2434−2445

with 4-AP to produce the I^+ cation in $[(4\text{-}NH_2\text{-}1\lambda^4\text{-}C_5H_4N)_2\text{-}1\mu\text{-}I^+][I_7^-]$ ($\mathbf{2}\cdot I_7^-$) without any evidence of a charge-transfer compound comparable to **1**·ICl. In this instance, additional iodine is also needed for the formation of I_7^- polyiodide instead of triiodide I_3^- analogous to IBr_2^- and, consequently, the reaction between I_2 and 4-AP takes place in a 2:1 molar ratio. A series of the charge-transfer compounds comparable to **1**·ICl has been previously reported for unsubstituted pyridine, C_5H_4N-IX (X = Cl, Br, I).[72,82] In these compounds, the N–I(X) bond lengths of 2.284(3) (X = Cl),[72] 2.304(3) (X = Br),[72] and 2.425(8) Å (X = I),[82] and the calculated (N)I–X bond orders[70] of 0.52 (d(I–Cl) = 2.523(1) Å[72]), 0.54 (d(I–Br) = 2.654(1) Å[72]), and 0.75 (d(I–I) = 2.8043(9) Å[82]) display the expected trend: the N–I bond is strengthening and the I–X bond is weakening when the polarity of the IX component is increasing (ICl > IBr > I_2). In light of these data, stabilization of the charge-transfer compound **1**·ICl and, in contrast, the apparent ready formation of the iodonium cation in $\mathbf{2}\cdot IBr_2^-$ and $\mathbf{2}\cdot I_7^-$ is somewhat surprising. It is conceivable, however, that the easier formation of the polyhalides IBr_2^- and I_7^- in comparison to the reaction with ICl provides the driving force for a rapid cleavage of the I–Br and I–I bonds and subsequent formation of an iodonium cation. On the basis of this study and a literature survey, there is a fine balance between the two components that, presumably, can also be controlled by the selection of substituents.

The chemical transformation between 4-AP and Br_2 exhibits unique reactivity in comparison to those involving ICl, IBr, and I_2. The reaction displays immediate protonation of the 4-AP ring, affording $[4\text{-}NH_2\text{-}1\lambda^4\text{-}C_5H_4N\text{-}1\text{-}H^+][Br^-]$ ($\mathbf{3}\cdot Br^-$) as the initial product. While the presence of a catalytic amount of HBr in the starting material to initiate the protonation cannot be completely ruled out,[74] the subsequent intriguing bromination–dimerization process and formation of pyridyl-pyridinium cations **4** and **5** indicates greater reactivity in the reactions with Br_2 in comparison to those of the other dihalogens. Consequently, the present study shows that, while the reactions between 4-AP and ICl, IBr, and I_2 conveniently produce N···I^+···N-bonded iodonium cations, potentially useful XB donors in applications, the chemical transformation with Br_2 is much more complex and the observed bromination–dimerization process merits further investigations.

■ ASSOCIATED CONTENT

Supporting Information

The Supporting Information is available free of charge on the ACS Publications website at DOI: 10.1021/acs.cgd.9b00119.

Crystallographic data, halogen bond geometries, and pertinent bond parameters for all compounds, crystallographic figures of compounds **1**·ICl and $\mathbf{2}\cdot Cl^-$ and $\mathbf{3}\cdot Br^-$, and ^1H NMR spectra of the bulk products (PDF)

Accession Codes

CCDC 1893191–1893202 contain the supplementary crystallographic data for this paper. These data can be obtained free of charge via www.ccdc.cam.ac.uk/data_request/cif, or by emailing data_request@ccdc.cam.ac.uk, or by contacting The Cambridge Crystallographic Data Centre, 12 Union Road, Cambridge CB2 1EZ, UK; fax: +44 1223 336033.

■ AUTHOR INFORMATION

Corresponding Author

*J.K.: e-mail, jari.a.konu@jyu.fi; tel, +358-40-805-4406.

ORCID

Matti Haukka: 0000-0002-6744-7208

Jari Konu: 0000-0002-7408-8995

Notes

The authors declare no competing financial interest.

■ ACKNOWLEDGMENTS

The authors gratefully acknowledge financial support from Jenny and Antti Wihuri Foundation, Magnus Ehrnrooth Foundation and the Academy of Finland (E.K, M.H., Project No. 295581).

■ REFERENCES

(1) Guthrie, F. XXVIII.—On the Iodide of Iodammonium. *J. Chem. Soc.* **1863**, *16*, 239–244.

(2) Moore, T. S.; Winmill, T. F. CLXXVII.—The State of Amines in Aqueous Solution. *J. Chem. Soc., Trans.* **1912**, *101*, 1635–1676.

(3) Řezáč, J.; Riley, K. E.; Hobza, P. Benchmark Calculations of Noncovalent Interactions of Halogenated Molecules. *J. Chem. Theory Comput.* **2012**, *8* (11), 4285–4292.

(4) Bundhun, A.; Ramasami, P.; Murray, J. S.; Politzer, P. Trends in σ-Hole Strengths and Interactions of F_3MX Molecules (M = C, Si, Ge and X = F, Cl, Br, I). *J. Mol. Model.* **2013**, *19* (7), 2739–2746.

(5) Kozuch, S.; Martin, J. M. L. Halogen Bonds: Benchmarks and Theoretical Analysis. *J. Chem. Theory Comput.* **2013**, *9* (4), 1918–1931.

(6) Politzer, P.; Murray, J. S.; Clark, T. Halogen Bonding and Other σ-Hole Interactions: A Perspective. *Phys. Chem. Chem. Phys.* **2013**, *15* (27), 11178–11189.

(7) Syzgantseva, O. A.; Tognetti, V.; Joubert, L. On the Physical Nature of Halogen Bonds: A QTAIM Study. *J. Phys. Chem. A* **2013**, *117* (36), 8969–8980.

(8) Mitoraj, M. P.; Michalak, A. Theoretical Description of Halogen Bonding – an Insight Based on the Natural Orbitals for Chemical Valence Combined with the Extended-Transition-State Method (ETS-NOCV). *J. Mol. Model.* **2013**, *19* (11), 4681–4688.

(9) Mu, X.; Wang, Q.; Wang, L.-P.; Fried, S. D.; Piquemal, J.-P.; Dalby, K. N.; Ren, P. Modeling Organochlorine Compounds and the σ-Hole Effect Using a Polarizable Multipole Force Field. *J. Phys. Chem. B* **2014**, *118* (24), 6456–6465.

(10) Wang, C.; Danovich, D.; Mo, Y.; Shaik, S. On The Nature of the Halogen Bond. *J. Chem. Theory Comput.* **2014**, *10* (9), 3726–3737.

(11) Arman, H. D.; Biella, S.; Bruce, D. W.; Fourmigué, M.; Hanks, T. W.; Karpfen, A.; Kochi, J. K.; Legon, A. C.; Metrangolo, P.; Pennington, W. T.; et al. *Halogen Bonding: Fundamentals and Applications*; Metrangolo, P., Resnati, G., Eds.; Springer-Verlag: Berlin, Heidelberg, 2008; Vol. *126*.

(12) Cavallo, G.; Metrangolo, P.; Pilati, T.; Resnati, G.; Sansotera, M.; Terraneo, G. Halogen Bonding: A General Route in Anion Recognition and Coordination. *Chem. Soc. Rev.* **2010**, *39* (10), 3772–3783.

(13) Bertani, R.; Sgarbossa, P.; Venzo, A.; Lelj, F.; Amati, M.; Resnati, G.; Pilati, T.; Metrangolo, P.; Terraneo, G. Halogen Bonding in Metal–organic–supramolecular Networks. *Coord. Chem. Rev.* **2010**, *254* (5–6), 677–695.

(14) Ding, X.; Tuikka, M.; Haukka, M. Halogen Bonding in Crystal Engineering. In *Recent Advances in Crystallography*; Benedict, J. B., Ed.; InTech: New York, 2012; pp 143–168.

(15) Priimagi, A.; Cavallo, G.; Metrangolo, P.; Resnati, G. The Halogen Bond in the Design of Functional Supramolecular Materials: Recent Advances. *Acc. Chem. Res.* **2013**, *46* (11), 2686–2695.

(16) Mukherjee, A.; Tothadi, S.; Desiraju, G. R. Halogen Bonds in Crystal Engineering: Like Hydrogen Bonds yet Different. *Acc. Chem. Res.* **2014**, *47* (8), 2514–2524.

(17) Rissanen, K.; Haukka, M. Halonium Ions as Halogen Bond Donors in the Solid State $[XL_2]Y$ Complexes. In *Halogen Bonding II.*

Topics in Current Chemistry; Metrangolo, P., Resnati, G., Eds.; Springer: Cham, Switzerland, 2015; pp 77−90.
(18) Cavallo, G.; Metrangolo, P.; Milani, R.; Pilati, T.; Priimagi, A.; Resnati, G.; Terraneo, G. The Halogen Bond. *Chem. Rev.* **2016**, *116* (4), 2478−2601.
(19) Haukka, M.; Hirva, P.; Rissanen, K. Dihalogens as Halogen Bond Donors. In *Non-covalent Interactions in the Synthesis and Design of New Compounds*; Maharramov, A. M., Mahmudov, K. T., Kopylovich, M. N., Pombeiro, A. J. L., Eds.; Wiley: 2016; pp 187−197.
(20) Kilah, N. L.; Wise, M. D.; Serpell, C. J.; Thompson, A. L.; White, N. G.; Christensen, K. E.; Beer, P. D. Enhancement of Anion Recognition Exhibited by a Halogen-Bonding Rotaxane Host System. *J. Am. Chem. Soc.* **2010**, *132* (34), 11893−11895.
(21) Chudzinski, M. G.; McClary, C. A.; Taylor, M. S. Anion Receptors Composed of Hydrogen- and Halogen-Bond Donor Groups: Modulating Selectivity With Combinations of Distinct Noncovalent Interactions. *J. Am. Chem. Soc.* **2011**, *133* (27), 10559−10567.
(22) Zapata, F.; Caballero, A.; Molina, P.; Alkorta, I.; Elguero, J. Open Bis(triazolium) Structural Motifs as a Benchmark To Study Combined Hydrogen- and Halogen-Bonding Interactions in Oxoanion Recognition Processes. *J. Org. Chem.* **2014**, *79* (15), 6959−6969.
(23) Sarwar, M. G.; Dragisic, B.; Sagoo, S.; Taylor, M. S. A Tridentate Halogen-Bonding Receptor for Tight Binding of Halide Anions. *Angew. Chem., Int. Ed.* **2010**, *49* (9), 1674−1677.
(24) Caballero, A.; White, N. G.; Beer, P. D. A Bidentate Halogen-Bonding Bromoimidazoliophane Receptor for Bromide Ion Recognition in Aqueous Media. *Angew. Chem., Int. Ed.* **2011**, *50* (8), 1845−1848.
(25) Zapata, F.; Caballero, A.; White, N. G.; Claridge, T. D. W.; Costa, P. J.; Félix, V.; Beer, P. D. Fluorescent Charge-Assisted Halogen-Bonding Macrocyclic Halo-Imidazolium Receptors for Anion Recognition and Sensing in Aqueous Media. *J. Am. Chem. Soc.* **2012**, *134* (28), 11533−11541.
(26) Lim, J. Y. C.; Marques, I.; Ferreira, L.; Félix, V.; Beer, P. D. Enhancing the Enantioselective Recognition and Sensing of Chiral Anions by Halogen Bonding. *Chem. Commun.* **2016**, *52* (32), 5527−5530.
(27) Bolton, O.; Lee, K.; Kim, H.-J.; Lin, K. Y.; Kim, J. Activating Efficient Phosphorescence from Purely Organic Materials by Crystal Design. *Nat. Chem.* **2011**, *3* (3), 205−210.
(28) Yan, D.; Delori, A.; Lloyd, G. O.; Friščić, T.; Day, G. M.; Jones, W.; Lu, J.; Wei, M.; Evans, D. G.; Duan, X. A Cocrystal Strategy to Tune the Luminescent Properties of Stilbene-Type Organic Solid-State Materials. *Angew. Chem., Int. Ed.* **2011**, *50* (52), 12483−12486.
(29) Yan, D.; Bučar, D.-K.; Delori, A.; Patel, B.; Lloyd, G. O.; Jones, W.; Duan, X. Ultrasound-Assisted Construction of Halogen-Bonded Nanosized Cocrystals That Exhibit Thermosensitive Luminescence. *Chem. - Eur. J.* **2013**, *19* (25), 8213−8219.
(30) Kwon, M. S.; Lee, D.; Seo, S.; Jung, J.; Kim, J. Tailoring Intermolecular Interactions for Efficient Room-Temperature Phosphorescence from Purely Organic Materials in Amorphous Polymer Matrices. *Angew. Chem., Int. Ed.* **2014**, *53* (42), 11177−11181.
(31) Schindler, S.; Huber, S. M. Halogen Bonds in Organic Synthesis and Organocatalysis. In *Halogen Bonding II. Topics in Current Chemistry*; Metrangolo, P., Resnati, G., Eds.; Springer: Cham, Switzerland, 2014; pp 167−203.
(32) Tamilselvi, A.; Mugesh, G. Interaction of Heterocyclic Thiols/thiones Eliminated from Cephalosporins with Iodine and Its Biological Implications. *Bioorg. Med. Chem. Lett.* **2010**, *20* (12), 3692−3697.
(33) Scholfield, M. R.; Vander Zanden, C. M.; Carter, M.; Ho, P. S. Halogen Bonding (X-Bonding): A Biological Perspective. *Protein Sci.* **2013**, *22* (2), 139−152.
(34) Wilcken, R.; Zimmermann, M. O.; Lange, A.; Joerger, A. C.; Boeckler, F. M. Principles and Applications of Halogen Bonding in Medicinal Chemistry and Chemical Biology. *J. Med. Chem.* **2013**, *56* (4), 1363−1388.
(35) Xu, Z.; Yang, Z.; Liu, Y.; Lu, Y.; Chen, K.; Zhu, W. Halogen Bond: Its Role beyond Drug−Target Binding Affinity for Drug Discovery and Development. *J. Chem. Inf. Model.* **2014**, *54* (1), 69−78.
(36) Ford, M. C.; Ho, P. S. Computational Tools To Model Halogen Bonds in Medicinal Chemistry. *J. Med. Chem.* **2016**, *59* (5), 1655−1670.
(37) Lu, Y.; Shi, T.; Wang, Y.; Yang, H.; Yan, X.; Luo, X.; Jiang, H.; Zhu, W. Halogen Bonding - A Novel Interaction for Rational Drug Design? *J. Med. Chem.* **2009**, *52* (9), 2854−2862.
(38) Carlsson, A.-C. C.; Veiga, A. X.; Erdélyi, M. Halogen Bonding in Solution. In *Halogen Bonding II. Topics in Current Chemistry*; Metrangolo, P., Resnati, G., Eds.; Springer: Cham, Switzerland, 2014; pp 49−76.
(39) Bedin, M.; Karim, A.; Reitti, M.; Carlsson, A.-C. C.; Topić, F.; Cetina, M.; Pan, F.; Havel, V.; Al-Ameri, F.; Sindelar, V.; Rissanen, K.; Gräfenstein, J.; Erdelyi, M. Counterion Influence on the N−I−N Halogen Bond. *Chem. Sci.* **2015**, *6* (7), 3746−3756.
(40) Koskinen, L.; Hirva, P.; Kalenius, E.; Jääskeläinen, S.; Rissanen, K.; Haukka, M. Halogen Bonds with Coordinative Nature: Halogen Bonding in a S−I^+−S Iodonium Complex. *CrystEngComm* **2015**, *17* (6), 1231−1236.
(41) Turunen, L.; Warzok, U.; Puttreddy, R.; Beyeh, N. K.; Schalley, C. A.; Rissanen, K. [N···I^+···N] Halogen-Bonded Dimeric Capsules from Tetrakis(3-Pyridyl)ethylene Cavitands. *Angew. Chem., Int. Ed.* **2016**, *55* (45), 14033−14036.
(42) Turunen, L.; Peuronen, A.; Forsblom, S.; Kalenius, E.; Lahtinen, M.; Rissanen, K. Tetrameric and Dimeric [N···I^+···N] Halogen-Bonded Supramolecular Cages. *Chem. - Eur. J.* **2017**, *23* (48), 11714−11718.
(43) Carlsson, A.-C. C.; Mehmeti, K.; Uhrbom, M.; Karim, A.; Bedin, M.; Puttreddy, R.; Kleinmaier, R.; Neverov, A. A.; Nekoueishahraki, B.; Gräfenstein, J.; et al. Substituent Effects on the [N−I−N]$^+$ Halogen Bond. *J. Am. Chem. Soc.* **2016**, *138* (31), 9853−9863.
(44) Desiraju, G. R.; Shing Ho, P.; Kloo, L.; Legon, A. C.; Marquardt, R.; Metrangolo, P.; Politzer, P.; Resnati, G.; Rissanen, K. Definition of the Halogen Bond (IUPAC Recommendations 2013)*. *Pure Appl. Chem.* **2013**, *85* (8), 1711−1713.
(45) Sarwar, M. G.; Dragisic, B.; Salsberg, L. J.; Gouliaras, C.; Taylor, M. S. Thermodynamics of Halogen Bonding in Solution: Substituent, Structural, and Solvent Effects. *J. Am. Chem. Soc.* **2010**, *132* (5), 1646−1653.
(46) Grabowski, S. J. Hydrogen and Halogen Bonds Are Ruled by the Same Mechanisms. *Phys. Chem. Chem. Phys.* **2013**, *15* (19), 7249−7259.
(47) Metrangolo, P.; Meyer, F.; Pilati, T.; Resnati, G.; Terraneo, G. Halogen Bonding in Supramolecular Chemistry. *Angew. Chem., Int. Ed.* **2008**, *47* (33), 6114−6127.
(48) Hassel, O.; Hope, H. Structure of the Solid Compound Formed by Addition of Two Molecules of Iodine to One Molecule of Pyridine. *Acta Chem. Scand.* **1961**, *15*, 407−416.
(49) Hakkert, S. B.; Erdélyi, M. Halogen Bond Symmetry: The N-X-N Bond. *J. Phys. Org. Chem.* **2015**, *28* (3), 226−233.
(50) Meazza, L.; Martí-Rujas, J.; Terraneo, G.; Castiglioni, C.; Milani, A.; Pilati, T.; Metrangolo, P.; Resnati, G. Solid-State Synthesis of Mixed Trihalides via Reversible Absorption of Dihalogens by Non Porous Onium Salts. *CrystEngComm* **2011**, *13* (13), 4427−4435.
(51) Lin, J.; Martí-Rujas, J.; Metrangolo, P.; Pilati, T.; Radice, S.; Resnati, G.; Terraneo, G. Solution and Solid State Synthesis of the Discrete Polyiodide I_7^{3-} under Modular Cation Templation. *Cryst. Growth Des.* **2012**, *12* (11), 5757−5762.
(52) Martí-Rujas, J.; Meazza, L.; Lim, G. K.; Terraneo, G.; Pilati, T.; Harris, K. D. M.; Metrangolo, P.; Resnati, G. An Adaptable and Dynamically Porous Organic Salt Traps Unique Tetrahalide Dianions. *Angew. Chem., Int. Ed.* **2013**, *52* (50), 13444−13448.

DOI: 10.1021/acs.cgd.9b00119
Cryst. Growth Des. 2019, 19, 2434−2445

(53) Yushina, I. D.; Kolesov, B. A.; Bartashevich, E. V. Raman Spectroscopy Study of New Thia- and Oxazinoquinolinium Triodides. *New J. Chem.* **2015**, *39* (8), 6163−6170.
(54) Bartashevich, E.; Troitskaya, E.; Tsirelson, V. Understanding the Bifurcated Halogen Bonding N···Hal···N in Bidentate Diazaheterocyclic Compounds. *Comput. Theor. Chem.* **2015**, *1053*, 229−237.
(55) Bartashevich, E. V.; Yushina, I. D.; Stash, A. I.; Tsirelson, V. G. Halogen Bonding and Other Iodine Interactions in Crystals of Dihydrothiazolo(oxazino)quinolinium Oligoiodides from the Electron-Density Viewpoint. *Cryst. Growth Des.* **2014**, *14* (11), 5674−5684.
(56) Bartashevich, E. V.; Matveychuk, Y. V.; Troitskaya, E. A.; Tsirelson, V. G. Characterizing the Multiple Non-Covalent Interactions in N, S-Heterocycles−diiodine Complexes with Focus on Halogen Bonding. *Comput. Theor. Chem.* **2014**, *1037*, 53−62.
(57) Bartashevich, E. V.; Troitskaya, E. A.; Tsirelson, V. G. The N···I Halogen Bond in Substituted Pyridines as Viewed by the Source Function and Delocalization Indices. *Chem. Phys. Lett.* **2014**, *601*, 144−148.
(58) Ding, X.; Tuikka, M. J.; Hirva, P.; Kukushkin, V. Y.; Novikov, A. S.; Haukka, M. Fine-Tuning Halogen Bonding Properties of Diiodine through Halogen−halogen Charge Transfer − Extended $[Ru(2,2'\text{-bipyridine})(CO)_2X_2]\cdot I_2$ Systems (X = Cl, Br, I). *CrystEngComm* **2016**, *18* (11), 1987−1995.
(59) *CrysAlis PRO*; Agilent Technologies Ltd: Yarnton, Oxfordshire, England, 2014.
(60) Dolomanov, O. V.; Bourhis, L. J.; Gildea, R. J.; Howard, J. A. K.; Puschmann, H. OLEX2 : A Complete Structure Solution, Refinement and Analysis Program. *J. Appl. Crystallogr.* **2009**, *42* (2), 339−341.
(61) Sheldrick, G. M. Crystal Structure Refinement with SHELXL. *Acta Crystallogr., Sect. C: Struct. Chem.* **2015**, *C71* (1), 3−8.
(62) Reiss, G. J.; Leske, P. B. The Twinned Crystal Structure of bis((4-Aminopyridin-1-Ium) Iodide Triiodide, $C_{20}H_{28}I_8N_8$. *Z. Kristallogr. NCS* **2014**, *229* (4), 452−454.
(63) Brayer, G. D.; James, M. N. G A charge-transfer complex: bis(2,4,6-trimethyl-1-pyridyl)iodonium perchlorate. *Acta Crystallogr., Sect. B: Struct. Crystallogr. Cryst. Chem.* **1982**, *B38*, 654−657.
(64) Okitsu, T.; Yumitate, S.; Sato, K.; In, Y.; Akimori Wada, A. Substituent Effect of Bis(pyridines)iodonium Complexes as Iodinating Reagents: Control of the Iodocyclization/Oxidation Process. *Chem. - Eur. J.* **2013**, *19*, 4992−4996.
(65) Batsanov, A. S.; Lightfoot, A. P.; Twiddle, S. J. R.; Whiting, A. *Acta Crystallogr., Sect. E: Struct. Rep. Online* **2006**, *E62*, o901−o902.
(66) Georgiou, D. C.; Butler, P.; Browne, E. C.; Wilson, D. J. D.; Dutton, J. L. On the Bonding in Bis-pyridine Iodonium Cations. *Aust. J. Chem.* **2013**, *66*, 1179−1188.
(67) Lommerse, J. P. M.; Stone, A. J.; Taylor, R.; Allen, F. H. The Nature and Geometry of Intermolecular Interactions between Halogens and Oxygen or Nitrogen. *J. Am. Chem. Soc.* **1996**, *118* (13), 3108−3116.
(68) Brammer, L.; Bruton, E. A.; Sherwood, P. Understanding the Behavior of Halogens as Hydrogen Bond Acceptors. *Cryst. Growth Des.* **2001**, *1* (4), 277−290.
(69) Zordan, F.; Brammer, L.; Sherwood, P. Supramolecular Chemistry of Halogens: Complementary Features of Inorganic (M−X) and Organic (C−X') Halogens Applied to M−X···X'−C Halogen Bond Formation. *J. Am. Chem. Soc.* **2005**, *127* (16), 5979−5989.
(70) Pauling, L. *The Nature of the Chemical Bond*, 3rd ed.; Cornell University Press: Ithaca, NY, 1960.
(71) Pyykkö, P.; Atsumi, M. Molecular Single-Bond Covalent Radii for Elements 1−118. *Chem. - Eur. J.* **2009**, *15* (1), 186−197.
(72) Jones, R. H.; Knight, K. S.; Marshall, W. G.; Clews, J.; Darton, R. J.; Pyatt, D.; Coles, S. J.; Horton, P. N. Colossal Thermal Expansion and Negative Thermal Expansion in Simple Halogen Bonded Complexes. *CrystEngComm* **2014**, *16* (2), 237−243.
(73) Batsanov, A. S.; Howard, J. A. K.; Lightfoot, A. P.; Twiddle, S. J. R.; Whiting, A. Stereoselcetive Chloro-Deboronation Reactions Induced by Substituted Pyridine-Iodine Chloride Complexes. *Eur. J. Org. Chem.* **2005**, *2005*, 1876−1883.
(74) The purity of the Br_2 starting material and the absence of, for example, significant amounts of HBr were subsequently confirmed by ^1H NMR spectroscopy. The presence of a catalytic amount of HBr in the reaction mixture, however, cannot be excluded.
(75) Harding, P.; Harding, D. J.; Pakawatchai, C.; Phetmung, H. Catena-Poly[[bis[-1-(2-Pyridyl)pyridinium-2-Thiolate]-2-N:S;-2-S:N-dicopper(I)]-Di-Chloro]. *Acta Crystallogr., Sect. E: Struct. Rep. Online* **2006**, *E62*, m1335−m1337.
(76) Owen, J. S.; Day, M. W.; Bercaw, J. E. CCDC 199233. *CSD Commun.* **2005**.
(77) Owen, J. S.; Labinger, J. A.; Bercaw, J. E. Pyridinium-Derived N-Heterocyclic Carbene Complexes of Platinum: Synthesis, Structure and Ligand Substitution Kinetics. *J. Am. Chem. Soc.* **2004**, *126* (26), 8247−8255.
(78) Piro, N. A.; Owen, J. S.; Bercaw, J. E. Pyridinium-Derived N-Heterocyclic Carbene Ligands: Syntheses, Structures and Reactivity of N-(2'-Pyridyl)pyridin-2-Ylidene Complexes of nickel(II), palladium-(II) and platinum(II). *Polyhedron* **2004**, *23* (17), 2797−2804.
(79) Kinoshita, I.; James Wright, L.; Kubo, S.; Kimura, K.; Sakata, A.; Yano, T.; Miyamoto, R.; Nishioka, T.; Isobe, K. Design and Synthesis of Copper Complexes of Novel Ligands Based on the Pyridine Thiolate Group. *Dalt. Trans.* **2003**, *0* (10), 1993−2003.
(80) Fox, B. A.; Threlfall, T. L. 2,3-diaminopyridine. *Org. Synth.* **2003**, *44*, 34−39.
(81) Lackova, D.; Ondrejkovicova, I.; Padelkova, Z.; Koman, M. Syntheses, crystal structures, and IR spectra of isonicotinamide-isonicotinamidium bis(isonicotinamide)-tetrakis(isothiocyanato)-ferrate(III) and isonicotinamidium chloride. *J. Coord. Chem.* **2014**, *67*, 1652−1663.
(82) Tuikka, M.; Haukka, M. Crystal Structure of the Pyridine-Diiodine (1/1) Adduct. *Acta Cryst., Sect. E: Cryst. Commun.* **2015**, *E71*, o463−o463.

DOI: 10.1021/acs.cgd.9b00119
Cryst. Growth Des. 2019, 19, 2434−2445

III

NONLINEAR OPTICAL PROPERTIES OF DIAROMATIC STILBENE, BUTADIENE AND THIOPHENE DERIVATIVES

by

Esa Kukkonen, Elmeri Lahtinen, Pasi Myllyperkiö, Matti Haukka and Jari Konu 2021

New J. Chem., 45 (15), 6640-6650

DOI: 10.1039/d1nj00456e

NJC

PAPER

View Article Online
View Journal

Cite this: DOI: 10.1039/d1nj00456e

Nonlinear optical properties of diaromatic stilbene, butadiene and thiophene derivatives†

Esa Kukkonen, [a] Elmeri Lahtinen, [a] Pasi Myllyperkiö, [b] Matti Haukka [a] and Jari Konu *[a]

Series of highly polar stilbene (**1a–e**), diphenylbutadiene (**2a–c**) and phenylethenylthiophene (**3a–c**) derivatives were prepared *via* Horner–Wadsworth–Emmons method with a view to produce new and efficient materials for second harmonic generation (SHG) in the solid-state. The single-crystal X-ray structures of compounds **1–3** reveal extensive polymorphism and a peculiar photodimerization of the 2-chloro-3,4-dimethoxy-4′-nitrostilbene derivative **1a** to afford two polymorphs of tetra-aryl cyclobutane **4**. The stilbene congeners 2-chloro-3,4-dimethoxy-4′-nitrostilbene (**1a**·non-centro), 5-bromo-2-hydroxy-3-nitro-4′-nitrostilbene (**1b**) and 4-dimethylamino-4′-nitrostilbene (**1e**), as well as 4′-fluoro-4″-nitro-1,4-diphenyl-1,3-butadiene (**2a**) present the ideal, non-centrosymmetric arrangement of the chromophores for nonlinear optical (NLO) activity. Compounds **1b** and **2a** exhibit only relatively low intensity for second harmonic generation (0.04 and 0.18 times that of urea reference, respectively), while the stilbene polymorph **1a**·non-centro shows NLO activity of over 32 times that of urea. In addition, the conjugated diaromatic compounds **1–3** display fluorescence behaviour in CH_2Cl_2 solutions with the exception of stilbene derivative **1b**.

Received 28th January 2021,
Accepted 19th March 2021

DOI: 10.1039/d1nj00456e

rsc.li/njc

Introduction

The study of nonlinear optical (NLO) materials has gained increasing interest especially owing to their significance in laser technology and optoelectronics. Ultrafast electro-optical switches, optical signal processing and computing, data storage, and photonic technologies are just some of the various applications where these materials have become indispensable.[1–8] One of the most sought-after nonlinear properties for these applications is the second harmonic generation (SHG), a phenomenon in which the material combines two photons into one, creating radiation with twice the frequency of the original. The fundamental requirement for a material to have SHG activity is to possess non-zero second-order nonlinear susceptibility $\chi^{(2)}$, which necessitates the compound to have non-zero first-order hyperpolarizability β at the molecular level.[9] It is highly beneficial if the NLO active material crystallizes in a non-centrosymmetric space group (lack of inversion symmetry) to avoid the effective cancelation of hyperpolarizability, even though centrosymmetric crystals have also been reported to display SHG through processes involving intermolecular interactions.[10,11]

Although most of the commercially available NLO crystals are based on inorganic compounds such as β-barium borate (BBO) and potassium titanyl phosphate (KTP), primarily owing to their high chemical and physical stability,[12–14] the academic research on new NLO active materials has largely focused on organic "push–pull" molecules for which high SHG activities have been observed frequently.[15–18] A group of compounds consistently showing remarkable SHG efficiencies are diarylethenes, commonly known as stilbenes (compound **1**, Scheme 1). They have been studied extensively by both theoretical and experimental methods,[19,20] and, for example, 3-methyl-4-methoxy-4′-nitrostilbene (MMONS, Scheme 1), the most efficient second order NLO material reported to date with the SHG efficiency of up to 1250 times of urea,[21] belongs to this group of conjugated systems. Additionally, a variety of heteroaromatic, diarylethene-based systems where one or both aryl moieties have been replaced with thiophene, thiazole, or pyrrole rings have also been investigated.[22–25] The primary aim of these studies was to increase the hyperpolarizability (β) of the chromophores by altering the charge-transfer properties. While the electric field induced second harmonic generation (EFISHG) measurements of especially thiophene containing diarylethenes in solution have shown to improve the NLO properties at molecular

[a] Department of Chemistry, University of Jyväskylä, P. O. Box 35, FI-40014 Jyväskylä, Finland. E-mail: jari.a.konu@jyu.fi; Tel: +358-40-805-4406
[b] Nanoscience Center, University of Jyväskylä, P. O. Box 35, FI-40014 Jyväskylä, Finland

† Electronic supplementary information (ESI) available: A pdf file containing tables of crystallographic data (Tables S1–S3) and pertinent bond parameters (Tables S4–S16, together with molecular figures for atomic numbering scheme) as well as ^{1}H NMR (Fig. S1–S11) and IR spectra (Fig. S12–S22) for all compounds. This material is available free of charge. CCDC 2058507–2058519 for compounds **1a**·centro, **1a**·non-centro, **1b**, **1c**, **1d**, **1e**, **4**·Pcell, **4**·Ccell, **2a**, **3a**·mono, **3a**·ortho, **3b**, and **3c**. For ESI and crystallographic data in CIF or other electronic format see DOI: 10.1039/d1nj00456e

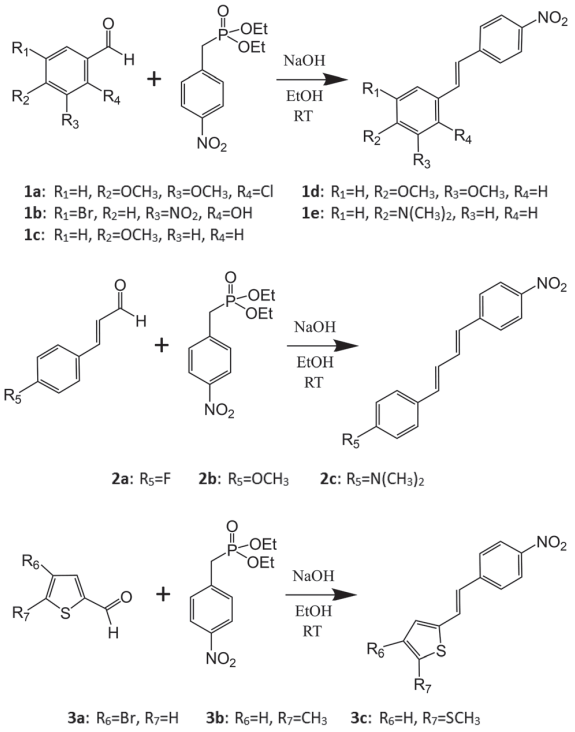

Scheme 1 Synthesis of the stilbene (**1**), diphenylbutadiene (**2**), and phenylethenylthiophene (**3**) derivatives.

level,[22–25] the information on SHG activity of these systems in the solid-state, requiring the most advantageous non-centrosymmetric molecular packing in the crystal lattice, is much more scarce.

We recently reported a novel method for producing NLO active lenses by stereolithographic (SLA) 3D printing technique.[26] This new approach avoids the often tedious and time-consuming process of growing large single crystals by utilizing microcrystalline powders of NLO active components similarly to the Kurtz–Perry powder method for determination of relative SHG intensities.[27] At the same time, the protective layer of photopolymer resin used in the SLA 3D printing could enable the use of labile organic chromophores as NLO active units.[26] In this context and with the above considerations in mind, we have now investigated the conjugated, $-NO_2$ substituted stilbene-based systems with the goal of producing new NLO active materials in the solid-state by the means of (1) changing the functional groups at the electron-donating end of stilbene, (2) extending the chain length between the aromatic groups to afford diarylbutadiene derivatives, and (3) changing one of the phenyl groups to thiophene. Consequently, we report here the synthesis, spectroscopic (^{1}H NMR, IR, UV-Visible and fluorescence) and structural characterization (single-crystal XRD), and the SHG properties (Kurtz–Perry powder method)[27] of stilbene (**1a–e**), diphenylbutadiene (**2a–c**), and phenylethenylthiophene (**3a–c**) derivatives (Scheme 1).

Experimental methods

Reagents and general procedures

The reactions were carried out in air. All the starting materials and solvents were purchased from commercial sources. Solvents were dried over 3 Å molecular sieves and the remaining reagents were used without further purification: diethyl(4-nitrobenzyl)-phosphonate (TCI Chemicals, >97.0%), 4-methoxy-3-methylbenzaldehyde (Sigma-Aldrich, 99%), 2-chloro-3,4-dimethoxybenzaldehyde (TCI Chemicals, >98.0%), 5-bromo-3-nitrosalicylaldehyde (TCI Chemicals, >97.0%), 4-bromothiophene-2-carboxaldehyde (TCI Chemicals, >98.0%), 5-methylthiophene-2-carboxaldehyde (TCI Chemicals, >97.0%), 4-fluorocinnamaldehyde (TCI Chemicals, >95.0%), sodium hydroxide (VWR Chemicals, 99%), 4-anisaldehyde (Merck, 99%), 3,4-dimethoxybenzaldehyde (Aldrich, 99%), 5-(methylthio)thiophenecarboxaldehyde (TCI Chemicals, >98.0%), 4-methoxycinnamaldehyde (Sigma-Aldrich, ≥98%), 4-dimethylaminocinnamaldehyde (TCI Chemicals, >98.0%), CH_2Cl_2 (VWR Chemicals, 99%), chloroform (Fisher Chemical, analytical reagent grade), acetone (Mallinckrodt, >99.5%), Ethanol (Altia, >99.5%). Elemental analyses were performed by analytical services at the Department of Chemistry, University of Jyväskylä.

Spectroscopic methods

The ^{1}H NMR spectra were obtained in CD_2Cl_2 at 30 °C on Bruker Avance III 300 spectrometer operating at 300.15 MHz. ^{1}H NMR spectra are referenced to the solvent signal and the chemical shifts are reported relative to $(CH_3)_4Si$. The IR spectra were measured with Bruker Alpha FTIR spectrometer. The extinction coefficients (molar absorptivity) were determined with PerkinElmer Lambda 650 spectrophotometer by measuring the absorbances of 1 mM and 10 μM solutions in CH_2Cl_2 (800 to 250 nm). The fluorescence spectra of the compounds were recorded on a Varian Cary Eclipse spectrophotometer from 0.1–10 μM solutions in CH_2Cl_2.

Nonlinear optical (NLO) measurements

The nonlinear optical properties of compounds **1a–e**, **2a–c**, and **3a–c** were measured with Kurtz–Perry powder method[27] by using femtosecond laser radiation at 1030 nm. In addition, the second harmonic generation (SHG) was double-checked by using spectrally resolving detection scheme using Kurtz–Perry sample geometry. For these experiments, both femtosecond and nanosecond laser pulses were used. Femtosecond experiments were performed with the setup consisting an amplified femtosecond laser source at 1030 nm (Pharos, Light Conversion Ltd) running at 600 kHz repetition rate. Generated SHG signal was detected by using a high-resolution spectrometer equipped with 300 mm spectrograph (Acton SpectraPro 300i) with spectroscopy CCD detector (Newton DU971N-BV, Andor). Nano-second laser pulses at 100 Hz repetition rate and at 1030 nm and 1060 nm were taken from the ns-OPO (Ekspla Ltd.). Spectrum of the SHG signal was recorded by using time-gated ICCD detector (ISTAR, Andor) with 150 mm spectrograph. (Acton SpectraPro 150i). The crystalline samples, apart from **1b**, were sieved to a particle size of <125 μm and placed into capillary

tubes for the determination of relative SHG intensity of the compounds. A capillary tube with urea sieved to the same particle size was used as a reference.

X-Ray crystallography. Crystallographic data for compounds **1a**·centro, **1a**·non-centro, **1b**, **1c**, **1d**, **1e**, **4**·Pcell, **4**·Ccell, **2a**, **3a**·mono, **3a**·ortho, **3b**, and **3c** are summarized in Tables S1–S3 (*cf.* ESI,† also for molecular figures with atomic numbering schemes and the tables of pertinent bond parameters). Crystals were coated with Fomblin®Y oil and mounted on a MiTeGen loop. Diffraction data were collected on Rikagu-Oxford SuperNova Single or Dual Source diffractometers equipped with Atlas CCD area-detector using graphite monochromatized CuKα radiation (λ = 1.54184 Å; **1a**·centro, **1a**·non-centro, **1b**, **1c**, **1e**, **4**·Pcell, **4**·Ccell, **2a**, and **3b**) or MoKα radiation (λ = 0.71073 Å; **1d**, **3a**·mono, **3a**·ortho, and **3c**) at −120 or −150 °C. The data were processed primarily by performing analytical numeric absorption correction using a multifaceted crystal with CrysAlisPro program.[28] All structures were solved by direct methods with SHELXS or SHELXT and refined by using SHELXL implemented in the Olex^2 program package.[29,30] After full-matrix least-squares refinement of the non-hydrogen atoms with anisotropic thermal parameters, the hydrogen atoms were placed in calculated positions (C–H = 0.93 Å for –CH and 0.98 Å for $–CH_3$ hydrogen atoms, and O–H = 0.82 Å for –OH hydrogen atoms). The isotropic thermal parameters of the calculated hydrogen atoms were fixed at 1.2 (–CH) or 1.5 ($–CH_3$) times that of the corresponding carbon or oxygen. In the final refinement, the calculated hydrogen atoms were riding on their respective carbon or oxygen atoms.

Preparation of 2-chloro-3,4-dimethoxy-4′-nitrostilbene (1a). 0.202 g (1.00 mmol) of 2-chloro-3,4-dimethoxybenzaldehyde was dissolved in 10 mL of ethanol and 0.22 mL (1.00 mmol) of diethyl(4-nitrobenzyl)phosphonate was added to the solution at 23 °C. 3 mL of 1.5 M of sodium hydroxide solution in ethanol was then added and the reaction mixture was stirred overnight. The resulting precipitate was then filtered and washed with 5 mL of cold ethanol. The reaction afforded 0.255 g of yellow powder (80% yield).

Anal. calcd (%): C, 60.10; H, 4.41; N, 4.38 found: C, 59.54; H, 4.19; N, 4.40%. ^{1}H NMR (CD_2Cl_2, 30 °C): δ 8.21 [m, 2H, $–C_6H_4NO_2$], δ 7.68 [m, 2H, $–C_6H_4NO_2$], δ 7.65 [d, 1H, –C*H*═CH–, ^3J (^{1}H,^{1}H) = 16 Hz], δ 7.49 [m, 1H, $–C_6H_2$], δ 7.05 [d, 1H, –C*H*═CH–, ^3J (^{1}H,^{1}H) = 17 Hz], δ 6.93 [m, 1H, $–C_6H_2$], δ 3.91 [s, 3H, $–OCH_3$], δ 3.85 [s, 3H, $–OCH_3$]. X-Ray quality crystals of the two polymorphs of compound **1a** (**1a**·centro and **1a**·non-centro) as well as two polymorphs of the subsequent dimerization products (**4**·Pcell and **4**·Ccell, *cf.* main text) were obtained by slow evaporation of ethanol/chloroform and ethanol/dichloromethane solutions at 23 °C.

Preparation of 5-bromo-2-hydroxy-3-nitro-4′-nitrostilbene (1b). 0.247 g (1.00 mmol) of solid 5-bromo-3-nitrosalicylaldehyde was dissolved in 15 mL of ethanol at 23 °C. 0.22 mL (1.00 mmol) of diethyl(4-nitrobenzyl)phosphonate was added to the solution. The flask was gently heated until all aldehyde had dissolved. 3 mL of 1.5 M solution of sodium hydroxide in ethanol was then added and the reaction mixture was stirred overnight. The resulting precipitate was then filtered and washed with 5 mL of cold ethanol, affording 0.200 g of red-brown product (55% yield). The product was then extracted with CH_2Cl_2/H_2O-mixture followed by evaporation of the organic phase to give an orange powder of 0.023 g (6% yield) as the spectroscopically pure product.

Anal. calcd (%): C, 46.05; H, 2.48; N, 7.67 found: C, 44.98; H, 2.64; N, 7.86%. ^{1}H NMR (CD_3CN, 30 °C): δ 11.10 [s, 1H, –O*H*], δ 8.24 [m, 3H, $–C_6H_4NO_2$ (2H) and $–C_6H_2$ (1H)], δ 8.04 [m, 1H, $–C_6H_2$], δ 7.72 [m, 2H, $–C_6H_4NO_2$], δ 7.58 [d, 1H, –C*H*═CH–, ^3J (^{1}H,^{1}H) = 16 Hz], δ 7.32 [d, 1H, –C*H*═CH–, ^3J (^{1}H,^{1}H) = 16 Hz]. X-Ray quality crystals of compound **1b** were obtained by slow evaporation of ethanol/chloroform solution at 23 °C.

Preparation of 4-methoxy-4′-nitrostilbene (1c). 0.133 g (1.00 mmol) of 4-anisaldehyde was dissolved in 10 mL of ethanol and 0.22 mL (1.00 mmol) of diethyl(4-nitrobenzyl)phosphonate was added at 23 °C. 3 mL of 1.5 M solution of sodium hydroxide in ethanol was then added and the reaction mixture was stirred overnight. The resulting precipitate was then filtered and washed with 5 mL of cold ethanol. The reaction afforded 0.170 g of yellow powder (66% yield).

Anal. calcd (%): C, 70.57; H, 5.13; N, 5.49 found: C, 69.83; H, 4.82; N, 5.52%. ^{1}H NMR (CD_2Cl_2, 30 °C): δ 8.19 [m, 2H, $–C_6H_4NO_2$], δ 7.63 [m, 2H, $–C_6H_4NO_2$], δ 7.52 [m, 2H, $–C_6H_4OMe$], δ 7.27 [d, 1H, –C*H*═CH–, ^3J (^{1}H,^{1}H) = 16 Hz], δ 7.05 [d, 1H, –C*H*═CH–, ^3J (^{1}H,^{1}H) = 16 Hz], δ 6.94 [m, 2H, $–C_6H_4OMe$], δ 3.84 [s, 3H, $–OCH_3$]. X-Ray quality crystals of compound **1c** were obtained by slow evaporation of methanol solution at 23 °C.

Preparation of 3,4-dimethoxy-4′-nitrostilbene (1d). 0.165 g (1.00 mmol) of solid 3,4-dimethoxybenzaldehyde was dissolved in 10 mL of ethanol at 23 °C. 0.22 mL (1.00 mmol) of diethyl-(4-nitrobenzyl)phosphonate was added to the solution. 3 mL of 1.5 M solution of sodium hydroxide in ethanol was then added and the reaction mixture was stirred overnight. The resulting precipitate was then filtered and washed with 5 mL of cold ethanol. The reaction afforded 0.219 g of yellow powder (77% yield).

Anal. calcd (%): C, 67.36; H, 5.30; N, 4.91 found: C, 66.46; H, 5.08; N, 4.81%. ^{1}H NMR (CD_2Cl_2, 30 °C): δ 8.20 [m, 2H, $–C_6H_4NO_2$], δ 7.64 [m, 2H, $–C_6H_4NO_2$], δ 7.26 [d, 1H, –C*H*═CH–, ^3J (^{1}H,^{1}H) = 16 Hz], δ 7.12 [m, 2H, $–C_6H_3$], δ 7.05 [d, 1H, –C*H*═CH–, ^3J (^{1}H,^{1}H) = 16 Hz], δ 6.90 [m, 2H, $–C_6H_3O$], δ 3.91 [s, 3H, $–OCH_3$] δ 3.87 [s, 3H, $–OCH_3$]. X-Ray quality crystals of compound **1d** were obtained by slow evaporation of methanol solution at 23 °C.

Preparation of 4-dimethylamino-4′-nitrostilbene (1e). 0.148 g (1.00 mmol) of 4-dimethylaminobenzaldehyde was dissolved in 10 mL of ethanol at 23 °C. 0.22 mL (1.00 mmol) of diethyl-(4-nitrobenzyl)phosphonate was added to the solution. 3 mL of 1.5 M solution of sodium hydroxide in ethanol was then added and the reaction mixture was stirred overnight. The resulting precipitate was then filtered and washed with 5 mL of cold ethanol. The reaction afforded 0.182 g of red powder (68% yield).

Anal. calcd (%): C, 71.62; H, 6.01; N, 10.44 found: C, 70.25; H, 5.81; N, 10.32%. ^{1}H NMR (CD_2Cl_2, 30 °C): δ 8.17 [m, 2H, $–C_6H_4NO_2$], δ 7.59 [m, 2H, $–C_6H_4NO_2$], δ 7.45 [m, 2H, $–C_6H_4NMe_2$], δ 7.24 [d, 1H, –C*H*═CH–, ^3J (^{1}H,^{1}H) = 16 Hz], δ 6.96 [d, 1H, –C*H*═CH–, ^3J (^{1}H,^{1}H) = 16 Hz], δ 6.72 [m, 2H,

–$C_6H_4NMe_2$], δ 3.01 [s, 6H, –N(CH_3)$_2$]. X-Ray quality crystals of the compound **1e** were obtained by slow evaporation of methanol solution at 23 °C.

Preparation of 4′-fluoro-4″-nitro-1,4-diphenyl-1,3-butadiene (2a). 0.151 g (1.00 mmol) of solid 4-fluorocinnamaldehyde was dissolved in 10 mL of ethanol at 23 °C. 0.22 mL (1.00 mmol) of diethyl(4-nitrobenzyl)phosphonate was added to the solution. 3 mL of 1.5 M solution of sodium hydroxide in ethanol was then added and the reaction mixture was stirred overnight. The resulting precipitate was then filtered and washed with 5 mL of cold ethanol. The reaction afforded 0.093 g of yellow powder (35% yield).

Anal. calcd (%): C, 71.36; H, 4.49; N, 5.20 found: C, 70.05; H, 4.33; N, 5.18%. ^{1}H NMR (CD_2Cl_2, 30 °C): δ 8.18 [m, 2H, –$C_6H_4NO_2$], δ 7.58 [m, 2H, –$C_6H_4NO_2$], δ 7.47 [m, 2H, –C_6H_4OMe], δ 7.18–6.71 [m, 6H, –C_6H_4OMe & –C*H*═CH–]. X-Ray quality crystals of compound **2a** were obtained by slow evaporation of acetone/water solution at 23 °C.

Preparation of 4′-methoxy-4″-nitro-1,4-diphenyl-1,3-butadiene (2b). 0.162 g (1.00 mmol) of solid 4-methoxycinnamaldehyde was dissolved in 10 mL of ethanol at 23 °C. 0.22 mL (1.00 mmol) of diethyl(4-nitrobenzyl)phosphonate was added to the solution. 3 mL of 1.5 M solution of sodium hydroxide in ethanol was then added and the reaction mixture was stirred overnight. The resulting precipitate was then filtered and washed with 5 mL of cold ethanol. The reaction afforded 0.175 g of orange powder (62% yield).

Anal. calcd (%): C, 72.58; H, 5.38; N, 4.98 found: C, 71.36; H, 5.27; N, 5.01%. ^{1}H NMR (CD_2Cl_2, 30 °C): δ 8.17 [m, 2H, –$C_6H_4NO_2$], δ 7.57 [m, 2H, –$C_6H_4NO_2$], δ 7.43 [m, 2H, –C_6H_4OMe], δ 7.14 [q, 1H, –C*H*═CH–], δ 6.90 [m, 3H, –C_6H_4OMe & –C*H*═CH–], δ 6.78 [d, 1H, –C*H*═CH–, ^3J (^{1}H,^{1}H) = 15 Hz], δ 6.69 [d, 1H, –C*H*═CH–, ^3J (^{1}H,^{1}H) = 16 Hz], δ 3.82 [s, 3H, –OCH_3]. X-Ray quality crystals of compound **2b** were obtained by slow evaporation of dichloromethane solution at 23 °C and the structure was confirmed to be analogous to that reported previously[31] by unit cell measurement.

Preparation of 4′-dimethylamino-4″-nitro-1,4-diphenyl-1,3-butadiene (2c). 0.175 g (1.00 mmol) of solid 4-dimethylaminocinnamaldehyde was dissolved in 15 mL of ethanol at 23 °C. 0.22 mL (1.00 mmol) of diethyl(4-nitrobenzyl)phosphonate was added to the solution. 3 mL of 1.5 M solution of sodium hydroxide in ethanol was then added and the reaction mixture was stirred overnight. The resulting precipitate was then filtered and washed with 5 mL of cold ethanol. The reaction afforded 0.1451 g of copper-brown product (49% yield).

Anal. calcd (%): C, 73.44; H, 6.16; N, 9.52 found: C, 72.83; H, 6.07; N, 9.47%. ^{1}H NMR (CD_2Cl_2, 30 °C): δ 8.15 [m, 2H, –$C_6H_4NO_2$], δ 7.54 [m, 2H, –$C_6H_4NO_2$], δ 7.36 [m, 2H, –$C_6H_4NMe_2$], δ 7.14 [q, 1H, –C*H*═CH–], δ 6.87–6.68 [m, 4H, –$C_6H_4NMe_2$ & –C*H*═CH–], δ 6.62 [d, 1H, –C*H*═CH–, ^3J (^{1}H,^{1}H) = 16 Hz], δ 2.99 [s, 6H, –N(CH_3)$_2$]. X-Ray quality crystals of compound **2c** were obtained by slow evaporation of dichloromethane solution at 23 °C and the structure was confirmed to be analogous to that reported previously[32] by unit cell measurement.

Preparation of 2-[(4-nitrophenyl)ethenyl]-4-bromothiophene (3a). 0.191 g (1.00 mmol) of solid 4-bromothiophene-2-carboxaldehyde was dissolved in 10 mL of ethanol at 23 °C. 0.22 mL (1.00 mmol) of diethyl(4-nitrobenzyl)phosphonate was added to the solution. 3 mL of 1.5 M solution of sodium hydroxide in ethanol was then added and the reaction mixture was stirred overnight. The resulting precipitate was then filtered and washed with 5 mL of cold ethanol. The reaction afforded 0.186 g of yellow powder (60% yield).

Anal. calcd (%): C, 46.47; H, 2.60; N, 4.52 found: C, 45.91; H, 2.62; N, 4.53%. ^{1}H NMR (CD_2Cl_2, 30 °C): δ 8.20 [m, 2H, –$C_6H_4NO_2$], δ 7.62 [m, 2H, –$C_6H_4NO_2$], δ 7.34 [d, 1H, –C*H*═CH–, ^3J (^{1}H,^{1}H) = 16 Hz], δ 7.23 [m, 1H, –C_4H_2S], δ 7.12 [m, 1H, –C_4H_2S], δ 7.01 [d, 1H, –C*H*═CH–, ^3J (^{1}H,^{1}H) = 16 Hz]. X-Ray quality crystals of compound **3a**·mono were obtained by slow evaporation of ethanol/chloroform solution at 23 °C, while the crystals of **3a**·ortho were obtained by slow evaporation of toluene solution at 23 °C.

Preparation of 2-[(4-nitrophenyl)ethenyl]-5-methylthiophene (3b). 0.11 mL (1.00 mmol) of liquid 5-methylthiophene-2-carboxaldehyde was dissolved in 10 mL of ethanol at 23 °C. 0.22 mL (1.00 mmol) of diethyl(4-nitrobenzyl)phosphonate was added to the solution. 3 mL of 1.5 M solution of sodium hydroxide in ethanol was then added and the reaction mixture was stirred overnight. The resulting precipitate was then filtered and washed with 5 mL of cold ethanol. The reaction afforded 0.191 g of yellow powder (78% yield).

Anal. calcd (%): C, 63.65; H, 4.52; N, 5.71 found: C, 62.70; H, 4.40; N, 5.59%. ^{1}H NMR (CD_2Cl_2, 30 °C): δ 8.18 [m, 2H, –$C_6H_4NO_2$], δ 7.58 [m, 2H, –$C_6H_4NO_2$], δ 7.35 [d, 1H, –C*H*═CH–, ^3J (^{1}H,^{1}H) = 16 Hz], δ 6.99 [m, 1H, –C_4H_2S], δ 6.84 [d, 1H, –C*H*═CH–, ^3J (^{1}H,^{1}H) = 16 Hz], δ 6.72 [m, 1H, –C_4H_2S], δ 2.51 [s, 3H, –CH_3]. X-Ray quality crystals of compound **3b** were obtained by slow evaporation of ethanol/chloroform solution at 23 °C.

Preparation of 2-[(4-nitrophenyl)ethenyl]-5-(methylthio)thiophe (3c). 0.152 g (1.00 mmol) of liquid (5-methylthio)thiophene-2-carboxaldehyde was dissolved in 10 mL of ethanol at 23 °C. 0.22 mL (1.00 mmol) of diethyl(4-nitrobenzyl)phosphonate was added to the solution. 3 mL of 1.5 M of sodium hydroxide in ethanol was then added and the reaction mixture was stirred overnight. The precipitate was then filtered and washed with 5 mL of cold ethanol. The reaction afforded 0.224 g of orange powder (81% yield).

Anal. calcd (%): C, 56.29; H, 4.00; N, 5.05 found: C, 55.53; H, 3.97; N, 5.05%. ^{1}H NMR (CD_2Cl_2, 30 °C): δ 8.19 [m, 2H, –$C_6H_4NO_2$], δ 7.59 [m, 2H, –$C_6H_4NO_2$], δ 7.33 [d, 1H, –C*H*═CH–, ^3J (^{1}H,^{1}H) = 16 Hz], δ 7.04 [m, 1H, –C_4H_2S], δ 6.96 [m, 1H, –C_4H_2S], δ 6.87 [d, 1H, –C*H*═CH–, ^3J (^{1}H,^{1}H) = 16 Hz], δ 2.55 [s, 3H, –CH_3]. X-Ray quality crystals of compound **3c** were obtained by slow evaporation of dichloromethane solution at 23 °C.

Results and discussion

Synthesis and crystal structures of compounds 1–4

Horner–Wadsworth–Emmons synthetic method[33] was used to synthesize the compounds **1–3** (Scheme 1). Equimolar amounts of aromatic aldehyde and phosphonate were reacted in basic conditions to yield spectroscopically and analytically pure products in good yields (*cf.* ESI† for the ^{1}H NMR and IR spectra). The reactions

resulted in the precipitation of pure products with the exception of compound **1b** which was extracted with a mixture of CH_2Cl_2 and H_2O followed by evaporation of the organic phase. All the compounds **1–3** possess $-NO_2$ group at the electron withdrawing end of the push–pull molecules. Various substituents at the electron donating end were selected with a view to have an effect on the charge-transfer properties and therefore the molecular hyperpolarizability as well as to increase the possibility for the ideal, non-centrosymmetric packing of the chromophores in the crystal lattice (Scheme 1).

Single-crystal X-ray structures of stilbene derivatives

Similarly to many reported stilbene derivatives,[20,21,34,35] the 2-chloro-3,4-dimethoxy-4′-nitrostilbene compound **1a** shows polymorphism by crystallization in both centrosymmetric ($P2_1/c$, **1a**·centro) and non-centrosymmetric ($P2_1$, **1a**·non-centro) space groups (Fig. 1, *cf.* ESI† for molecular figures of all the structures with atomic numbering schemes and the tables of pertinent bond parameters). Analogously to 3-methyl-4-methoxy-4′-nitrostilbene (MMONS),[34] the discrete molecules in the centrosymmetric form **1a**·centro are nearly planar with *ca.* 3.8° angle between the aryl rings. By contrast, more pronounced twisting is notable in the non-centrosymmetric polymorph **1a**·non-centro as evidenced by the corresponding angle of *ca.* 19.2° in the molecule. The primary driving force of the crystal packing in both polymorphs of **1a** seems to be π–π interactions, and while in **1a**·centro this leads to a herringbone-like linear arrangement of molecular chains (Fig. 1a), in **1a**·non-centro half of the molecules are rotated by *ca.* 90° (Fig. 1b). Consequently, only **1a**·non-centro displays intermolecular Cl···ONO interactions of 3.27 Å whereas the remaining close contacts (*e.g.* MeO···H, NO_2···H) are virtually insignificant in both polymorphs.

Stilbene **1a** was also noted to go through, presumably, a photodimerization process of the ethenyl linkage to afford tetra-aryl cyclobutane compound **4** (Fig. 2). Analogous behaviour has been previously observed with other stilbenes and diaromatic olefins where a distance of *ca.* 3.5–4.2 Å between the central C=C bonds of adjacent molecules facilitates the solid state photodimerization process.[36–38] Suitable alignment of molecules and a distance of *ca.* 3.7 Å between the double bonds can be found in **1a**·centro whereas no such arrangement is observable in **1a**·non-centro therefore suggesting that the former polymorph is the primary source for the formation of tetra-aryl cyclobutane dimer **4**.

The cyclobutane dimer **4** also shows polymorphism with crystallization in two monoclinic space groups, $P2_1/n$ (**4**·Pcell) and $C2/c$ (**4**·Ccell). The difference in crystal packing can also be seen in a slightly different orientation of the phenyl groups around the central cyclobutane unit (Fig. 2). The dimerization results in the expected lengthening of the double bond in the ethenyl part of the original monomers from 1.333(2)–1.333(4) Å in **1a**·non-centro and **1a**·centro to 1.546(2)–1.558(2) Å in **4**·Pcell and **4**·Ccell. In addition, the C–C bonds between the two stilbene units in cyclobutane rings in **4**·Pcell and **4**·Ccell are slightly longer than within each stilbene unit at 1.583(2)–1.600(2) Å *vs.* 1.546(2)–1.558(2) Å, respectively (*cf.* ESI†).

Stilbene derivative **1b** with –OH, –Br and two $-NO_2$ substituents crystallizes in a non-centrosymmetric space group Cc. The phenyl rings within each molecule are strongly twisted compared to both polymorphs of **1a** with an angle of 29.7° between the aryl groups (Fig. 3a). Similarly to **1a**, the crystal packing in **1b** can be primarily contributed to π–π interactions even though weak Br···ONO halogen contacts of *ca.* 3.51 and 3.37 Å, analogous to the Cl···ONO contacts in **1a**·non-centro, also exist. The two orientations of independent molecules in **1b** (Fig. 3b) and those observed in **1a**·non-centro (Fig. 1b) also bear a close resemblance.

Stilbene **1c** with $-NO_2$ and –MeO substituents displays three independent molecules in the crystal lattice arranged in a rather random manner in triclinic space group $P\bar{1}$ (Fig. 4a). In contrast to the structures of **1a** and **1b**, there is an apparent lack of π–π interactions in **1c**. Instead, one of the three independent molecules forms centrosymmetric dimers through weak H···OMe hydrogen bonds between the MeO group and one of the hydrogens of the phenyl rings (Fig. 4b).

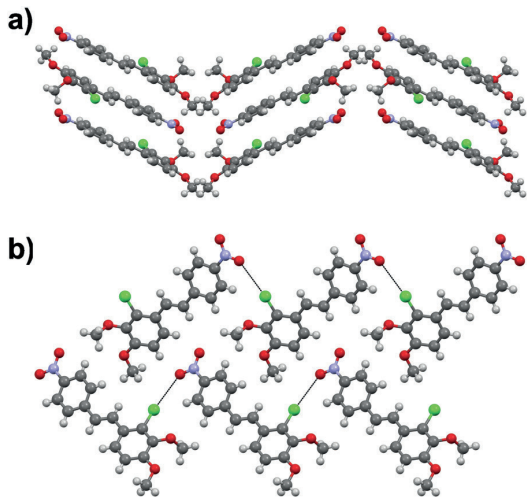

Fig. 1 Molecular packing in (a) **1a**·centro (along *c*-axis) and (b) **1a**·non-centro (along *a*-axis).

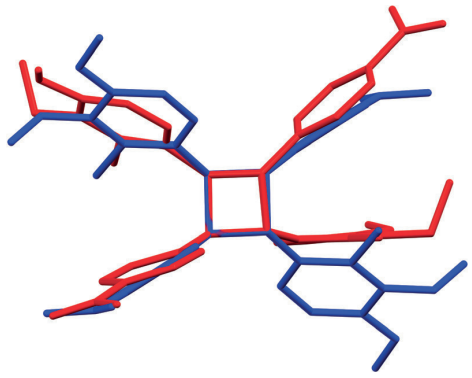

Fig. 2 The difference in phenyl ring and substituent orientations between P-cell (red) and C-cell (blue) tetra-aryl cyclobutanes **4**.

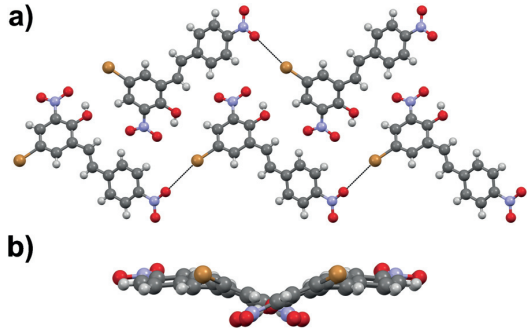

Fig. 3 (a) Crystal packing in compound **1b** showing the orientation of the molecules within each layer (along *a*-axis) and (b) side view of the layer revealing the molecular distortion.

Stilbene derivative **1d** with one $-NO_2$ and two –MeO groups crystallizes in a centrosymmetric space group $P2_1/c$. The aromatic rings within each molecule are heavily twisted with an angle of 43.7° between the rings (Fig. 5a). The molecules in **1d** form dimeric units through MeO···H_3CO interactions (Fig. 5b) while the overall arrangement of molecules in the crystal lattice is rather arbitrary.

Stilbene congener **1e** with $-NO_2$ and $-NMe_2$ substituents crystallizes in a non-centrosymmetric space group $P2_1$. The structure shows disorder in which the molecules are organized in two orientations in the crystal lattice in 60 : 40 ratio (*cf.* ESI† for a molecular figure of disorders in **1e**). The slightly twisted stilbene molecules form planes along *a*-axis, and chains through weak $NO_2\cdots(H_3C)N$ hydrogen bonding along *c*-axis with alternating chain directions in the planes (Fig. 6).

Single-crystal X-ray structures of diphenylbutadiene derivatives

The diphenylbutadiene **2a** crystallizes in non-centrosymmetric space group *Pc*. Despite multiple crystallizations and several data collections, the crystal structure consistently shows orientational disorder where adjacent molecules are placed opposite

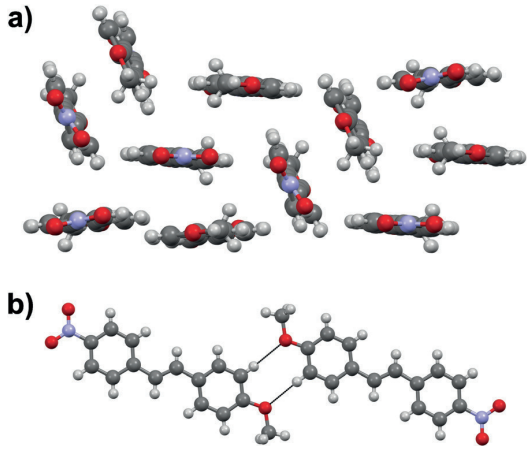

Fig. 4 (a) Orientation of stilbene molecules in the crystal lattice, and (b) close contacts in **1c**.

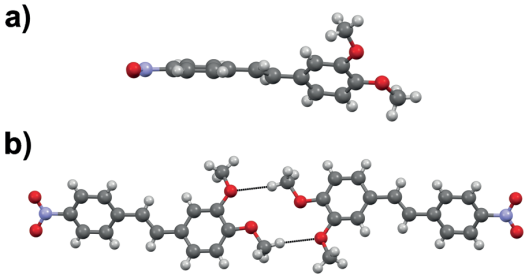

Fig. 5 (a) Rotation of the phenyl rings, and (b) the dimeric unit in **1d**.

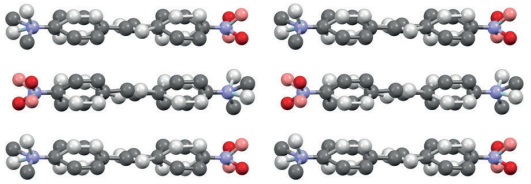

Fig. 6 Molecular packing of stilbene derivative **1e** viewed along *a*-axis (H atoms removed for clarity, disorder indicated with lighter colours).

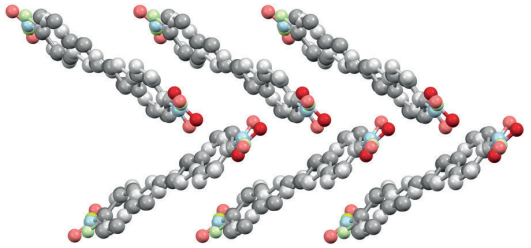

Fig. 7 Crystal structure of **2a** with herringbone-style layers viewed along *a*-axis (H atoms removed for clarity, disorder indicated with lighter colours).

directions in head-to-tail fashion (*cf.* ESI† for a molecular figure of disorder in **2a**).[39] The slightly twisted diphenylbutadienes in **2a** form planes along *a*-axis with alternating orientation of the molecules within each plane, and a herringbone style layering between the planes (Fig. 7). The crystal structures of diphenylbutadienes **2b** and **2c** have been reported previously (CSD entries YIQJEQ and EDUSAA).[31,32] The former crystallizes in centrosymmetric space group $P\bar{1}$ with head-to-tail organization of the molecules. Despite the increase in chain length compared to stilbenes derivatives **1a–e**, the conjugated molecules in **2b** are notably planar (Fig. 8) forming a sheet-like structure with π–π interactions leading to a relatively short distance of 3.70 Å between centroids of the phenyl rings. The diphenylbutadiene **2c** crystallizes in centrosymmetric space group $P2_1/c$ and, analogously to **2b**, with markedly planar geometry within the molecules. In contrast to **2b**, however, there is some angling of the molecules between the layers (Fig. 8c), and therefore no π–π interactions can be observed. Despite the extensive crystallization

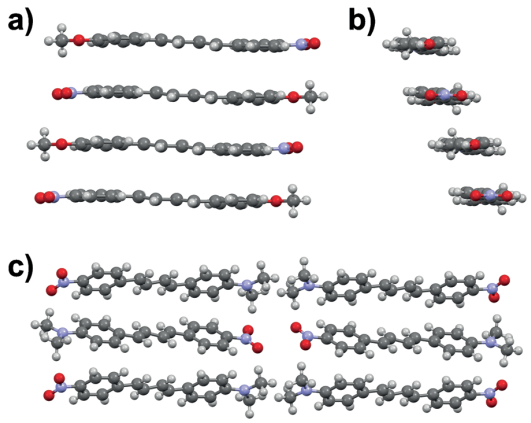

Fig. 8 (a) Side view and (b) end view of molecular arrangement in **2b** (CSD entry "YIQJEQ"),[31] and (c) molecular arrangement in **2c** (CSD entry "EDUSAA").[32] Disorder in **2c** has been removed for clarity.

efforts, no polymorphism and discovery of new, non-centrosymmetric crystal structures of **2b** and **2c** were observed.

Single-crystal X-ray structures of phenylethenylthiophene derivatives

Similarly to stilbene **1a**, the phenylethenylthiophene **3a** displays polymorphism by crystallizing in two centrosymmetric space groups, monoclinic $P2_1/c$ (**3a**·mono) and orthorhombic *Pbca* (**3a**·ortho). Most notably, the phenyl and thiophene rings in **3a**·mono are significantly twisted (by 12.4° and 17.5° in two independent molecules, respectively) while the analogous twisting in **3a**·ortho is less pronounced (4.7°). Both polymorphs exhibit significant halogen bonding through $NO_2\cdots$Br contacts of *ca.* 3.06 and 3.00 Å in **3a**·mono and **3a**·ortho, respectively. Overall, the molecules form layered structure in **3a**·mono (Fig. 9a) whereas in **3a**·ortho the distortion between layers is notable (Fig. 9b).

Phenylethenylthiophene derivative **3b** crystallizes in a centrosymmetric space group $P2_1/n$ (Fig. 10a). The crystal structure displays two independent molecules in the unit cell with only slight deviation from planarity (*ca.* 6.8° and 5.7° angles between the aromatic rings, respectively). One of the two molecules in asymmetric unit exhibits significant rotation of the $-NO_2$ substituent with respect to the phenyl ring (3.6° *vs.* 27.8° in the two distinct molecules). This behaviour is similar to **3a**·mono, in which the $-NO_2$ groups show various degrees of rotation (3.2° and 13.7° degrees), whereas in **3a**·ortho all the substituents are virtually planar with respect to the phenyl and thiophene rings. The weak $NO_2\cdots H_3C$ interactions result in chain formation with alternating directions and V-shaped geometry along the chains (Fig. 10b).

Phenylethenylthiophene **3c** crystallizes in centrosymmetric space group $P2_1/n$. The molecular chains form herringbone-style planes with altering direction of the chains within each layer (Fig. 11). The only intermolecular interactions are the weak $NO_2\cdots H_3CS$ contacts between the two substituents.

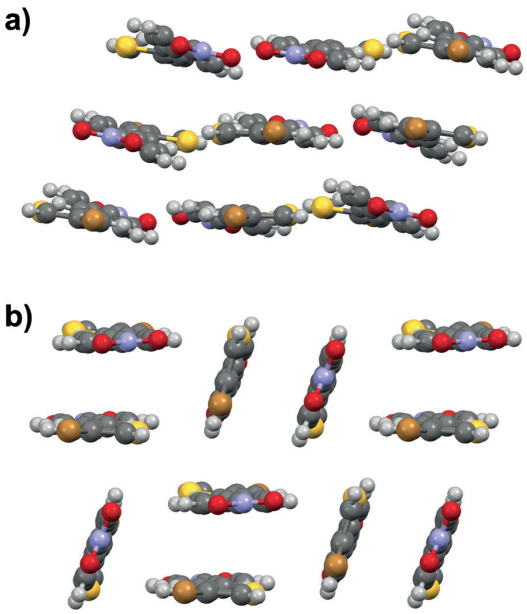

Fig. 9 (a) Crystal structure of **3a**·mono viewed along *b*-axis, and (b) side view of **3a**·ortho.

Nonlinear optical properties of compounds 1a–e, 2a–c and 3a–c

The nonlinear optical properties of compounds **1a–e**, **2a–c**, and **3a–c** were initially measured with Kurtz–Perry powder method[27] by using femtosecond laser radiation at 1030 nm. In these experiments the SHG efficiency of MMONS (Scheme 1) displayed intensity of 61 times compared to that of urea (Table 1), far from the reported literatures values of *ca.* 750–1250 times urea.[21] In view of the possible competing processes, such as two-photon fluorescence, the SHG intensities of MMONS, urea and the most promising new stilbene derivative, **1a**·non-centro, were also measured by using nanosecond laser radiation at both 1030 and 1060 nm to closely reproduce the literature experiments (Table 1 and Fig. 12).[21] While the switch from femtosecond to nanosecond laser source did increase the SHG intensity of MMONS from 61 to *ca.* 200 times to that of urea, the change of the wavelength from 1030 to 1060 nm did not show significant effect on the SHG intensity consistently with the solid-state absorption maxima of MMONS reported at lower wavelength (346 and 474 nm)[21] than either of the SHG signals at 515 and

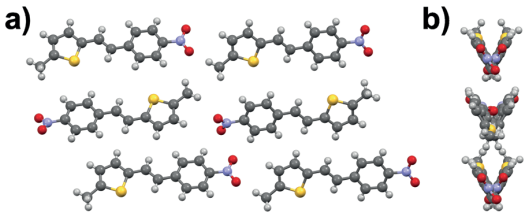

Fig. 10 (a) Crystal structure of compound **3b** viewed along *b*-axis, and (b) side view of the layers showing the V-shaped arrangement.

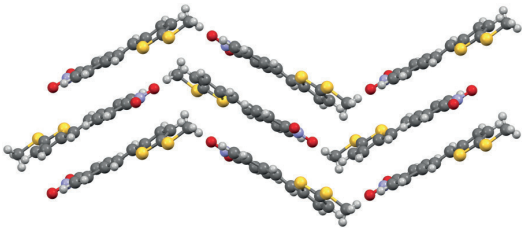

Fig. 11 Herringbone style layers of **3c** viewed along *a*-axis.

Table 1 Areas of SHG signals of **1a**·non-centro, **1b** and **2a** compared to urea and MMONS[a]

Femtosecond laser radiation at 1030 nm (laser power: [b]1.3 mW, [c]6.2 mW)					
Sample[a]	Signal area[b] (a.u.)	Relative area[b] (times urea)	Sample[b]	Signal area[c] (a.u.)	Relative area[c] (times urea)
Urea	31 000	1	Urea	397 800	1
MMONS	1 890 000	61.0	**1b**	15 600	0.04
1a·non-centro	169 700	5.5	**2a**	71 300	0.18
Nanosecond laser radiation at [d]1030 and [e]1060 nm					
Sample[a]	Signal area[d] (a.u.)	Relative area (times urea)[d]	Sample[d]	Signal area[e] (a.u.)	Relative area[e] (times urea)
Urea	4760	1	Urea	7120	1
MMONS	977 100	205	MMONS	1 498 300	210
1a·non-centro	36 640	7.7	**1a**·non-centro	230 650	32.4

[a] Crystalline samples sieved to particle size of <125 μm.

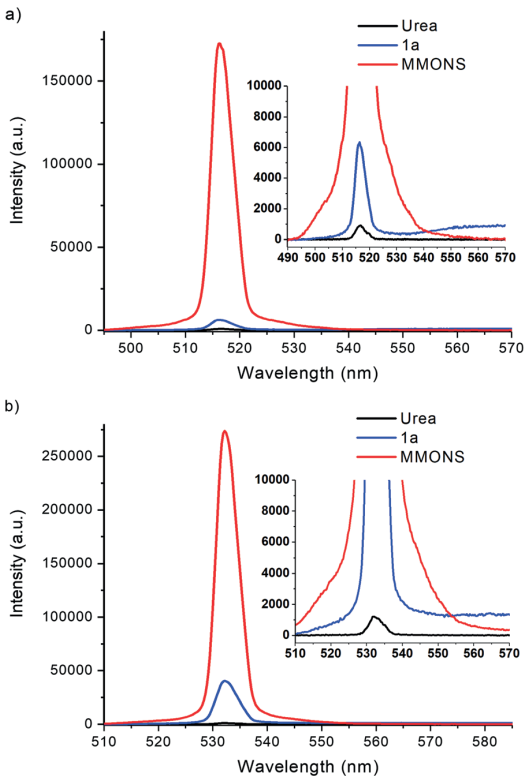

Fig. 12 SHG signals of **1a**·non-centro, MMONS and urea generated at (a) 1030 nm and (b) 1060 nm with nanosecond laser source.

530 nm. However, the SHG intensity of MMONS still remained notably lower than the literature values (200 *vs.* 750–1250 times of urea) possibly owing to the fragmentation of fragile MMONS samples into too small microcrystalline material in the sieving process to reduce the SHG intensity,[21] or because of partial contamination of the samples with inactive polymorphs of MMONS.[34] The latter, however, was rendered unlikely by space group determinations of several individual crystals and by X-ray powder measurements.

Hand-picked crystalline sample of the non-centrosymmetric polymorph **1a**·non-centro displays SHG intensity of *ca.* 5.5 times to that of urea in the femtosecond laser experiments at 1030 nm. The SHG intensity of **1a**·non-centro increases to 7.7 and, significantly, 32.4 times to that of urea when nanosecond laser source is used at 1030 and 1060 nm wavelength, respectively. In all measurements the microcrystalline sample of **1a**·non-centro shows detectable broad fluorescence indicating that some SHG efficiency is lost due to electronic excitation of the material, namely two-photon absorption of the laser radiation or absorption of the generated SH signal. The absorbance at 515 nm is virtually non-existing in CH_2Cl_2 solution (see below), but in the microcrystalline sample signal faces multiple interactions increasing absorption significantly. This may explain the observed difference in the intensity of SHG signal between two fundamental wavelengths. In addition, fluorescence is not evident to be two-photon induced process as the intensity is not clearly dependent on the duration of laser pulse, suggesting that the generated SHG signal is to some extent absorbed in the sample.

The stilbene derivatives **1b** and **1e** also display non-centrosymmetric crystal packing in the solid state with the space groups *Cc* and $P2_1$, respectively. However, only negligible SHG activity is observed for compound **1b** (0.04 times that of urea), and virtually no SHG activity is detected for **1e** with femtosecond laser experiments at 1030 nm. The stilbene derivative **1c** has also been reported to give rise to SHG signal, and polymorphism by crystallization in both centrosymmetric and non-centrosymmetric triclinic space groups.[20,40,41] However, our investigation revealed only centrosymmetric space group ($P\bar{1}$) and no SHG activity for **1c**.[42]

While the stilbene derivatives **1a–e** expectedly display varying degree of SHG activity in the solid state depending on the efficiency of crystal packing, the alterations in the chain length between aryl groups to give diarylbutadienes **2** and changing one of the aryl groups to thiophene in compounds **3** resulted primarily in centrosymmetric arrangements of the chromophores despite the extensive crystallization efforts to obtain non-centrosymmetric polymorphs. Consequently, among all the derivatives of **2** and **3**, only the diarylbutadiene compound **2a** shows SHG intensity (0.18 times of urea) consistently with the non-centrosymmetric space group *Pc*.

It has been suggested that the highest recorded SHG activity of 3-methyl-4-methoxy-4′-nitrostilbene (MMONS) arises partly from the strong π–π interactions that enhance the intermolecular charge-transfer and, consequently, the second order polarizability.[21] In accordance, MMONS displays distances as short as *ca.* 3.56 Å between the phenyl ring centroids despite the two distinct orientations of the molecules. The same distances in stilbene derivatives **1a**·non-centro and **1b** are *ca.* 4.22 and 3.82 Å, respectively, even though it is the former chromophore that displays higher SHG intensity. This is likely a result of the better arrangement of polar centres in the crystal lattice of **1a**·non-centro and the presence of electron withdrawing $-NO_2$ group also in the "push" part of the chromophore **1b**. In contrast to the aforementioned compounds, the non-centrosymmetric stilbene derivative **1e** does not show significant π–π interactions, which is possibly contributing to the virtual absence of SHG activity.

Optical spectroscopy of compounds 1–3

The absorption spectra of compounds **1–3** were measured in CH_2Cl_2 at room temperature (Table 2 and Fig. 13). All compounds display one high and one low energy absorption maximum in solution, albeit the former is observable only as a small shoulder with the solvent signal in the case of stilbene derivatives **1a** and **1c**. Additionally, stilbene congener **1b**, the only compound with $-NO_2$ group at both ends of the molecule, displays a distinct shoulder also at 410 nm. The high energy (low wavelength) absorption maxima show relatively narrow range of 278–303 nm for stilbene derivatives **1**, 289–322 nm for diphenylbutadiene compounds **2**, and 272–291 nm for phenylethenylthiophene species **3**, while the corresponding low energy (high wavelength) bands exhibit significantly broader range of 336–439 nm for **1a–e**, 381–452 nm for **2a–c** and 358–397 nm for **3a–c**. Expectedly, all the extinction coefficient values of *ca.* 9–37 × 10^3 M^{-1} cm^{-1} are in the range typically observed for π → π* transition. Given the wider wavelength range observed for the low energy absorption maxima, these bands are likely reflecting the modifications made by substituent alterations at the electron donating part of compounds **1–3** whereas the high energy bands in the absorption spectra are contributed to the electron withdrawing, $-NO_2$ substituted end of the conjugated push–pull systems where no alterations were made within each series. Consistently, both diphenylbutadiene (**2**) and phenylethenylthiophene (**3**) derivatives exhibit a steady red shift in the low energy absorption maximum following the approximate order of increasing electron donating power of the substituents: F (**2a**, 381 nm) < OCH_3 (**2b**, 401 nm) < NMe_2 (**2c**, 452 nm), and Br (**3a**, 358 nm) < CH_3 (**3b**, 390 nm) < SCH_3 (**3c**, 397 nm), respectively. Similarly, stilbene derivative **1e** with the strongest

Table 2 Absorption and fluorescence spectroscopic properties of compounds **1–3**

Absorption bands[a]						
	λ_{Abs}[b] (nm)	ε[c] (M^{-1} cm^{-1})		λ_{Abs}[b] (nm)	ε[c] (M^{-1} cm^{-1})
1a	365	17 200	**2a**	381	23 350
				289	10 700
1b	336	23 800	**2b**	401	36 450
	278	13 700		301	16 350
1c	376	23 100	**2c**	452	35 350
				322	18 450
1d	385	24 350	**3a**	358	10 600
	280	13 000		272	13 750
1e	439	23 850	**3b**	390	16 300
	303	12 750		278	10 800
			3c	397	27 350
				291	8850

Fluorescence bands[d]							
	λ_{Ex}[e] (nm)	λ_{Em}[f] (nm)	$\Delta\nu$[g] (cm^{-1})		λ_{Ex}[e] (nm)	λ_{Em}[f] (nm)	$\Delta\nu$[g] (cm^{-1})
1a	380	560	9540	**2a**	380	550	8065
1c	380	585	9502	**2b**	400	615	8677
1d	390	605	9445	**2c**	460	780	9303
1e	450	730	9080	**3a**	380	520	8702
				3b	395	570	8097
				3c	400	635	9441

[a] 1 mM and 10 μM sol. in CH_2Cl_2 at 23 °C. [b] Absorption maximum. [c] Extinction coefficient. [d] 0.1–10 μM solutions in CH_2Cl_2 at 23 °C. [e] Excitation maximum. [f] Emission maximum. [g] Stokes shift in wavenumbers calculated by the equation $(10^7/\lambda_{Abs}) - (10^7/\lambda_{Em})$.

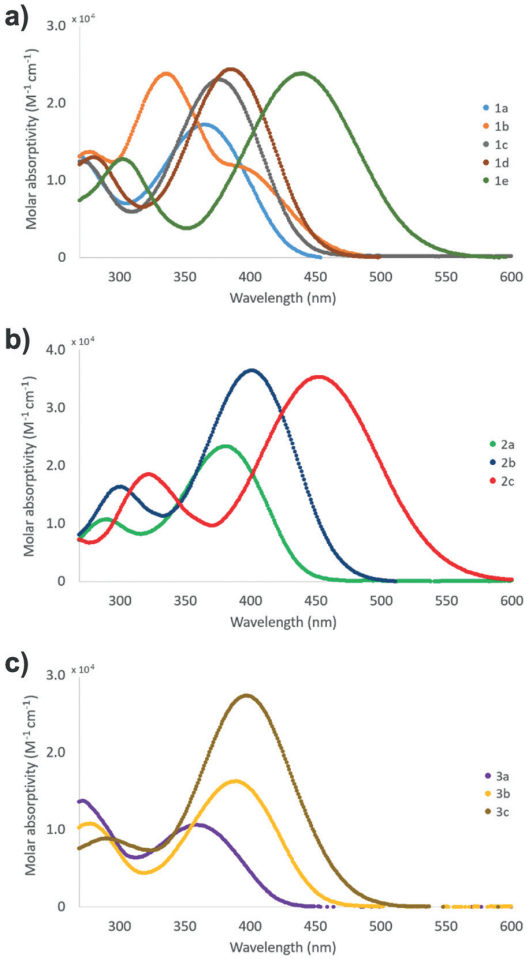

Fig. 13 Visible spectra of compounds (a) **1a–e**, (b) **2a–c** and (c) **3a–c** (1 mM and 10 μM sol. in CH_2Cl_2 at 23 °C).

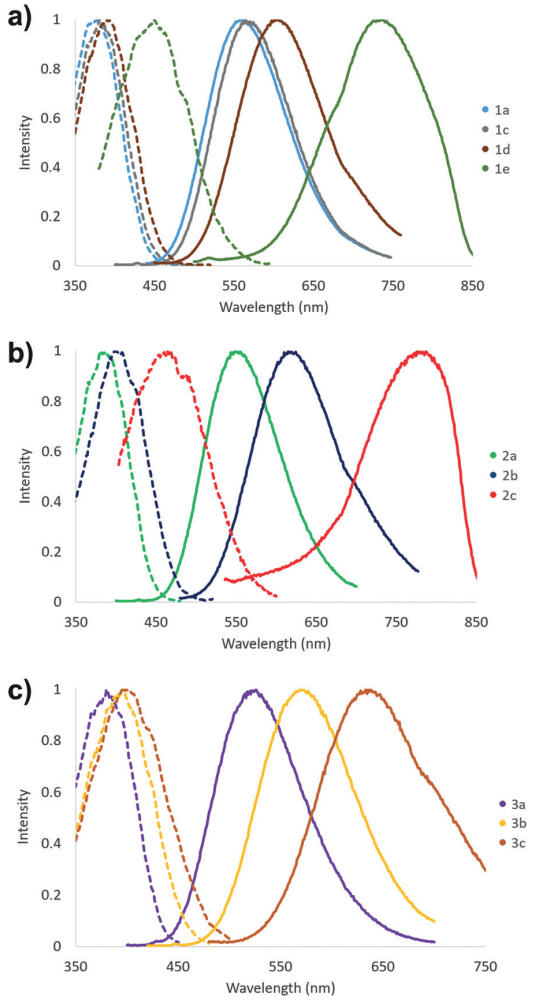

Fig. 14 Fluorescence spectra of compounds (a) **1a**, **1c–1e**, (b) **2a–c** and (c) **3a–c** (emission spectra: solid line, excitation spectra: dotted line, 0.1–10 μM sol. in CH_2Cl_2 at 23 °C).

electron donating group (NMe_2) gives the lowest energy absorption maximum of the series at 439 nm.

The fluorescent nature of stilbene and its derivatives is well established and various aspects of their optical, photophysical and photochemical properties have been exhaustively studied.[43–47] Consistently with the high optical activity, the stilbene (**1**), diphenylbutadiene (**2**) and phenylethenylthiophene (**3**) derivatives in this investigation all show fluorescent properties with the exception of compound **1b** (Table 2 and Fig. 14). In contrast to the two absorption bands, only single maximum with poorly resolved shoulders is observed in the excitation spectra of all the compounds **1–3** in CH_2Cl_2 at room temperature. However, the wavelength of the excitation maximum of each derivative displays close correlation with the corresponding low energy absorption band. Similarly to the absorption spectra, both the excitation and emission spectra of compounds **1–3** exhibit more pronounced red shift together with the increasing electron donating power of the substituent(s) within each series. Accordingly, the $-NMe_2$ containing derivatives **1e** and **2c** give rise to the highest wavelength excitation and emission maxima. The large Stokes red shift values expectedly indicate high dipole moment in the excited state for all the compounds **1–3** in CH_2Cl_2 as has been previously demonstrated, for example, for compound **1e**.[43]

Conclusions

We report here the preparation and characterization of conjugated stilbene, diphenylbutadiene and phenylethenylthiophene based diaromatic compounds and their SHG activities measured from the crystalline samples by the Kurtz–Perry powder method. The most significant activity was observed for the stilbene **1a**, which produces SHG signal with intensity *ca.* 32 times stronger than that of the urea reference when nanosecond laser radiation at 1060 nm is applied. The stilbene derivative **1b** and diphenylbutadiene **2a** also display SHG activity, albeit with significantly lower intensity compared to **1a**. The often high SHG intensities reported for stilbene derivatives have been contributed, in part, to the strong π–π interactions that enhance the intermolecular charge-transfer and, consequently, the second order polarizability.[21] Consistently, the stilbene derivative **1a** exhibits somewhat weaker π–π interactions compared to 3-methyl-4-methoxy-4′-nitrostilbene (MMONS, Scheme 1) with significantly higher SHG intensity.

Our efforts to further investigate the effect of weak interactions to the NLO properties by changing the functional groups at the electron-donating end of stilbene, the extended chain length between the aromatic groups in diarylbutadienes and with thiophene derivatives were hampered by the extensive polymorphism that resulted in mainly centrosymmetric, NLO inactive chromophores despite the comprehensive crystallization efforts. Even the stilbene **1a** with notable SHG activity also crystallizes in centrosymmetric, inactive space group and goes through, presumably, a photodimerization process to form two polymorphs of the tetraaryl cyclobutane **4**. Nevertheless, the high SHG intensities of especially 3-methyl-4-methoxy-4′-nitrostilbene (MMONS) and congeneric derivative **1a** make them attractive chromophores for future studies to produce NLO active lenses by stereolithographic 3D printing technique.[26] Furthermore, the current study illustrates the versatility of the structural, chemical and optical properties in these diaromatic, conjugated systems as also evidenced by their fluorescent nature in solution.

Conflicts of interest

There are no conflicts to declare.

Acknowledgements

The authors gratefully acknowledge financial support from the Finnish Cultural Foundation and the Magnus Ehrnrooth Foundation.

References

1 S. Tao, T. Miyagoe, A. Maeda, H. Matsuzaki, H. Ohtsu, M. Hasegawa, S. Takaishi, M. Yamashita and H. Okamoto, *Adv. Mater.*, 2007, **19**, 2707–2710.
2 J. M. Hales, S. Zheng, S. Barlow, S. R. Marder and J. W. Perry, *J. Am. Chem. Soc.*, 2006, **128**, 11362–11363.
3 B. Champagne, A. Plaquet, J.-L. Pozzo, V. Rodriguez and F. Castet, *J. Am. Chem. Soc.*, 2012, **134**, 8101–8103.
4 J. N. Zhang, X. Q. Wang, Q. Ren, H. L. Yang, J. W. Chen, Q. Sun, G. C. Li and T. B. Li, *Opt. Laser Technol.*, 2011, **43**, 679–682.
5 S. Di Bella, C. Dragonetti, M. Pizzotti, D. Roberto, F. Tessore and R. Ugo, in *Molecular Organometallic Materials for Optics, Topics in Organometallic Chemistry*, ed. H. Le Bozec and V. Guerchais, Coordination and Organometallic Complexes as Second-Order Nonlinear Optical Molecular Materials, Springer, Berlin, Heidelberg, ch. 1, vol. 28, 2010, pp. 1–55.
6 K. B. Manjunatha, R. Dileep, G. Umesh and B. R. Bhat, *Opt. Laser Technol.*, 2013, **52**, 103–108.
7 V. Nalla, R. Medishetty, Y. Wang, Z. Bai, H. Sun, J. Wei and J. J. Vittal, *IUCrJ*, 2015, **2**, 317–321.
8 C.-F. Sun, C.-L. Hu, X. Xu, J.-B. Ling, T. Hu, F. Kong, X.-F. Long and J.-G. Mao, *J. Am. Chem. Soc.*, 2009, **131**, 9486–9487.
9 R. W. Boyd, *Nonlinear Optics*, Academic Press, 3rd edn, 2008.
10 G. J. Ashwell, G. Jefferies, D. G. Hamilton, D. E. Lynch, M. P. S. Roberts, G. S. Bahra and C. R. Brown, *Nature*, 1995, **375**, 385–388.
11 G. J. Ashwell, *Adv. Mater.*, 1996, **8**, 248–250.
12 C. Chuantian, W. Bochang, J. Aidong and Y. Guiming, *Sci. Sin., Ser. B*, 1985, **28**, 235–243.
13 F. C. Zumsteg, J. D. Bierlein and T. E. Gier, *J. Appl. Phys.*, 1976, **47**, 4980–4985.
14 J. D. Bierlein and H. Vanherzeele, *J. Opt. Soc. Am. B*, 1989, **6**, 622.
15 I. Ledoux, C. Lepers, A. Périgaud, J. Badan and J. Zyss, *Opt. Commun.*, 1990, **80**, 149–154.
16 S. R. Marder, J. W. Perry and C. P. Yakymyshyn, *Chem. Mater.*, 1994, **6**, 1137–1147.
17 P. S. Patil, S. M. Dharmaprakash, H.-K. Fun and M. S. Karthikeyan, *J. Cryst. Growth*, 2006, **297**, 111–116.
18 B. F. Levine, C. G. Bethea, C. D. Thurmond, R. T. Lynch and J. L. Bernstein, *J. Appl. Phys.*, 1979, **50**, 2523–2527.
19 L. T. Cheng, W. Tam, S. H. Stevenson, G. R. Meredith, G. Rikken and S. R. Marder, *J. Phys. Chem.*, 1991, **95**, 10631–10643.
20 Y. Wang, W. Tam, S. H. Stevenson, R. A. Clement and J. Calabrese, *Chem. Phys. Lett.*, 1988, **148**, 136–141.
21 W. Tam, B. Guerin, J. C. Calabrese and S. H. Stevenson, *Chem. Phys. Lett.*, 1989, **154**, 93–96.
22 P. R. Varanasi, A. K.-Y. Jen, J. Chandrasekhar, I. N. N. Namboothiri and A. Rathna, *J. Am. Chem. Soc.*, 1996, **118**, 12443–12448.
23 A. K.-Y. Jen, Y. Cai, P. V. Bedworth and S. R. Marder, *Adv. Mater.*, 1997, **9**, 132–135.
24 K. Mandal, T. Kar, P. K. Nandi and S. P. Bhattacharyya, *Chem. Phys. Lett.*, 2003, **376**, 116–124.
25 V. P. Rao, A. K.-Y. Jen, K. Y. Wong and K. J. Drost, *Tetrahedron Lett.*, 1993, **34**, 1747–1750.
26 E. Kukkonen, E. Lahtinen, P. Myllyperkiö, J. Konu and M. Haukka, *ACS Omega*, 2018, **3**, 11558–11561.
27 S. K. Kurtz and T. T. Perry, *J. Appl. Phys.*, 1968, **39**, 3798–3813.
28 CrysAlis PRO, Agilent Technologies Ltd, Yarnton, Oxfordshire, England.
29 O. V. Dolomanov, L. J. Bourhis, R. J. Gildea, J. A. K. Howard and H. Puschmann, *J. Appl. Crystallogr.*, 2009, **42**, 339–341.
30 G. M. Sheldrick, *Acta Crystallogr., Sect. C: Struct. Chem.*, 2015, **71**, 3–8.
31 Crystal structure of compound **2b** has been deposited to CCDC database: S. P. Kelley, K. Yang, N. Corretjer, S. Gadban, R. Glaser, M. M. Kozak and B. A. Hathaway, CSD Private Commun, 2018, CCDC 1879519.
32 M. Rawal, K. E. Garrett, L. E. Johnson, W. Kaminsky, E. Jucov, D. P. Shelton, T. Timofeeva, B. E. Eichinger, A. F. Tillack, B. H. Robinson, D. L. Elder and L. R. Dalton, *J. Opt. Soc. Am. B*, 2016, **33**, E160.
33 W. S. Wadsworth and W. D. Emmons, *J. Am. Chem. Soc.*, 1961, **83**, 1733–1738.
34 P. Munshi, B. W. Skelton, J. J. McKinnon and M. A. Spackman, *CrystEngComm*, 2008, **10**, 197–206.
35 S. N. Oliver, P. Pantelis and P. L. Dunn, *Appl. Phys. Lett.*, 1990, **56**, 307–309.
36 G. Marras, P. Metrangolo, F. Meyer, T. Pilati, G. Resnati and A. Vij, *New J. Chem.*, 2006, **30**, 1397.
37 M. A. Sinnwell and L. R. MacGillivray, *Angew. Chem., Int. Ed.*, 2016, **55**, 3477–3480.
38 G. W. Coates, A. R. Dunn, L. M. Henling, J. W. Ziller, E. B. Lobkovsky and R. H. Grubbs, *J. Am. Chem. Soc.*, 1998, **120**, 3641–3649.
39 Analogous disorder with detailed examination of correct space group has been reported for (*trans*)-4-chloro-4′-nitrostilbene: N.-R. Behrnd, G. Labat, P. Venugopalan, J. Hulliger and H.-B. Bürgi, *CrystEngComm*, 2010, **12**, 4101–4108.
40 Preliminary single-crystal and powder X-ray studies with non-centrosymmetric space group *P*1 and some SHG activity has been reported for compound **1c**: P. M. Dinakaran, G. Bhagavannarayana and S. Kalainathan, *Spectrochim. Acta, Part A*, 2012, **97**, 995–1001; these results were subsequently challenged, *cf.* ref. 41.
41 B. R. Srinivasan, Z. Tylczynski and V. S. Nadkarni, *Opt. Mater.*, 2013, **35**, 1616–1618.
42 An analogous crystal structure of compound **1c** was deposited to CCDC database during the time of writing this contribution: T. H. Chunhua, A. C. Soegiarto and M. D. Ward, CSD Private Commun., 2020, CCDC 1976072.
43 H. Gruen and H. Goerner, *J. Phys. Chem.*, 1989, **93**, 7144–7152.
44 D. Pines, E. Pines and W. Rettig, *J. Phys. Chem. A*, 2003, **107**, 236–242.
45 T. Nakabayashi, M. Wahadoszamen and N. Ohta, *J. Am. Chem. Soc.*, 2005, **127**, 7041–7052.
46 R. Lapouyade, K. Czeschka, W. Majenz, W. Rettig, E. Gilabert and C. Rulliere, *J. Phys. Chem.*, 1992, **96**, 9643–9650.
47 D. Schulte-Frohlinde, H. Blume and H. Güsten, *J. Phys. Chem.*, 1962, **66**, 2486–2491.

DEPARTMENT OF CHEMISTRY, UNIVERSITY OF JYVÄSKYLÄ
RESEARCH REPORT SERIES

1. Vuolle, Mikko: Electron paramagnetic resonance and molecular orbital study of radical ions generated from (2.2)metacyclophane, pyrene and its hydrogenated compounds by alkali metal reduction and by thallium(III)trifluoroacetate oxidation. (99 pp.) 1976
2. Pasanen, Kaija: Electron paramagnetic resonance study of cation radical generated from various chlorinated biphenyls. (66 pp.) 1977
3. Carbon-13 Workshop, September 6-8, 1977. (91 pp.) 1977
4. Laihia, Katri: On the structure determination of norbornane polyols by NMR spectroscopy. (111 pp.) 1979
5. Nyrönen, Timo: On the EPR, ENDOR and visible absorption spectra of some nitrogen containing heterocyclic compounds in liquid ammonia. (76 pp.) 1978
6. Talvitie, Antti: Structure determination of some sesquiterpenoids by shift reagent NMR. (54 pp.) 1979
7. Häkli, Harri: Structure analysis and molecular dynamics of cyclic compounds by shift reagent NMR. (48 pp.) 1979
8. Pitkänen, Ilkka: Thermodynamics of complexation of 1,2,4-triazole with divalent manganese, cobalt, nickel, copper, zinc, cadmium and lead ions in aqueous sodium perchlorate solutions. (89 pp.) 1980
9. Asunta, Tuula: Preparation and characterization of new organometallic compounds synthesized by using metal vapours. (91 pp.) 1980
10. Sattar, Mohammad Abdus: Analyses of MCPA and its metabolites in soil. (57 pp.) 1980
11. Bibliography 1980. (31 pp.) 1981
12. Knuuttila, Pekka: X-Ray structural studies on some divalent 3d metal compounds of picolinic and isonicotinic acid N-oxides. (77 pp.) 1981
13. Bibliography 1981. (33 pp.) 1982
14. 6^{th} National NMR Symposium, September 9-10, 1982, Abstracts. (49 pp.) 1982
15. Bibliography 1982. (38 pp.) 1983
16. Knuuttila, Hilkka: X-Ray structural studies on some Cu(II), Co(II) and Ni(II) complexes with nicotinic and isonicotinic acid N-oxides. (54 pp.) 1983
17. Symposium on inorganic and analytical chemistry May 18, 1984, Program and Abstracts. (100 pp.) 1984
18. Knuutinen, Juha: On the synthesis, structure verification and gas chromatographic determination of chlorinated catechols and guaiacols occuring in spent bleach liquors of kraft pulp mill. (30 pp.) 1984
19. Bibliography 1983. (47 pp.) 1984
20. Pitkänen, Maija: Addition of BrCl, B_2 and Cl_2 to methyl esters of propenoic and 2-butenoic acid derivatives and ^{13}C NMR studies on methyl esters of saturated aliphatic mono- and dichlorocarboxylic acids. (56 pp.) 1985
21. Bibliography 1984. (39 pp.) 1985
22. Salo, Esa: EPR, ENDOR and TRIPLE spectroscopy of some nitrogen heteroaromatics in liquid ammonia. (111 pp.) 1985

23. Humppi, Tarmo: Synthesis, identification and analysis of dimeric impurities of chlorophenols. (39 pp.) 1985
24. Aho, Martti: The ion exchange and adsorption properties of sphagnum peat under acid conditions. (90 pp.) 1985
25. Bibliography 1985 (61 pp.) 1986
26. Bibliography 1986. (23 pp.) 1987
27. Bibliography 1987. (26 pp.) 1988
28. Paasivirta, Jaakko (Ed.): Structures of organic environmental chemicals. (67 pp.) 1988
29. Paasivirta, Jaakko (Ed.): Chemistry and ecology of organo-element compounds. (93 pp.) 1989
30. Sinkkonen, Seija: Determination of crude oil alkylated dibenzothiophenes in environment. (35 pp.) 1989
31. Kolehmainen, Erkki (Ed.): XII National NMR Symposium Program and Abstracts. (75 pp.) 1989
32. Kuokkanen, Tauno: Chlorocymenes and Chlorocymenenes: Persistent chlorocompounds in spent bleach liquors of kraft pulp mills. (40 pp.) 1989
33. Mäkelä, Reijo: ESR, ENDOR and TRIPLE resonance study on substituted 9,10-anthraquinone radicals in solution. (35 pp.) 1990
34. Veijanen, Anja: An integrated sensory and analytical method for identification of off-flavour compounds. (70 pp.) 1990
35. Kasa, Seppo: EPR, ENDOR and TRIPLE resonance and molecular orbital studies on a substitution reaction of anthracene induced by thallium(III) in two fluorinated carboxylic acids. (114 pp.) 1990
36. Herve, Sirpa: Mussel incubation method for monitoring organochlorine compounds in freshwater recipients of pulp and paper industry. (145 pp.) 1991
37. Pohjola, Pekka: The electron paramagnetic resonance method for characterization of Finnish peat types and iron (III) complexes in the process of peat decomposition. (77 pp.) 1991
38. Paasivirta, Jaakko (Ed.): Organochlorines from pulp mills and other sources. Research methodology studies 1988-91. (120 pp.) 1992
39. Veijanen, Anja (Ed.): VI National Symposium on Mass Spectrometry, May 13-15, 1992, Abstracts. (55 pp.) 1992
40. Rissanen, Kari (Ed.): The 7. National Symposium on Inorganic and Analytical Chemistry, May 22, 1992, Abstracts and Program. (153 pp.) 1992
41. Paasivirta, Jaakko (Ed.): CEOEC'92, Second Finnish-Russian Seminar: Chemistry and Ecology of Organo-Element Compounds. (93 pp.) 1992
42. Koistinen, Jaana: Persistent polychloroaromatic compounds in the environment: structure-specific analyses. (50 pp.) 1993
43. Virkki, Liisa: Structural characterization of chlorolignins by spectroscopic and liquid chromatographic methods and a comparison with humic substances. (62 pp.) 1993
44. Helenius, Vesa: Electronic and vibrational excitations in some

biologically relevant molecules. (30 pp.) 1993

45. Leppä-aho, Jaakko: Thermal behaviour, infrared spectra and x-ray structures of some new rare earth chromates(VI). (64 pp.) 1994
46. Kotila, Sirpa: Synthesis, structure and thermal behavior of solid copper(II) complexes of 2-amino-2- hydroxymethyl-1,3-propanediol. (111 pp.) 1994
47. Mikkonen, Anneli: Retention of molybdenum(VI), vanadium(V) and tungsten(VI) by kaolin and three Finnish mineral soils. (90 pp.) 1995
48. Suontamo, Reijo: Molecular orbital studies of small molecules containing sulfur and selenium. (42 pp.) 1995
49. Hämäläinen, Jouni: Effect of fuel composition on the conversion of fuel-N to nitrogen oxides in the combustion of small single particles. (50 pp.) 1995
50. Nevalainen, Tapio: Polychlorinated diphenyl ethers: synthesis, NMR spectroscopy, structural properties, and estimated toxicity. (76 pp.) 1995
51. Aittola, Jussi-Pekka: Organochloro compounds in the stack emission. (35 pp.) 1995
52. Harju, Timo: Ultrafast polar molecular photophysics of (dibenzylmethine)borondifluoride and 4-aminophthalimide in solution. (61 pp.) 1995
53. Maatela, Paula: Determination of organically bound chlorine in industrial and environmental samples. (83 pp.) 1995
54. Paasivirta, Jaakko (Ed.): CEOEC'95, Third Finnish-Russian Seminar: Chemistry and Ecology of Organo-Element Compounds. (109 pp.) 1995
55. Huuskonen, Juhani: Synthesis and structural studies of some supramolecular compounds. (54 pp.) 1995
56. Palm, Helena: Fate of chlorophenols and their derivatives in sawmill soil and pulp mill recipient environments. (52 pp.) 1995
57. Rantio, Tiina: Chlorohydrocarbons in pulp mill effluents and their fate in the environment. (89 pp.) 1997
58. Ratilainen, Jari: Covalent and non-covalent interactions in molecular recognition. (37 pp.) 1997
59. Kolehmainen, Erkki (Ed.): XIX National NMR Symposium, June 4-6, 1997, Abstracts. (89 pp.) 1997
60. Matilainen, Rose: Development of methods for fertilizer analysis by inductively coupled plasma atomic emission spectrometry. (41 pp.) 1997
61. Koistinen, Jari (Ed.): Spring Meeting on the Division of Synthetic Chemistry, May 15-16, 1997, Program and Abstracts. (36 pp.) 1997
62. Lappalainen, Kari: Monomeric and cyclic bile acid derivatives: syntheses, NMR spectroscopy and molecular recognition properties. (50 pp.) 1997
63. Laitinen, Eira: Molecular dynamics of cyanine dyes and phthalimides in solution: picosecond laser studies. (62 pp.) 1997
64. Eloranta, Jussi: Experimental and theoretical studies on some

quinone and quinol radicals. (40 pp.) 1997

65. Oksanen, Jari: Spectroscopic characterization of some monomeric and aggregated chlorophylls. (43 pp.) 1998
66. Häkkänen, Heikki: Development of a method based on laser-induced plasma spectrometry for rapid spatial analysis of material distributions in paper coatings. (60 pp.) 1998
67. Virtapohja, Janne: Fate of chelating agents used in the pulp and paper industries. (58 pp.) 1998
68. Airola, Karri: X-ray structural studies of supramolecular and organic compounds. (39 pp.) 1998
69. Hyötyläinen, Juha: Transport of lignin–type compounds in the receiving waters of pulp mills. (40 pp.) 1999
70. Ristolainen, Matti: Analysis of the organic material dissolved during totally chlorine-free bleaching. (40 pp.) 1999
71. Eklin, Tero: Development of analytical procedures with industrial samples for atomic emission and atomic absorption spectrometry. (43 pp.) 1999
72. Välisaari, Jouni: Hygiene properties of resol-type phenolic resin laminates. (129 pp.) 1999
73. Hu, Jiwei: Persistent polyhalogenated diphenyl ethers: model compounds syntheses, characterization and molecular orbital studies. (59 pp.) 1999
74. Malkavaara, Petteri: Chemometric adaptations in wood processing chemistry. (56 pp.) 2000
75. Kujala Elena, Laihia Katri, Nieminen Kari (Eds.): NBC 2000, Symposium on Nuclear, Biological and Chemical Threats in the 21st Century. (299 pp.) 2000
76. Rantalainen, Anna-Lea: Semipermeable membrane devices in monitoring persistent organic pollutants in the environment. (58 pp.) 2000
77. Lahtinen, Manu: *In situ* X-ray powder diffraction studies of Pt/C, CuCl/C and Cu_2O/C catalysts at elevated temperatures in various reaction conditions. (92 pp.) 2000
78. Tamminen, Jari: Syntheses, empirical and theoretical characterization, and metal cation complexation of bile acid-based monomers and open/closed dimers. (54 pp.) 2000
79. Vatanen, Virpi: Experimental studies by EPR and theoretical studies by DFT calculations of α-amino-9,10-anthraquinone radical anions and cations in solution. (37 pp.) 2000
80. Kotilainen, Risto: Chemical changes in wood during heating at 150-260 °C. (57 pp.) 2000
81. Nissinen, Maija: X-ray structural studies on weak, non-covalent interactions in supramolecular compounds. (69 pp.) 2001
82. Wegelius, Elina: X-ray structural studies on self-assembled hydrogen-bonded networks and metallosupramolecular complexes. (84 pp.) 2001
83. Paasivirta, Jaakko (Ed.): CEOEC'2001, Fifth Finnish-Russian Seminar: Chemistry and Ecology of Organo-Element Compounds. (163 pp.) 2001
84. Kiljunen, Toni: Theoretical studies on spectroscopy and

atomic dynamics in rare gas solids. (56 pp.) 2001

85. Du, Jin: Derivatives of dextran: synthesis and applications in oncology. (48 pp.) 2001
86. Koivisto, Jari: Structural analysis of selected polychlorinated persistent organic pollutants (POPs) and related compounds. (88 pp.) 2001
87. Feng, Zhinan: Alkaline pulping of non-wood feedstocks and characterization of black liquors. (54 pp.) 2001
88. Halonen, Markku: Lahon havupuun käyttö sulfaattiprosessin raaka-aineena sekä havupuun lahontorjunta. (90 pp.) 2002
89. Falábu, Dezsö: Synthesis, conformational analysis and complexation studies of resorcarene derivatives. (212 pp.) 2001
90. Lehtovuori, Pekka: EMR spectroscopic studies on radicals of ubiquinones Q-*n*, vitamin K_3 and vitamine E in liquid solution. (40 pp.) 2002
91. Perkkalainen, Paula: Polymorphism of sugar alcohols and effect of grinding on thermal behavior on binary sugar alcohol mixtures. (53 pp.) 2002
92. Ihalainen, Janne: Spectroscopic studies on light-harvesting complexes of green plants and purple bacteria. (42 pp.) 2002
93. Kunttu, Henrik, Kiljunen, Toni (Eds.): 4th International Conference on Low Temperature Chemistry. (159 pp.) 2002
94. Väisänen, Ari: Development of methods for toxic element analysis in samples with environmental concern by ICP-AES and ETAAS. (54 pp.) 2002
95. Luostarinen, Minna: Synthesis and characterisation of novel resorcarene derivatives. (200 pp.) 2002
96. Louhelainen, Jarmo: Changes in the chemical composition and physical properties of wood and nonwood black liquors during heating. (68 pp.) 2003
97. Lahtinen, Tanja: Concave hydrocarbon cyclophane π-prismands. (65 pp.) 2003
98. Laihia, Katri (Ed.): NBC 2003, Symposium on Nuclear, Biological and Chemical Threats – A Crisis Management Challenge. (245 pp.) 2003
99. Oasmaa, Anja: Fuel oil quality properties of wood-based pyrolysis liquids. (32 pp.) 2003
100. Virtanen, Elina: Syntheses, structural characterisation, and cation/anion recognition properties of nano-sized bile acid-based host molecules and their precursors. (123 pp.) 2003
101. Nättinen, Kalle: Synthesis and X-ray structural studies of organic and metallo-organic supramolecular systems. (79 pp.) 2003
102. Lampiselkä, Jarkko: Demonstraatio lukion kemian opetuksessa. (285 pp.) 2003
103. Kallioinen, Jani: Photoinduced dynamics of $Ru(dcbpy)_2(NCS)_2$ – in solution and on nanocrystalline titanium dioxide thin films. (47 pp.) 2004
104. Valkonen, Arto (Ed.): VII Synthetic Chemistry Meeting and XXVI Finnish NMR Symposium. (103 pp.) 2004

105. Vaskonen, Kari: Spectroscopic studies on atoms and small molecules isolated in low temperature rare gas matrices. (65 pp.) 2004
106. Lehtovuori, Viivi: Ultrafast light induced dissociation of $Ru(dcbpy)(CO)_2I_2$ in solution. (49 pp.) 2004
107. Saarenketo, Pauli: Structural studies of metal complexing Schiff bases, Schiff base derived *N*-glycosides and cyclophane π-prismands. (95 pp.) 2004
108. Paasivirta, Jaakko (Ed.): CEOEC'2004, Sixth Finnish-Russian Seminar: Chemistry and Ecology of Organo-Element Compounds. (147 pp.) 2004
109. Suontamo, Tuula: Development of a test method for evaluating the cleaning efficiency of hard-surface cleaning agents. (96 pp.) 2004
110. Güneş, Minna: Studies of thiocyanates of silver for nonlinear optics. (48 pp.) 2004
111. Ropponen, Jarmo: Aliphatic polyester dendrimers and dendrons. (81 pp.) 2004
112. Vu, Mân Thi Hong: Alkaline pulping and the subsequent elemental chlorine-free bleaching of bamboo (*Bambusa procera*). (69 pp.) 2004
113. Mansikkamäki, Heidi: Self-assembly of resorcinarenes. (77 pp.) 2006
114. Tuononen, Heikki M.: EPR spectroscopic and quantum chemical studies of some inorganic main group radicals. (79 pp.) 2005
115. Kaski, Saara: Development of methods and applications of laser-induced plasma spectroscopy in vacuum ultraviolet. (44 pp.) 2005
116. Mäkinen, Riika-Mari: Synthesis, crystal structure and thermal decomposition of certain metal thiocyanates and organic thiocyanates. (119 pp.) 2006
117. Ahokas, Jussi: Spectroscopic studies of atoms and small molecules isolated in rare gas solids: photodissociation and thermal reactions. (53 pp.) 2006
118. Busi, Sara: Synthesis, characterization and thermal properties of new quaternary ammonium compounds: new materials for electrolytes, ionic liquids and complexation studies. (102 pp.) 2006
119. Mäntykoski, Keijo: PCBs in processes, products and environment of paper mills using wastepaper as their raw material. (73 pp.) 2006
120. Laamanen, Pirkko-Leena: Simultaneous determination of industrially and environmentally relevant aminopolycarboxylic and hydroxycarboxylic acids by capillary zone electrophoresis. (54 pp.) 2007
121. Salmela, Maria: Description of oxygen-alkali delignification of kraft pulp using analysis of dissolved material. (71 pp.) 2007
122. Lehtovaara, Lauri: Theoretical studies of atomic scale impurities in superfluid ^{4}He. (87 pp.) 2007
123. Rautiainen, J. Mikko: Quantum chemical calculations of structures, bonding, and spectroscopic properties of some sulphur and selenium iodine cations. (71 pp.) 2007
124. Nummelin, Sami: Synthesis, characterization, structural and

retrostructural analysis of self-assembling pore forming dendrimers. (286 pp.) 2008

125. Sopo, Harri: Uranyl(VI) ion complexes of some organic aminobisphenolate ligands: syntheses, structures and extraction studies. (57 pp.) 2008
126. Valkonen, Arto: Structural characteristics and properties of substituted cholanoates and *N*-substituted cholanamides. (80 pp.) 2008
127. Lähde, Anna: Production and surface modification of pharmaceutical nano- and microparticles with the aerosol flow reactor. (43 pp.) 2008
128. Beyeh, Ngong Kodiah: Resorcinarenes and their derivatives: synthesis, characterization and complexation in gas phase and in solution. (75 pp.) 2008
129. Välisaari, Jouni, Lundell, Jan (Eds.): Kemian opetuksen päivät 2008: uusia oppimisympäristöjä ja ongelmalähtöistä opetusta. (118 pp.) 2008
130. Myllyperkiö, Pasi: Ultrafast electron transfer from potential organic and metal containing solar cell sensitizers. (69 pp.) 2009
131. Käkölä, Jaana: Fast chromatographic methods for determining aliphatic carboxylic acids in black liquors. (82 pp.) 2009
132. Koivukorpi, Juha: Bile acid-arene conjugates: from photoswitchability to cancer cell detection. (67 pp.) 2009
133. Tuuttila, Tero: Functional dendritic polyester compounds: synthesis and characterization of small bifunctional dendrimers and dyes. (74 pp.) 2009
134. Salorinne, Kirsi: Tetramethoxy resorcinarene based cation and anion receptors: synthesis, characterization and binding properties. (79 pp.) 2009
135. Rautiainen, Riikka: The use of first-thinning Scots pine (*Pinus sylvestris*) as fiber raw material for the kraft pulp and paper industry. (73 pp.) 2010
136. Ilander, Laura: Uranyl salophens: synthesis and use as ditopic receptors. (199 pp.) 2010
137. Kiviniemi, Tiina: Vibrational dynamics of iodine molecule and its complexes in solid krypton - Towards coherent control of bimolecular reactions? (73 pp.) 2010
138. Ikonen, Satu: Synthesis, characterization and structural properties of various covalent and non-covalent bile acid derivatives of N/O-heterocycles and their precursors. (105 pp.) 2010
139. Siitonen, Anni: Spectroscopic studies of semiconducting single-walled carbon nanotubes. (56 pp.) 2010
140. Raatikainen, Kari: Synthesis and structural studies of piperazine cyclophanes – Supramolecular systems through Halogen and Hydrogen bonding and metal ion coordination. (69 pp.) 2010
141. Leivo, Kimmo: Gelation and gel properties of two- and three-component Pyrene based low molecular weight organogelators. (116 pp.) 2011
142. Martiskainen, Jari: Electronic energy transfer in light-harvesting complexes isolated from *Spinacia oleracea* and from three

photosynthetic green bacteria *Chloroflexus aurantiacus*, *Chlorobium tepidum*, and *Prosthecochloris aestuarii*. (55 pp.) 2011

143. Wichmann, Oula: Syntheses, characterization and structural properties of [O,N,O,X´] aminobisphenolate metal complexes. (101 pp.) 2011
144. Ilander, Aki: Development of ultrasound-assisted digestion methods for the determination of toxic element concentrations in ash samples by ICP-OES. (58 pp.) 2011
145. The Combined XII Spring Meeting of the Division of Synthetic Chemistry and XXXIII Finnish NMR Symposium. Book of Abstracts. (90 pp.) 2011
146. Valto, Piia: Development of fast analysis methods for extractives in papermaking process waters. (73 pp.) 2011
147. Andersin, Jenni: Catalytic activity of palladium-based nanostructures in the conversion of simple olefinic hydro- and chlorohydrocarbons from first principles. (78 pp.) 2011
148. Aumanen, Jukka: Photophysical properties of dansylated poly(propylene amine) dendrimers. (55 pp.) 2011
149. Kärnä, Minna: Ether-functionalized quaternary ammonium ionic liquids – synthesis, characterization and physicochemical properties. (76 pp.) 2011
150. Jurček, Ondřej: Steroid conjugates for applications in pharmacology and biology. (57 pp.) 2011
151. Nauha, Elisa: Crystalline forms of selected Agrochemical actives: design and synthesis of cocrystals. (77 pp.) 2012
152. Ahkola, Heidi: Passive sampling in monitoring of nonylphenol ethoxylates and nonylphenol in aquatic environments. (92 pp.) 2012
153. Helttunen, Kaisa: Exploring the self-assembly of resorcinarenes: from molecular level interactions to mesoscopic structures. (78 pp.) 2012
154. Linnanto, Juha: Light excitation transfer in photosynthesis revealed by quantum chemical calculations and exiton theory. (179 pp.) 2012
155. Roiko-Jokela, Veikko: Digital imaging and infrared measurements of soil adhesion and cleanability of semihard and hard surfaces. (122 pp.) 2012
156. Noponen, Virpi: Amides of bile acids and biologically important small molecules: properties and applications. (85 pp.) 2012
157. Hulkko, Eero: Spectroscopic signatures as a probe of structure and dynamics in condensed-phase systems – studies of iodine and gold ranging from isolated molecules to nanoclusters. (69 pp.) 2012
158. Lappi, Hanna: Production of Hydrocarbon-rich biofuels from extractives-derived materials. (95 pp.) 2012
159. Nykänen, Lauri: Computational studies of Carbon chemistry on transition metal surfaces. (76 pp.) 2012
160. Ahonen, Kari: Solid state studies of pharmaceutically important molecules and their derivatives. (65 pp.) 2012

161. Pakkanen, Hannu: Characterization of organic material dissolved during alkaline pulping of wood and non-wood feedstocks. (76 pp.) 2012
162. Moilanen, Jani: Theoretical and experimental studies of some main group compounds: from closed shell interactions to singlet diradicals and stable radicals. (80 pp.) 2012
163. Himanen, Jatta: Stereoselective synthesis of Oligosaccharides by *De Novo* Saccharide welding. (133 pp.) 2012
164. Bunzen, Hana: Steroidal derivatives of nitrogen containing compounds as potential gelators. (76 pp.) 2013
165. Seppälä, Petri: Structural diversity of copper(II) amino alcohol complexes. Syntheses, structural and magnetic properties of bidentate amino alcohol copper(II) complexes. (67 pp.) 2013
166. Lindgren, Johan: Computational investigations on rotational and vibrational spectroscopies of some diatomics in solid environment. (77 pp.) 2013
167. Giri, Chandan: Sub-component self-assembly of linear and non-linear diamines and diacylhydrazines, formulpyridine and transition metal cations. (145 pp.) 2013
168. Riisiö, Antti: Synthesis, Characterization and Properties of Cu(II)-, Mo(VI)- and U(VI) Complexes With Diaminotetraphenolate Ligands. (51 pp.) 2013
169. Kiljunen, Toni (Ed.): Chemistry and Physics at Low Temperatures. Book of Abstracts. (103 pp.) 2013
170. Hänninen, Mikko: Experimental and Computational Studies of Transition Metal Complexes with Polydentate Amino- and Aminophenolate Ligands: Synthesis, Structure, Reactivity and Magnetic Properties. (66 pp.) 2013
171. Antila, Liisa: Spectroscopic studies of electron transfer reactions at the photoactive electrode of dye-sensitized solar cells. (53 pp.) 2013
172. Kemppainen, Eeva: Mukaiyama-Michael reactions with α-substituted acroleins – a useful tool for the synthesis of the pectenotoxins and other natural product targets. (190 pp.) 2013
173. Virtanen, Suvi: Structural Studies of Dielectric Polymer Nanocomposites. (49 pp.) 2013
174. Yliniemelä-Sipari, Sanna: Understanding The Structural Requirements for Optimal Hydrogen Bond Catalyzed Enolization – A Biomimetic Approach.(160 pp.) 2013
175. Leskinen, Mikko V: Remote β-functionalization of β'-keto esters. (105 pp.) 2014
176. 12th European Conference on Research in Chemistry Education (ECRICE2014). Book of Abstracts. (166 pp.) 2014
177. Peuronen, Anssi: N-Monoalkylated DABCO-Based N-Donors as Versatile Building Blocks in Crystal Engineering and Supramolecular Chemistry. (54 pp.) 2014
178. Perämäki, Siiri: Method development for determination and recovery of rare earth elements from industrial fly ash. (88 pp.) 2014

179. Chernyshev, Alexander, N.: Nitrogen-containing ligands and their platinum(IV) and gold(III) complexes: investigation and basicity and nucleophilicity, luminescence, and aurophilic interactions. (64 pp.) 2014
180. Lehto, Joni: Advanced Biorefinery Concepts Integrated to Chemical Pulping. (142 pp.) 2015
181. Tero, Tiia-Riikka: Tetramethoxy resorcinarenes as platforms for fluorescent and halogen bonding systems. (61 pp.) 2015
182. Löfman, Miika: Bile acid amides as components of microcrystalline organogels. (62 pp.) 2015
183. Selin, Jukka: Adsorption of softwood-derived organic material onto various fillers during papermaking. (169 pp.) 2015
184. Piisola, Antti: Challenges in the stereoselective synthesis of allylic alcohols. (210 pp.) 2015
185. Bonakdarzadeh, Pia: Supramolecular coordination polyhedra based on achiral and chiral pyridyl ligands: design, preparation, and characterization. (65 pp.) 2015
186. Vasko, Petra: Synthesis, characterization, and reactivity of heavier group 13 and 14 metallylenes and metalloid clusters: small molecule activation and more. (66 pp.) 2015
187. Topić, Filip: Structural Studies of Nano-sized Supramolecular Assemblies. (79 pp.) 2015
188. Mustalahti, Satu: Photodynamics Studies of Ligand-Protected Gold Nanoclusters by using Ultrafast Transient Infrared Spectroscopy. (58 pp.) 2015
189. Koivisto, Jaakko: Electronic and vibrational spectroscopic studies of gold-nanoclusters. (63 pp.) 2015
190. Suhonen, Aku: Solid state conformational behavior and interactions of series of aromatis oligoamide foldamers. (68 pp.) 2016
191. Soikkeli, Ville: Hydrometallurgical recovery and leaching studies for selected valuable metals from fly ash samples by ultrasound-assisted extraction followed by ICP-OES determination. (107 pp.) 2016
192. XXXVIII Finnish NMR Symposium. Book of Abstracts. (51 pp.) 2016
193. Mäkelä, Toni: Ion Pair Recognition by Ditopic Crown Ether Based bis-Urea and Uranyl Salophen Receptors. (75 pp.) 2016
194. Lindholm-Lehto, Petra: Occurrence of pharmaceuticals in municipal wastewater treatment plants and receiving surface waters in Central and Southern Finland. (98 pp.) 2016
195. Härkönen, Ville: Computational and Theoretical studies on Lattice Thermal conductivity and Thermal properties of Silicon Clathrates. (89 pp.) 2016
196. Tuokko, Sakari: Understanding selective reduction reactions with heterogeneous Pd and Pt: climbing out of the black box. (85 pp.) 2016
197. Nuora, Piia: Monitapaustutkimus LUMA-Toimintaan liittyvissä oppimisympäristöissä tapahtuvista kemian oppimiskokemuksista. (171 pp.) 2016

198. Kumar, Hemanathan: Novel Concepts on The Recovery of By-Products from Alkaline Pulping. (61 pp.) 2016
199. Arnedo-Sánchez, Leticia: Lanthanide and Transition Metal Complexes as Building Blocks for Supramolecular Functional Materials. (227 pp.) 2016
200. Gell, Lars: Theoretical Investigations of Ligand Protected Silver Nanoclusters. (134 pp.) 2016
201. Vaskuri, Juhani: Oppiennätyksistä opetussuunnitelman perusteisiin - lukion kemian kansallisen opetussuunnitelman kehittyminen Suomessa vuosina 1918-2016. (314 pp.) 2017
202. Lundell Jan, Kiljunen Toni (Eds.): 22nd Horizons in Hydrogen Bond Research. Book of Abstracts. 2017
203. Turunen, Lotta: Design and construction of halogen-bonded capsules and cages. (61 pp.) 2017
204. Hurmalainen, Juha: Experimental and computational studies of unconventional main group compounds: stable radicals and reactive intermediates. (88 pp.) 2017
205. Koivistoinen Juha: Non-linear interactions of femtosecond laser pulses with graphene: photo-oxidation, imaging and photodynamics. (68 pp.) 2017
206. Chen, Chengcong: Combustion behavior of black liquors: droplet swelling and influence of liquor composition. (39 pp.) 2017
207. Mansikkamäki, Akseli: Theoretical and Computational Studies of Magnetic Anisotropy and Exchange Coupling in Molecular Systems. (190 p. + included articles) 2018.
208. Tatikonda, Rajendhraprasad: Multivalent N-donor ligands for the construction of coordination polymers and coordination polymer gels. (62 pp.) 2018
209. Budhathoki, Roshan: Beneficiation, desilication and selective precipitation techniques for phosphorus refining from biomass derived fly ash. (64 pp.) 2018
210. Siitonen, Juha: Synthetic Studies on 1-azabicyclo[5.3.0]decane Alkaloids. (140 pp.) 2018
211. Ullah, Saleem: Advanced Biorefinery Concepts Related to Non-wood Feedstocks. (57 pp.) 2018
212. Ghalibaf, Maryam: Analytical Pyrolysis of Wood and Non-Wood Materials from Integrated Biorefinery Concepts. (106 pp.) 2018

DEPARTMENT OF CHEMISTRY, UNIVERSITY OF JYVÄSKYLÄ
DISSERTATIONS PUBLISHED IN THE JYU DISSERTATIONS RESEARCH SERIES

1. Bulatov, Evgeny: Synthetic and structural studies of covalent and non-covalent interactions of ligands and metal center in platinum(II) complexes containing 2,2′-dipyridylamine or oxime ligands. (58 pp.) 2019. JYU Dissertations 70.
2. Annala, Riia: Conformational Properties and Anion Complexes of Aromatic Oligoamide Foldamers. (80 pp.) 2019. JYU Dissertations 84.
3. Isoaho, Jukka Pekka: Dithionite Bleaching of Thermomechanical Pulp - Chemistry and Optimal Conditions. (73 pp.) 2019. JYU Dissertations 85.
4. Nygrén, Enni: Recovery of rubidium from power plant fly ash. (98 pp.) 2019. JYU Dissertations 136.
5. Kiesilä, Anniina: Supramolecular chemistry of anion-binding receptors based on concave macromolecules. (68 pp.) 2019. JYU Dissertations 137.
6. Sokolowska, Karolina: Study of water-soluble p-MBA-protected gold nanoclusters and their superstructures. (60 pp.) 2019. JYU Dissertations 167.
7. Lahtinen, Elmeri: Chemically Functional 3D Printing: Selective Laser Sintering of Customizable Metal Scavengers. (71 pp.) 2019. JYU Dissertations 175.
8. Larijani, Amir: Oxidative reactions of cellulose under alkaline conditions. (102 pp.) 2020. JYU Dissertations 217.
9. Kolari, Kalle: Metal-metal contacts in late transition metal polymers. (60 pp.) 2020. JYU Dissertations 220.
10. Kauppinen, Minttu: Multiscale computational investigation of catalytic properties of zirconia supported noble metals. (87 pp.) 2020. JYU Dissertations 231.
11. Ding, Xin: Halogen Bond in Crystal Engineering: Structural Studies on Crystals with Ruthenium Centered Complexes and 1-(4-Pyridyl)-4-thiopyridine Zwitterion as Halogen Bond Acceptors. (59 pp.) 2020. JYU Dissertations 323.
12. Neuvonen, Antti: Toward an Understanding of Hydrogen-Bonding Bifunctional Organocatalyst Conformations and Their Activity in Asymmetric Mannich Reactions. (77 pp.) 2020. JYU Dissertations 336.
13. Kortet, Sami: 2,5-Diarylpyrrolidines and Pyroglutamic-Acid-Derived 2-Diarylmethyl-5-Aryl-Pyrrolidines: Their Synthesis and Use in Asymmetric Synthesis. (221 pp.) 2020. JYU Dissertations 337.
14. Saarnio, Ville: Fluorescent probes, noble metal nanoparticles and their nanocomposites: detection of nucleic acids and other biological targets. (80 pp.) 2021. JYU Dissertations 361.
15. Chernysheva, Maria: σ-hole interactions: the effect of the donors and acceptors nature in selenoureas, thioureas, halogenated species, substituted benzenes, and their adducts. (72 pp.) 2021. JYU Dissertations 370.
16. Bulatova, Margarita: Noncovalent interactions as a tool for supramolecular self-assembly of metallopolymers. (62 pp.) 2021. JYU Dissertations 377.

DEPARTMENT OF CHEMISTRY, UNIVERSITY OF JYVÄSKYLÄ
DISSERTATIONS PUBLISHED IN THE JYU DISSERTATIONS RESEARCH SERIES

17. Romppanen, Sari: Laser-spectroscopic studies of rare earth element- and lithium-bearing minerals and rocks. (66 pp.) 2021. JYU Dissertations 393.